ON MULTI-POINT SIMILARITY SOLUTIONS IN TURBULENT FREE-SHEAR FLOWS

Ву

Daniel Ewing

A dissertation submitted to the
Faculty of the Graduate School of the
State University of New York at Buffalo
in partial fulfillment of the requirements
for the degree of
Doctor of Philosophy
September 1995

Acknowledgements

I would like to thank Dr. William K. George for all his assistance in carrying out this research and in the preparation the document. I would also like to thank Drs. Dale Taulbee, Peyman Givi, and Mike Rogers for sitting on my committee. In addition, I would like to acknowledge the contribution of Drs. Robert Moser and Mike Rogers to this research.

I would also like to thank the State University of the New York at Buffalo, the National Science Foundation, and the Center for Turbulence Research at Stanford University for providing the financial support which made this research possible.

Finally, and most importantly, I would like to thank my family and close friends for all their support.

Abstract

The equations that govern the two-point velocity correlation tensor in three different free-shear flows: a temporally developing wake, a spatially evolving axisymmetric jet, and a spatially evolving plane jet, are examined in order to determine if these equations admit similarity solutions. Following the approach suggested by George (1989), this investigation is carried out by allowing the different correlations in these equations to have their own similarity scales. The allowable choices for these scales are then determined by examining the equations of motion. It is demonstrated that the full equations that govern the two-point velocity correlation tensor in the temporally developing wake and the spatially developing axisymmetric jet admit similarity solutions for idealized virtual sources. In these solutions, the scales for all of the members in the two-point velocity correlation tensor and the turbulent transfer terms are proportional, consistent with the traditional self-preservation (similarity) approach (v. Townsend 1956). The equations that govern the similarity profiles are dependent on the growth rates of the flows, though, indicating that the solutions for these profiles depend on the source conditions of the flows, in contrast to the traditional self-preservation arguments.

The governing equations for the two-point velocity correlation in the spatially evolving plane jet do not admit similarity solutions because this is not a constant-Reynolds-number flow. The Reynolds number of the jet approaches infinity, however, as the flow evolves downstream. In this limit, it is possible to demonstrate that the first order equations that govern the evolution of the two-point velocity correlation tensor for large separation distances (which emphasize the large-scale motions) and the equations governing the second-order structure functions (which emphasize the

small-scale motions) each admit similarity solutions. The similarity solutions for the small-scale motions are consistent with the solution proposed by Kolmogorov (1941).

Contents

A	f Acknowledgements $f Abstract$			
A				
Ta	able (of Con	tents	iv
Li	st of	Figur	es	vi
N	omer	ıclatur	·e	x
1	\mathbf{Intr}	oduct	ion	1
	1.1	Revie	w of Similarity Analysis	3
		1.1.1	Single-Point Similarity Analysis	4
		1.1.2	Similarity Analysis of Two-Point Information	9
		1.1.3	Kolmogorov's Hypothesis	13
	1.2	Objec	tive of This Research	14
2	The	Temp	oorally Developing Plane Wake	18
	2.1	Revie	w of Spatially Evolving Wake Literature	19
	2.2	Flow	Geometry	23
	2.3	Simila	arity of the Single-Point Moments	24

	2.3.1	Analysis of the Velocity Field	25
2.4	Analys	sis of the Two-Point Correlations	36
	2.4.1	The Two-Point Velocity Correlation Tensor	36
	2.4.2	Pressure-Velocity Correlation	43
	2.4.3	Other Statistical Measures of The Flow	45
	2.4.4	One-Dimensional Spectra Of the Velocity Field	47
2.5	Length	and Velocity Scales	49
2.6	Compa	arison of Theory to Data	52
	2.6.1	Simulations	52
	2.6.2	Evolution of the Reynolds Number and Similarity Length Scale	55
	2.6.3	Single-Point Moments	56
	2.6.4	Computation of One-Dimensional Spectra	57
	2.6.5	One-Dimensional Spectra of the Fluctuating Velocity	60
	2.6.6	Taylor Microscales	65
	2.6.7	Velocity Correlation in the Non-Homogeneous Direction	67
2.7	Analys	sis of the Two-Point, Two-Time Correlations	70
2.8	Analys	sis of a Scalar Field	79
	2.8.1	Single-Point Moments: The Two-Stream Field	80
	2.8.2	Analysis of Scalar-Deficit Flow	86
2.9	Analys	sis of the Two-Point Scalar Correlation	88
2.10	Comparison of Theory to Data: Scalar Field		
	2.10.1	Simulation: Scalar Field	92
	2.10.2	One-Dimensional Spectra of the Scalar Field	92
	2.10.3	Taylor Microscales of the Scalar Field	93

3	The	Spati	ally Developing Axisymmetric Jet	160
	3.1	Simila	rity Analysis of the Two-Point Velocity Correlation Tensor	161
	3.2	The P	ressure Field	172
	3.3	Simila	rity of the Velocity-Gradient Moments	178
4	The	Spati	ally Developing Plane Jet	183
	4.1	Review	w of the Results of the Single-Point Similarity Analysis	184
	4.2	Simila	rity Analysis of the Two-Point Velocity Correlation Tensor	185
		4.2.1	The Large-Scale Motions	187
		4.2.2	The Small-Scale Motions	193
5	Imp	licatio	ons of the Hypothesis	206
	5.1	Single	-Point Similarity Solution For Finite-Reynolds-Number Flows .	207
	5.2	The R	epresentation of the Velocity Field	208
		5.2.1	The Temporally Evolving, Plane Wake	210
		5.2.2	The Spatially Developing Axisymmetric Jet	214
6	Sun	nmary	and Concluding Remarks	218
Bi	bliog	graphy		226
A	Rev	iew of	Single-Point Similarity Hypothesis	231
В	Equ	ation	for the Structure Function	239

List of Figures

1.1	Geometry of the spatially evolving plane wake	17
2.1	Instantaneous realization of the temporally evolving wake simulation	95
2.2	Geometry of the temporally evolving wake flow	96
2.3	Evolution of Reynolds number in the temporally developing wake sim-	
	ulations	97
2.4	Evolution of the similarity length scale in the temporally evolving wake	
	simulations	98
2.5	Scaled value of $\overline{u_1u_1}$ in the unforced wake	99
2.6	Scaled value of $\overline{u_2u_2}$ in the unforced wake	100
2.7	Scaled value of $\overline{u_3u_3}$ in the unforced wake	101
2.8	Scaled value of $\overline{u_1u_1}$ in the forced wake	102
2.9	Scaled value of $\overline{u_2u_2}$ in the forced wake	103
2.10	Scaled value of $\overline{u_3u_3}$ in the forced wake	104
2.11	One-dimensional spectra in the unforced wake at $x_2/\delta=0$	105
2.12	One-dimensional spectra in the forced wake at $x_2/\delta = 0$	106
2.13	One-dimensional spectra of $\overline{u_1u_1}$ at different x_2 -positions in the forced	
	wake	107

2.14	One-dimensional spectra of u_2u_2 at different x_2 -positions in the forced	
	wake	108
2.15	Scaled one-dimensional spectra F^1_{11} in the unforced wake	109
2.16	Scaled one-dimensional spectra F_{22}^1 in the unforced wake	110
2.17	Scaled one-dimensional spectra F^1_{33} in the unforced wake	111
2.18	Scaled one-dimensional spectra F^1_{11} in the forced wake	112
2.19	Scaled one-dimensional spectra F_{22}^1 in the forced wake	113
2.20	Scaled one-dimensional spectra F^1_{33} in the forced wake	114
2.21	Scaled one-dimensional spectra F_{11}^3 in the unforced wake	115
2.22	Scaled one-dimensional spectra F_{22}^3 in the unforced wake	116
2.23	Scaled one-dimensional spectra F_{33}^3 in the unforced wake	117
2.24	Scaled one-dimensional spectra F_{11}^3 in the forced wake	118
2.25	Scaled one-dimensional spectra F_{22}^3 in the forced wake	119
2.26	Scaled one-dimensional spectra F_{33}^3 in the forced wake	120
2.27	Magnitude of one-dimensional spectra F_{12}^1 at $\eta{=}0.0$ in the unforced wake	.121
2.28	Scaled magnitude of the spectra F_{12}^1 at $\eta=0.0$ in the unforced wake.	122
2.29	Scaled magnitude of the spectra F_{12}^1 at $\eta=0.0$ in the forced wake	123
2.30	Scaled magnitude of the spectra F_{12}^1 at $\eta=0.5$ and $\eta=1.0$ in the	
	unforced wake	124
2.31	Scaled magnitude of the spectra F_{12}^1 at $\eta=0.5$ and $\eta=1.0$ in the	
	forced wake	125
2.32	Scaled magnitude of the spectra F_{12}^3 at $\eta=0.0$ and $\eta=0.5$ in the	
	unforced wake	126
2.33	Taylor microscales in the x_1 -direction in the unforced wake	127
2.34	Taylor microscales in the x_3 -direction in the unforced wake	128

2.35	Taylor microscales in the x_1 -direction in the forced wake 129
2.36	Taylor microscales in the x_3 -direction in the forced wake 130
2.37	Scaled autocorrelation of $\overline{u_1u_1'}$ about $\eta = 0.0$; unforced wake 131
2.38	Scaled autocorrelation of $\overline{u_1u_1'}$ about $\eta = \pm 0.5$; unforced wake 132
2.39	Structure function of the u_1 component at $\eta = 0.0$ in the unforced wake.133
2.40	Structure function of the u_1 component at $\eta=\pm 0.5$ in the unforced
	wake
2.41	Structure function of the u_2 component at $\eta=0.0$ in the unforced wake.135
2.42	Structure function of the u_2 component at $\eta=\pm 0.5$ in the unforced
	wake
2.43	Structure function of the u_3 component at $\eta = 0.0$ in the unforced wake.137
2.44	Structure function of the u_3 component at $\eta=\pm 0.5$ in the unforced
	wake
2.45	Scaled autocorrelation of $\overline{u_1u_2'}$ about $\eta=0.0$ in the unforced wake 139
2.46	Scaled autocorrelation of $\overline{u_1u_2'}$ about $\eta=\pm 0.5$ in the unforced wake 140
2.47	Scaled autocorrelation of $\overline{u_2u_1'}$ about $\eta=0.0$ in the unforced wake 141
2.48	Scaled autocorrelation of $\overline{u_2u_1'}$ about $\eta=\pm 0.5$ in the unforced wake 142
2.49	Structure function of the u_1 component at $\eta = 0.0$ in the forced wake. 143
2.50	Structure function of the u_1 component at $\eta = \pm 0.5$ in the forced wake. 144
2.51	Structure function of the u_2 component at $\eta = 0.0$ in the forced wake. 145
2.52	Structure function of the u_2 component at $\eta=\pm 0.5$ in the forced wake. 146
2.53	Structure function of the u_3 component at $\eta = 0.0$ in the forced wake. 147
2.54	Structure function of the u_3 component at $\eta=\pm 0.5$ in the forced wake. 148
2.55	Geometry of the two-stream scalar field in the temporally developing
	wake

2.56	Geometry of the scalar-deficit field in the temporally developing wake.	150
2.57	One-dimensional scalar spectra $F^1_{\theta\theta}$ at $\eta{=}0.0$ in the unforced wake	151
2.58	Scaled one-dimensional spectra $F^1_{\theta\theta}$ at $\eta{=}0.0$ and η =0.5 in the unforced	
	wake	152
2.59	Scaled one-dimensional spectra $F_{\theta\theta}^3$ at $\eta{=}0.0$ and η =0.5 in the unforced	
	wake	153
2.60	Scaled one-dimensional spectra $F^1_{\theta\theta}$ at $\eta{=}0.0$ and η =0.5 in the forced	
	wake	154
2.61	Scaled one-dimensional spectra $F_{\theta\theta}^3$ at $\eta{=}0.0$ and η =0.5 in the forced	
	wake	155
2.62	Taylor microscales of the scalar field in the x_1 -direction in the unforced	
	wake	156
2.63	Taylor microscales of the scalar field in the x_3 -direction in the unforced	
	wake	157
2.64	Taylor microscales of the scalar field in the x_1 -direction in the forced	
	wake	158
2.65	Taylor microscales of the scalar field in the x_3 -direction in the forced	
	wake	159
3.1	Geometry of the spatially developing axisymmetric wake	182
4.1	Geometry for the spatially developing plane jet	205

Nomenclature

 d_{u_i} Similarity profile for the dissipation of the normal Reynolds stresses. D_{u_i} Similarity scale for the dissipation of the normal Reynolds stresses. Rate-of-strain tensor. e_{ij} fSimilarity profile for U_1 . F(r,t)Longitudinal correlation function (for isotropic turbulence). k_1 Wavenumber in physical variables for the homogeneous x_1 direction. \tilde{k}_1 Wavenumber in similarity variables for the homogeneous x_1 direction. k_2 ratio of time scales for the velocity field in the temporally evolving wake. Similarity profile for the normal Reynolds stresses. k_{u_i} Turbulence transfer function (for isotropic turbulence). K(r,t) K_{u_i} Similarity scale for the normal Reynolds stresses. One-dimensional Fourier transform of the $\overline{u_j u_k'}$ correlation in the *i* direction. F_{jk}^i

- g Similarity profile for $\overline{u_1u_2}$.
- l_s Characteristic length scale of the small-scale motion in the plane jet.
- L_{jk}^{i} Integral length scale of the $\overline{u_{j}u_{k}'}$ correlation in the *i* direction.
- M_0 Momentum deficit/ surplus in the flow.
- p Fluctuating pressure.
- $p_{,j}^1$ Similarity profile for the two-point pressure-velocity correlation.
- P Average pressure.
- Pe Peclet number.
- $P_1^{,j}$ Similarity scale for the two-point pressure-velocity correlation.
- $q_{i,j}$ Similarity profile for the two-point velocity correlation.
- $Q^{i,j}$ Similarity scale for the two-point velocity correlation.
- r Separation distance between two points.
- $r_{u_2\theta}$ Similarity profile for $\overline{u_2\theta}$.

- r_1^{θ} Similarity profile for the two-point scalar-velocity correlation.
- Re Reynolds number.
- $R_{i,j}$ Unscaled two-point velocity correlation tensor.
- R_s Similarity scale for $\overline{u_1u_2}$.
- R_{θ}^{1} Similarity scale for the two-point scalar-velocity correlation.
- $R_{u_2\theta}$ Similarity scale for $\overline{u_2\theta}$.
- s_c Similarity profile for the mean value of the scalar.
- s_k^1 Similarity profile for $\overline{u_k\theta\theta'}$.
- S_c Similarity scale for the mean value of the scalar.
- S_k^1 Similarity scale for $\overline{u_k\theta\theta'}$.
- t Time.
- tr_{u_i} Similarity profile for the single-point turbulent transport terms.
- $tt^1_{ki,j}$ Similarity profile for the two-point turbulent transfer terms.

Similarity scale for the two-point turbulent transfer terms. Tr_{u_i} Similarity scale for the single-point turbulent transport terms. Fluctuating velocity in the x_i direction u_i Kolmogorov velocity scale. u_k Mean velocity in the x_i direction U_i U_s^d Scale for difference in the mean velocity between two points. U_{∞} Mean free stream velocity in the wake. U_s Similarity scale for the U_1 . Coordinate system in physical variables. x_i Mean-flow direction. x_1 Cross-flow direction in the cartesian coordinate system. x_2 Radial direction in cylindrical coordinate system. Infinite homogeneous direction in cartesian coordinate system. x_3 Azimuthal direction in the cylindrical coordinate system.

xiv

 \tilde{x}_k separation coordinate in analysis of small-scale motions in the plane jet. average position of two points in analysis of small-scale motions. \hat{x}_k molecular diffusivity of a scalar. α Similarity scale for the two-point scalar correlation. χ δ Similarity length scale for the velocity field. δ_d Displacement thickness of the wake. δ_{θ} Similarity length scale for the scalar field. Rate of dissipation of turbulent kinetic energy per unit mass. ϵ Similarity coordinate in the x_2 direction. η Kolmogorov length scale. η_k separation distance in the x_3 direction for temporally evolving wake. γ similarity variable in the x_3 direction for the small scale motions in the plane jet. Taylor microscale of the $\overline{u_ju_k'}$ correlation in the i direction. λ_{jk}^{i}

λ^n	Eigenvalue of the proper orthogonal decomposition.
ν	kinematic viscosity.
ω_i	Vorticity vector.
π^1_j	Similarity profile of the two-point pressure-velocity correlation (spatially evolving flow).
π_{u_i}	Similarity profile for pressure-strain terms.
Π_j^1	Similarity scale for the two-point pressure-velocity correlation (spatially evolving flow).
Π_{u_i}	Similarity scale for pressure-strain terms.
Ψ	Orthogonal functions used in the proper orthogonal decomposition.
au	Separation distance in similarity time scale \tilde{t} for the temporally evolving wake.
θ	Momentum thickness of the velocity field in the wake.
	Fluctuating value of the passive scalar in the temporally evolving wake.
	Separation in the azimuthal coordinate for the cylindrical coordinate system.
Θ	Mean value of the scalar in the temporally evolving wake.
	xvi

- v Separation distance in the similarity coordinate in spatially evolving flows.
- ς Separation distance in the x_1 direction in physical variables.
- φ Similarity profile for the two-point scalar correlation.
- ξ Similarity coordinate in the x_1 direction.
- ζ Similarity variable in the x_3 direction.

Chapter 1

Introduction

The complex nature of turbulent flows seems to preclude the possibility of finding an analytical solution to its governing equations, even for an incompressible flow of a Newtonian, single component fluid in simple geometries, such as simple jets or wakes. Recent advances in computational capabilities, however, have allowed the simulation of some simple flows for all the relevant scales of motion. At present these simulations can only be carried out for moderate Reynolds numbers. Of course, as the computer technology advances the quality of the simulations will improve. Even so, these simulations, themselves, can only answer the question 'what happens?' and not 'why does it happen?'. In order to understand the 'why' it is necessary to construct simplified models of the turbulence that exhibit the features one suspects to be important.

The analysis of turbulence is complicated by the fact that the non-linear nature of the equations of motion amplifies any uncertainty in the initial and boundary conditions as the flow evolves, so eventually the instantaneous velocity at any point in the flow cannot be predicted with any certainty. Thus, it is conventional to average

the governing equations to generate a set of equations for statistical measures of the flow. These equations, unfortunately, do not form a closed set (c.f. Batchelor, 1953) so they cannot be solved without a closure model, which is essentially an assumption about how the flow evolves. Hence, it is useful to gain insight into how the turbulent flows evolve in order to construct better closure models.

One hypothesis, which has been examined extensively is that the turbulence in many free-shear flows asymptotically approaches an 'equilibrium' or 'similarity' state. In a similarity analysis it is hypothesized that a solution exists to the governing equations in which the statistical moments of the velocity can be written as the product of a scale that is dependent on the downstream position of the point and a similarity function that is dependent on the cross-stream position of the point normalized by a characteristic length scale. Hence, it is assumed that the profiles of the velocity moments have a similar shape at different downstream positions and, in fact, can be collapsed to a single profile. It can be shown that the governing equations for the single-point moments admit similarity solutions when the flow evolves such that all of the terms in the governing equation make the same relative contribution; i.e., the flow evolves such that the terms in the governing equations are in equilibrium. Of course, the similarity solution is at best an approximate model of an actual flow because it requires that the profiles at all streamwise positions in the flow collapse. This cannot be true for profiles near the origin of most (if not all) turbulent flows. Thus, the similarity solution is, at most, an asymptotic solution for the flow.

For non-homogeneous shear flows, the similarity analysis has traditionally only

been carried out for the equations which govern the evolution of the single-point moments; *i.e.*, moments where all of the variables are evaluated at a single point in space and time. A question to be resolved (eg., Townsend, 1956 or Bonnet et al., 1986) is whether the structure of the turbulence itself is in an 'equilibrium' or 'similarity' state when the flow evolves such that the single-point moments are in agreement with a similarity hypothesis. In other words, does the flow evolve such that the structures of the turbulence and the probability density functions describing their occurrence at one point in the flow are related to those at another point in the flow by a similarity transformation?

One technique which can be utilized to address this question is to demonstrate that equations that govern the evolution of more complex statistical moments, such as the two-point velocity correlation tensor, admit similarity solutions. It is important to note that the two-point velocity correlation tensor cannot be utilized to uniquely determine the structure of the turbulence. Thus, demonstrating that the governing equations for the two-point velocity correlation tensor admit similarity solutions does not imply that the turbulent structure is similar. However, it can be argued that the similarity hypothesis for the turbulent structure is consistent with the equations of motion, at least to the level of the two-point velocity correlation tensor.

1.1 Review of Similarity Analysis

Similarity analysis has been utilized extensively in laminar fluid dynamics and heat transfer (v. Batchelor 1967 and Burmeister 1983) since the early work on laminar

boundary layer theory carried out by Blasius (v. Batchelor, 1967). Similarity analysis can be utilized to transform one dependent variable from the differential equations governing the flow, thereby simplifying the mathematical description of the problem. Unlike laminar flows, the application of the similarity analysis to single-point equations in turbulent flows, by itself, cannot be used to elicit solutions because of the closure problem. However, the analysis is still useful because it offers insight into the evolution of these flows; i.e., that they evolve towards an 'equilibrium' state.

1.1.1 Single-Point Similarity Analysis

There are essentially two different approaches to find if the governing equations solutions for non-homogeneous free-shear flows admit similarity solutions. The traditional approach to the similarity analysis (c.f. Townsend, 1956 and Tennekes and Lumley, 1972) is to choose the similarity scales for all of the moments in the equations which are being analyzed. These scales are chosen by making a 'self-preservation' hypothesis, in which case it is assumed that the profiles of the statistical moment in the flow can be rescaled using a single length and velocity scale. For instance; the scales for Reynolds stresses are chosen equal to the square of the scale for the mean velocity profile. It is then determined if these hypothesized similarity solutions are consistent with the equations of motion. Further, in the traditional approach it is usually argued that the asymptotic similarity solution for each type of flow (such as all plane wakes) is universal or unique, independent of the initial (or source) conditions of the flow.

The second approach, suggested by George (1989), is to carry out the similarity analysis using arbitrary scales for all of the statistical moments in the transport equations. The allowable choices for these scales are then determined by examining the constraints that must be imposed so the transport equations admit similarity solutions. Consequently, the scales for all of the velocity moments are not necessarily powers of the scale used for the mean velocity. This second approach can yield the solutions derived using the traditional approach, and is thus more general. Further, in this second approach the equations of motion are used to determine whether the all flows of a certain type evolve to universal or unique similarity solution.

An example of the difference in the two approaches can be seen in the analysis of the spatially evolving plane wake flow (v. fig. 1.1). The experimental results of Wygnanski et al. (1986) demonstrate that the Reynolds stresses measured in the plane wake generated behind several different types of bodies do not collapse when they are scaled with the traditional similarity variables (nor were the spreading rates of the wakes the same) despite the fact that the mean velocity profile in the different wakes do collapse. These differences occurred in both the normal Reynolds stresses, in particular $\overline{u_1u_1}$, and the Reynolds shear-stress, $\overline{u_1u_2}$.

In the traditional approach to the similarity analysis (Townsend 1956), it is assumed that the governing equations admit similarity solutions where the mean velocity profile, U_1 , can be written as

$$U_{\infty} - U_1 = U_s(x_1) f(\eta), \tag{1.1}$$

while the similarity solution for the Reynolds stress, $\overline{u_1u_2}$, is chosen (arbitrarily) as

$$\overline{u_1 u_2} = U_s^2(x_1) g(\eta), \tag{1.2}$$

where

$$\eta = \frac{x_2}{\delta}.\tag{1.3}$$

Substituting the hypothesized similarity solutions into the first-order differential and mean momentum equations (Wygnanski *et al.* 1986) yields

$$[U_{\infty}U_{s}\delta] \int_{-\infty}^{\infty} f(\tilde{\eta})d\tilde{\eta} = M_{0}$$
(1.4)

and

$$-\frac{d\eta f(\eta)}{d\eta} = \left[\frac{2M_0}{U_\infty}\right] \left[\frac{d\delta^2}{dx_1}\right]^{-1} \left(\int_{-\infty}^{\infty} f(\tilde{\eta}) d\tilde{\eta}\right)^{-1} \frac{dg(\eta)}{d\eta},\tag{1.5}$$

where M_0 is the momentum deficit of the wake. Thus, the traditional similarity solutions are consistent with the mean momentum equation only when

$$\frac{d\delta^2}{dx_1} \propto const \tag{1.6}$$

Further, if the functional forms of the mean velocity and the Reynolds stress similarity profiles are to be independent of the wake generator, then so must be the growth rate of the wake. As Wygnanski et al. (1986) point out, the growth rates in the data they reported were not the same for all wakes. Thus, their results are either inconsistent with the hypothesis that all flows reach an universal equilibrium state or the experiments have not gone far enough to reach this state.

In contrast, following the approach suggested by George (1989) it is hypothesized that the mean momentum equations in the wake admit similarity solutions where the mean velocity profile is given by equation 1.1 and the Reynolds shear-stress is given by

$$\overline{u_1 u_2} = R_s(x_1) g(\eta). \tag{1.7}$$

In this case the differential mean momentum equation can be reduced to

$$-\frac{d\eta f(\eta)}{d\eta} = \frac{dg(\eta)}{d\eta} \tag{1.8}$$

when the scale for the Reynolds stress $\overline{u_1u_2}$ is chosen as

$$R_s = U_\infty U_s \frac{d\delta}{dx_1}. (1.9)$$

George illustrated that the similarity profiles for Reynolds shear-stress in wakes with different growth rates do collapse when this scale is utilized for the data reported by Wygnanski *et al.* (1986).

One key difference between this approach and the traditional approach is that the growth rate of the similarity length scale, δ , is not determined from the analysis of the mean momentum equation since the scale for the Reynolds stress is arbitrary at this point in the analysis. George (1989) suggested that the growth rate of the wake could be determined by examining the governing equation for the turbulent kinetic energy and using physical scaling arguments to choose the similarity scale for the rate of dissipation of turbulent kinetic energy. George found that this equation admits a similarity solution only when

$$\frac{d\delta^2}{dx_1} = const,\tag{1.10}$$

which is the same constraint derived from the traditional approach. In fact, on the surface, the similarity solution outlined by George (1989) is consistent with the similarity solution derived using the traditional approach except for one important difference. George found that the equation for the similarity profile of the turbulent kinetic energy is dependent on the growth rate of the wake. From this, George concluded that the functional forms of the similarity profiles for the normal stresses may

not be unique or independent of the source conditions. Such is, indeed, the case for the $\overline{u_1u_1}$ Reynolds stress measurements reported by Wygnanski *et al.* (1986). George did argue though that since the mean momentum equation is independent of this the growth rate factor when the Reynolds stress, $\overline{u_1u_2}$, is scaled as in equation 1.9 then the similarity solution of the properly scaled mean velocity and the Reynolds stress, $\overline{u_1u_2}$, should be independent of the source conditions, consistent with observations (George 1989).

Later analyses (George 1994 or Ewing and George 1994) demonstrated that the growth rate of the similarity length scale in several free-shear flows can be determined by applying the similarity analysis to the equations that govern the individual Reynolds stresses, $\overline{u_i u_j}$, without requiring physical scaling arguments for the rate of dissipation of the kinetic energy. In this case, the scale for the dissipation rate is a predicted outcome of the analysis. A comparison of the scale derived for the rate of dissipation using the similarity analysis and that derived from physical arguments led George (1994) to conclude that similarity solutions are only possible for constant-Reynolds-number, free-shear, flows or free-shear flows in the infinite-Reynolds-number limit.

In summary, the approach to similarity analysis suggested by George introduces two modifications of the traditional similarity analysis. Firstly, it uses the equations of motion to determine the appropriate choice for the similarity scales. This emphasizes one of the key physical characteristics of the similarity solution; namely that the equations governing the statistical moments evolve in an 'equilibrium' manner when the evolution of the flow is consistent with a similarity hypothesis (i.e., the ratios of

the terms in the equations are independent of the downstream position in the flow). The second idea introduced by George (1989) is the possibility that the similarity states of the turbulence may depend on the source conditions of the flow.¹ This dependence can occur in two different places in the solution: First, the appropriate scale for the statistical moments may be a function of the initial conditions. And second, the functional form of the similarity solutions may depend on the source conditions.

1.1.2 Similarity Analysis of Two-Point Information

Previously, there have been a few attempts to find two-point similarity solutions in turbulent flows. These include similarity analyses of decaying isotropic turbulence (e.g., von Karman and Howarth 1938, Batchelor 1948, Speziale and Bernard 1992, and George 1992), homogeneous shear flow (v. George and Gibson 1992), and the spatially evolving, axisymmetric jet (Ewing and George 1994). ²

For decaying isotropic turbulence, von Karmen and Howarth (1938) found that the governing equation for the two-point longitudinal correlation is given by

$$\frac{\partial F(r,t)}{\partial t} = \left(\frac{\partial}{\partial r} + \frac{4}{r}\right) K(r,t) + 2\nu \left(\frac{\partial^2}{\partial r^2} + \frac{4}{r}\frac{\partial}{\partial r}\right) F(r,t)$$
 (1.11)

(where F(r) and K(r) are $u^2f(r)$ and $u^3k(r)$ in the notation of von Karman and Howarth 1938). They then hypothesized that a similarity solution existed for this

¹It is important to note that the approach suggested by George does not exclude the possibility that all flows of a certain type settle into the same similarity state. It simply argues that the governing equations for each flow admit similarity solutions (of the hypothesized kind). These solutions may or may not all be the same.

²The similarity hypothesis for the small scale motion in an infinite Reynolds number turbulence proposed by Kolmogorov is considered separately.

equation where

$$F(r,t) = U_s^2 f(\eta) \tag{1.12}$$

and

$$K(r,t) = U_s^3 k(\eta). \tag{1.13}$$

Substituting these hypothesized solutions into equation 1.11, it is straightforward to demonstrate that this equation admits a similarity solution of this type only when

$$Re_{\delta} = \frac{U_s \delta}{\nu} = const.$$
 (1.14)

This condition is not normally satisfied in experimental measurements of decaying isotropic turbulence at finite Reynolds numbers. Batchelor (1948) carried out a similarity analysis of this problem in Fourier space and argued that a similarity solution could be found during the final period of decay when the nonlinear terms become negligible.

On the other hand, George (1992) argued that a similarity solution could exist for the full equation (at least during the early period of decay) if it is not assumed a priori that the scale for the turbulent transfer terms is U_s^3 . For example, if the hypothesized similarity solutions for equation 1.11 are given by

$$F(r,t) = \tilde{F}(t)\tilde{f}(\eta) \tag{1.15}$$

and

$$K(r,t) = \tilde{K}(t)\tilde{k}(\eta), \tag{1.16}$$

it is straightforward to demonstrate that the solutions are consistent with the equation 1.11 if

$$\frac{d\delta^2}{dt} \propto const \tag{1.17}$$

and

$$\tilde{K}(t) = \frac{\nu \tilde{F}}{\delta}.\tag{1.18}$$

It is conventional to define \tilde{F} such that

$$\tilde{F} = U_s^2, \tag{1.19}$$

where U_s^2 is the scale for the turbulent kinetic energy, in which case the scale for the turbulent transfer term can be written as

$$\tilde{K}(t) = \frac{U_s^3}{Re_{\delta}}. (1.20)$$

Thus, instead of requiring the Reynolds number to be constant, this approach has absorbed the Reynolds number dependence into the scale for the turbulent transfer terms.

It is important to note that this similarity solution is fundamentally different from the tradition solution, except for the special case where the Reynolds number is constant during the decay.³ In order to fully appreciate the difference between these two similarity solutions it is useful to examine the differences in the physical model which may have motivated the two approaches. Probably the simplest physical model that

³George (1989) argued that the similarity solution derived using the two methods are consistent in the limit of infinite Reynolds number since in this case the Reynolds number of the turbulence remains constant.

would lead to the traditional similarity solution is one in which the turbulent structures in the flow and the probability density functions that describe their occurrences at different points in the flow evolution are similar. That is, the turbulence at one time is simply bigger (or smaller) and less (or more) energetic than at another point in time, so the differences in the statistical measures be removed by normalizing the measures by a single length and velocity scale. Although this may not be the only type of flow that yields correlation functions consistent with the traditional similarity solution, it is a useful model to contrast to the similarity solution derived by George (1992). In that solution the skewness of the fluctuating velocity components and the skewness of the velocity derivatives (George, 1992) in physical variables vary inversely with the Reynolds number of the flow, based on the Taylor microscale, as the flow evolves. For example,

$$\frac{\overline{u_l^3}}{\overline{u_l^2}^{3/2}} = \lim_{r \to 0} \frac{K(r, t)}{F(r, t)^{3/2}} = \frac{1}{Re_\lambda} \frac{\tilde{k}(\eta)}{\tilde{f}(\eta)^{3/2}},\tag{1.21}$$

where u_l is the longitudinal velocity component and λ (the Taylor microscale) is the similarity length scale (George 1989). Thus, either the turbulence structures and/or the probability distribution function describing their occurrences (or more formally the probability distribution functions of the velocity field) are varying continuously as the flow evolves so that the velocity skewness and velocity derivative skewness vary continuously as the flow evolves. This model of the turbulent flow is significantly different from any self-preserving model which would produce statistical measures consistent with the traditional similarity solution. Thus, for decaying isotropic turbulence the more general similarity approach suggested by George leads to a solution which is significantly different from the solution generated using the traditional approach. Note, George also suggested (but could not prove) that the region of applicability of this solution was limited by an upper bound on the derivative skewness.

George and Gibson (1992) illustrated that an analogous similarity solution exists for homogeneous shear turbulence, although in this case the turbulent kinetic energy of the flow and the Reynolds number increase exponentially as the flow evolves, while the similarity length (the Taylor microscale) is a constant. In this solution, the scale for the turbulent transfer terms is again u^3/Re^{-1} . Hence, the discussion regarding the nature of George's similarity solution for isotropic turbulence is equally applicable to the similarity solution for this flow. However, George and Gibson (1992) argue there is no bound on the validity of the solution for this flow since the derivative skewness decreases as the energy and Reynolds number increase.

Although the similarity analyses outlined by George (1992) and George and Gibson (1992) are by no means universally accepted, the experimental evidence illustrated in both papers appears to be in agreement with the theories. Whether the theory is true or not, they do seem to make an important point. It may not be appropriate to simply assume a priori that all of the velocity moments in the turbulence scale as a simple power of a single velocity scale and are independent of Reynolds number, without recognizing the inherent limitations this assumption imposes on the evolution of the turbulent flow being considered.

1.1.3 Kolmogorov's Hypothesis

Kolmogorov (1941, 1963) outlined a series of similarity hypotheses about the nature of small-scale turbulence in the infinite-Reynolds-number limit. The essence of these

hypotheses is that probability density function for the small-scale motions is dependent only on two flow dependent parameters: the rate of dissipation of kinetic energy per unit mass and the viscosity of the fluid. Hence, the statistical measures of the small-scale turbulence are universal and can be characterized by a single length and velocity scale given by

$$\eta_k = \left(\frac{\nu^3}{\epsilon}\right)^{1/4} \tag{1.22}$$

and

$$u_k = (\nu \epsilon)^{1/4} \,. \tag{1.23}$$

Thus, Kolmogorov's hypotheses fall very much in line with the classical self-preservation ideas (or *vice versa*). Kolmogorov's hypotheses have been well documented elsewhere (v. Monin and Yaglom 1975 or Batchelor 1947), so the reader is referred to these sources for any further introduction.

It is important to note that Kolmogorov's hypotheses assume that the Reynolds number of the turbulence is very large and are only formally exact in the infinite Reynolds number limit (Batchelor, 1953). There are a significant number of spectral measurements that appear to be in agreement with the predictions of the theories (v. Monin and Yaglom, 1975), but careful experimental investigation of the higher-order moments and spectra, such as those carried out by Champagne (1978), illustrate that there is a residual Reynolds number dependence even for fairly large Reynolds number flows.

1.2 Objective of This Research

The objective of the present analysis is to determine whether the equations that govern the evolution of the two-point velocity correlation tensor in several turbulent free-shear flows admit to similarity solutions. Following the methodology outlined by George (1989), this is accomplished by hypothesizing that the relevant equations admit similarity solutions where the two-point velocity correlation tensor can be written as the product of a scale that indicates how the moment varies as the flow evolves and a similarity function. The scales for these similarity solutions are then determined by examining the governing equations.

The flows examined here fall in three categories: First, a constant-Reynolds-number, temporally developing flow. Second, a constant-Reynolds-number, spatially developing flow with a constant growth rate. Finally, a varying-Reynolds-number, spatially developing flow with a constant growth rate. The flows examined in each of these groups should be considered as representative flows, so the analyses applied to these flows can easily be extended to other flows that are in the same group. It is not possible to directly extend the similarity analysis of the two-point equations in spatially evolving flows with a constant growth rates to those with non-constant growth rates, as is the case for the temporally evolving flows. Spatially developing flows with a non-constant growth rates (eg., the spatially developing plane and axisymmetric wakes) will be considered in later analyses.

In the case of the temporally evolving wake, the equation that governs the twopoint scalar correlation is also examined for two different sets of initial/boundary conditions. The first is a two-stream mixing field in which the mean value of the

scalar differs on the two sides of the wake, while the second is a scalar field with a mean deficit or surplus in the wake.

The data from Direct Numerical Simulations of the temporally evolving wake computed by Moser and Rogers (1994) are also examined as a test of the two-point similarity hypothesis. It is, of course, not possible to simulate a flow that is infinite in extent in the homogeneous directions, so instead the wake in an infinite environment is modeled using the flow in a box with periodic boundary conditions these directions. It is argued that scales of motion which are somewhat smaller than the dimensions of the box should evolve like a flow in an infinite environment. Hence, it is not expected that the similarity solution for the infinite wake should be a good model for the largest motions in the box, but it should accurately describe the the moderate- and small-scale motions. Thus, the comparison of data and the predictions of the theory can be viewed as a test of both the two-point similarity hypothesis and the ability of the simulation to model a wake in an infinite environment. Agreement between the theory and the data adds credence to both the similarity hypothesis and to the idea that motions in the finite box evolve like those in an infinite environment (in the sense that they both evolve in a 'equilibrium' manner).

In all of these cases information from the single-point analysis is utilized to facilitate the analysis of the two-point equations, but this does not imply that the similarity solutions for the two-point moments follows from the single-point solutions. In fact, the opposite is true. When the equation that govern the two-point velocity correlation tensor admit similarity solutions, the Reynolds stresses can also be written in a similarity form since these moments are a special case of the two-point correlations.

Similarly, the two-point velocity correlation tensor is similar when the structure of the turbulence is similar, but the opposite is not necessarily be true.

Figure 1.1: Geometry of the spatially evolving plane wake

Chapter 2

A Constant-Reynolds-Number, Non-Homogeneous, Temporally Developing Flow: The Plane Wake

The temporally evolving wake flow illustrated in figure 2.1 is a non-homogeneous shear flow in which a momentum deficit, which is infinite in extent in two homogeneous directions, evolves in time. Although this flow is not a naturally occurring flow, it is useful in the sense that it is easier to carry out a Direct Numerical Simulation of this flow than its spatially evolving counterpart. The Direct Numerical Simulations approach also has an advantage over experimental investigation since it yields complete knowledge of the instantaneous field (at a somewhat lower Reynolds number), so these data bases can be utilized to test theoretical hypotheses about the turbulence. Thus, it is useful to query if the equations that govern the two-point velocity correlation in this flow admit similarity solutions.

The temporally developing plane wake can be thought of as a model of the spatially developing wake in the asymptotic small-deficit limit. Therefore, although the spatially developing wake is not considered here, it is useful first to briefly review the literature for the spatially developing wake.

2.1 Review of Spatially Evolving Wake Literature

There has been a great deal of interest in the spatially evolving wake flow because it appears in many engineering applications. The studies this flow can be separated into three groups defined by the regions of the wake examined. These are: the near-wake region, $0 \le x/d \le 10$; the intermediate-wake region, $10 \le x/d \le 60$; and the far-wake region, x/d > 250. These studies have included investigations of both the Reynolds averaged statistics and the large-scale coherent structures in the turbulent flow.

Many of the recent investigations in the near and intermediate regions of the wake have been primarily interested in the dynamics of the large-scale structures in these regions. For example, in an investigation of the near-wake region behind a circular cylinder, Cantwell and Coles (1983) found a periodic turbulent structure that closely resembled a Karman vortex street. This organized structure contained approximately half of the turbulent stresses in the near-wake region. In addition, they found that the turbulent production and the entrainment of the non-vortical fluid in this region was closely related to the saddle points that occurred in the these structures. Investigations in the intermediate wake (v. Hayakawa and Hussain 1989 or Zhou and Antonia 1993) found a similar vortical structure in this region of the wake, though

¹The definitions do vary but these are nominally the defining values.

21

Hayakawa and Hussain (1989) noted a significant amount of three dimensionality existed in the spanwise structures of the intermediate wake. They concluded that this three dimensionality was primarily due to kinking of the spanwise vortices producing horseshoe vortices that were inclined relative to the cross-stream coordinate direction.

There have also been numerous studies in the far-wake region (which are of primary interest here). The earlier work on the spatially evolving wake including the classical similarity analysis of the single-point, Reynolds-averaged equations documented by Townsend (1956). The first two-point velocity correlations measurements in the far field of the wake led investigators (v. Grant 1958 and Townsend 1970) to conclude that a double-roller eddy structure existed in the far field of the wake. This structure consisted of two parallel vortical motions of opposite sign inclined forward relative to the non-homogeneous cross-stream direction in the far field of the wake. Grant (1958) reported that the correlation of the velocity component u_1 was positive when the probes were situated on opposite sides of the layer. This led Grant to conclude that the double-roller eddy structure was symmetric about the centerline of the wake and it occurred on both side of the wake simultaneously. Payne and Lumley (1967) found a similar structure in the far wake by applying the proper orthogonal decomposition technique (v. Lumley 1970) to the correlation measurements reported by Grant (1958). In order to investigate whether these types of structures actually exist in the far field of the wake, Mumford (1983) applied a pattern recognition technique to the instantaneous measured velocity field utilizing patterns analogous to those identified by Grant and Townsend. Mumford did find evidence of the existence of double roller structures in the far wake, although the structures were predominantly confined to a single side of the wake unlike the model suggested by Grant (1958).

22

Bonnet et al. (1986) also carried out measurements of the two-point velocity correlation tensor in a turbulent wake behind a flat plate. They found that the correlation of the u_1 component was negative when the probes were on opposite sides of the wake, in contrast to the results reported by Grant (1958). They also noted that the correlation of the u_1 component in the homogeneous spanwise direction was always positive in their measurements, also in contrast to the correlation reported by Grant (1958), which had several zero crossings over the same separation distance. Consequently, Bonnet et al. argued that the double-roller eddy structure proposed by Grant (1958) did not describe the structure in their flow. Bonnet et al. attributed the differences in the measurements to the fact that the boundary layers on their plate were turbulent before they left the end of the plate, while the previous investigations including Grant's, were carried out behind a body that had laminar boundary layers. They argued that the transition which occurs in the wake behind a body with laminar boundary layers would create different structures than those that occur in a wake when two independent turbulent boundary layers are joined at the back of a body, such as a plate. This hypothesis was supported by a recent experimental investigation of the wake behind a plate with both laminar and turbulent boundary layers reported by Weygandt and Metha (1993). They found significantly more three dimensionality in the time-averaged velocity field measured in near and intermediate regions of a wake behind a flat plate with laminar boundary layers compared to the wake formed behind the same plate with a boundary layers that are tripped to be turbulent. Weygandt and Metha also reported that this three dimensionality appears to influence the turbulence measurements in the far wake, although the time-averaged velocity field is two dimensional in this region. Parsad and Williamson (1993,1993)

23

also noted that the structure of the turbulence in the far wake could be related to the turbulence in the near wake and the vortex shedding from the cylinder, although their observations were in wakes of somewhat lower Reynolds number. In addition, they noted that the transitional flow in the wake was highly sensitive to external disturbances and these disturbances influenced the state of the turbulence in the far wake.

Of course, the difference between the measurements reported by Bonnet *et al.* and Grant may also be due to the fact that the bodies which produced the wakes were different (*i.e.*, a cylinder versus a flat plate). The measurement of the far behind different wake generators reported by Wygnanski *et al.* (1986) demonstrate that even the cross-stream distribution of the single-point moments depended on the type of body that produced the wake, in agreement with the results of the similarity hypothesis outlined by George (1989). Thus, it is not difficult to imagine that the coherent structures in the wakes may also differ.

The plane wake literature also contains evidence that supports the general hypothesis that the turbulent structure (or at least the two-point correlation tensor) in this flow may be similar. Grant (1958) illustrated that the correlation of the streamwise component u_1 in spanwise direction at two different locations downstream of the cylinder collapsed in similarity variables. In addition, Wygnanski *et al.* showed that the shape of the spectra at different downstream positions in the wake collapsed when the frequency was scaled by similarity-type variables. They did not scale the magnitude of the spectra though, so a complete collapse of the data was not achieved. In both cases these occurrences were commented on, but no attempt was made to

demonstrate that this type of similarity solution was consistent with the governing equations. It is this question that will be addressed here for the temporally evolving plane wake (an approximate model of the asymptotic far field of the spatially evolving wake, v. Moser and Rogers 1994).

2.2 Flow Geometry

The temporally evolving wake is non-homogeneous in one direction, x_2 , and homogeneous in two directions, x_1 and x_3 , which includes the mean flow direction, x_1 (v. fig. 2.2). One consequence of the homogeneity in the mean flow direction is that the mean convection terms in the Reynolds-averaged, single-point equations (that dominate the spatially developing wake) are zero. Their role is, in part, picked up by the unsteady terms, which are non-zero in this flow (and zero in the single-point equations for the stationary, spatially developing flow). Another consequence of the homogeneity is that the mean cross-stream velocity component (i.e., U_2) is zero so that the spread of the temporally evolving wake occurs only through turbulent (and molecular) diffusion, in contrast to the spatially developing wake, which has a small but finite entrainment velocity in the direction normal to the wake centerline.

The temporally developing wake also differs from the spatially evolving wake in that different integral constraints are satisfied for the two flows. In the temporally evolving wake the mass and momentum deficits of the wake are conserved. Thus, both the displacement thickness of the wake, δ_d , given by

$$\delta_d = \frac{+ \int_{-\infty}^{\infty} (U_{\infty} - U_1) dx_2}{U_{\infty} - U_{cl}(t_o)},$$
(2.1)

where U_{∞} is the mean free-stream velocity and $U_{cl}(t_o)$ is the centerline velocity at the initial time, and the momentum thickness of the layer, θ , given by

$$\theta = \frac{+\int_{-\infty}^{\infty} U_{\infty}(U_{\infty} - U_1)dx_2}{U_{\infty}^2}$$
(2.2)

are constant as the wake evolves. In the case where the initial centerline velocity is zero, the displacement thickness of the temporally evolving wake is equal to the momentum thickness of the wake. In the spatially evolving wake the momentum thickness is constant as the flow evolves, but the displacement thickness is not. The displacement thickness of the spatially developing wake is only a constant in the limit of zero velocity deficit (c.f. Wygnanski et al., 1986).

2.3 Similarity of the Single-Point Moments

It is conventional (c.f. Tennekes and Lumley 1972) to examine whether the governing equations for the single-point moments admit similarity solutions for high- (or formally infinite-) Reynolds-number flows. That is, it is assumed that the molecular diffusion terms are negligible relative to the turbulent diffusion or transport terms. For example, in the mean momentum equation given by

$$\frac{\partial U_1}{\partial t} = -\frac{\partial \overline{u_1 u_2}}{\partial x_2} + \nu \frac{\partial^2 U_1}{\partial x_2^2},\tag{2.3}$$

where ν is the kinematic viscosity, this assumption implies that the viscous stresses are negligible compared to the turbulent Reynolds stresses (Tennekes and Lumley, 1972).

These assumptions can also be used to simplify the equation for the Reynolds stress components given by

$$\frac{\partial \overline{u_i u_j}}{\partial t} = \frac{\overline{p} \left(\frac{\partial u_i}{\partial x_j} + \frac{\partial u_j}{\partial x_i} \right)}{\overline{p} \left(\frac{\partial u_i}{\partial x_k} + \frac{\partial u_j}{\partial x_k} \right)} - \nu \left[\frac{\overline{\partial u_i}}{\partial x_k} \frac{\partial u_j}{\partial x_k} - \frac{\overline{\partial u_k}}{\partial x_i} \frac{\partial u_k}{\partial x_j} \right]
- \frac{\partial}{\partial x_2} \left(\overline{u_2 u_i u_j} + \frac{\overline{p} u_i}{\rho} \delta_{j2} + \frac{\overline{p} u_j}{\rho} \delta_{i2} - 2\nu \left\{ u_i e_{j2} + u_j e_{i2} \right\} \right)
- \overline{u_j u_2} \frac{\partial U_1}{\partial x_2} \delta_{i1} - \overline{u_i u_2} \frac{\partial U_1}{\partial x_2} \delta_{j1} - 4\nu \overline{e_{ik} e_{jk}}, \tag{2.4}$$

where e_{ik} is the fluctuating rate of strain tensor. In this case, the standard high-Reynolds-number assumption includes neglecting the viscous transport terms relative to the turbulent transport terms. It is also normally assumed that the small-scale motions in the flow are 'locally' isotropic, in which case the dissipations of the Reynolds stresses other than the normal stresses are zero and the viscous redistribution terms given by

$$-\nu \left[\frac{\partial u_i}{\partial x_k} \frac{\partial u_j}{\partial x_k} - \frac{\partial u_k}{\partial x_i} \frac{\partial u_k}{\partial x_j} \right]$$
 (2.5)

are zero.

As it will be shown later, it is possible to find a similarity solution without making these assumptions for both the velocity and scalar field, but to do this formally it is necessary to examine the equations that govern the two-point correlations in order to gain enough information to evaluate the velocity gradient terms in equation 2.4.

2.3.1 Analysis of the Velocity Field

The similarity analysis of the temporally evolving flow differs from that of the spatially evolving flow in that the length scales and velocity scales utilized in the analysis

are functions of time instead of the streamwise coordinate. Thus, the objective of the single-point similarity analysis is to determine if the governing equations allow solutions that are the product of a time-dependent scale and a similarity function.

Utilizing the standard high-Reynolds-number assumption, the mean-momentum equation (in deficit form) can be written as

$$\frac{\partial (U_{\infty} - U_1)}{\partial t} = +\frac{\partial \overline{u_1 u_2}}{\partial x_2} \tag{2.6}$$

Equation 2.6 can be integrated across the layer to yield an integral constraint for this flow given by

$$\frac{\partial}{\partial t} \int_{-\infty}^{\infty} (U_{\infty} - U_1) dx_2 = + \left. \overline{u_1 u_2} \right|_{-\infty}^{\infty} \tag{2.7}$$

Thus, if the free stream turbulence is negligible, the mass deficit and the momentum deficit in the temporally wake are conserved; *i.e.*,

$$\int_{-\infty}^{\infty} (U_{\infty} - U_1) dx_2 = \frac{M_0}{U_{\infty}}$$
(2.8)

where M_0 is the momentum deficit of the wake.

It is hypothesized that the mean momentum equations (eqn. 2.6 and 2.8) admit similarity solutions in which the mean velocity profile and the Reynolds stress $\overline{u_1u_2}$ are given by

$$U_{\infty} - U_1(x_2, t) = U_s(t) f(\eta)$$
 (2.9)

and

$$\overline{u_1 u_2}(x_2, t) = R_s(t)g(\eta), \tag{2.10}$$

where the similarity coordinate, η , is given by

$$\eta = \frac{x_2}{\delta(t)}. (2.11)$$

Following George (1989), individual scales have been chosen for each of the moments to avoid over-constraining the analysis. In particular, it has not been assumed a priori that the scale for the Reynolds stress $\overline{u_1u_2}$ is U_s^2 .

Substituting the hypothesized similarity solutions into equations 2.6 and 2.8 yields

$$\left[\frac{dU_s}{dt}\right]f - \left[\frac{U_s}{\delta}\frac{d\delta}{dt}\right]\eta\frac{df}{d\eta} = \left[\frac{R_s}{\delta}\right]\frac{dg}{d\eta}$$
(2.12)

and

$$[U_s \delta] \int_{-\infty}^{\infty} f(\tilde{\eta}) d\tilde{\eta} = \left[\frac{M_o}{U_{\infty}} \right]. \tag{2.13}$$

The time-dependent portion of each term in equations 2.12 and 2.13 is contained in square brackets (a convention which will be utilized throughout this analysis).

Mathematically, the mean momentum equations admit similarity solutions if it is possible to remove the explicit time dependence from equations 2.12 and 2.13. Thus, the hypothesized similarity solutions are consistent with the equations if the terms in square brackets are proportional; *i.e.*,

$$[U_s \delta] \propto \left[\frac{M_o}{U_\infty} \right] \tag{2.14}$$

and

$$\left[\frac{dU_s}{dt}\right] \propto \left[\frac{U_s}{\delta} \frac{d\delta}{dt}\right] \propto \left[\frac{R_s}{\delta}\right]. \tag{2.15}$$

Physically, this implies a solution exists to the mean momentum equation where all of the terms in this equation make the same relative contribution as the flow evolves.

It is straightforward to demonstrate that the constraints in equations 2.14 and

2.15 are satisfied when

$$U_s \propto \frac{M_o}{U_\infty \delta} \tag{2.16}$$

and

$$R_s \propto U_s \frac{d\delta}{dt}.$$
 (2.17)

At this point the growth rate of the layer is not yet determined because the scale for the Reynolds stress $\overline{u_1u_2}$ is not yet defined. However, the constraint in equation 2.16 implies that the Reynolds number of this flow based on the similarity variables must be a constant; *i.e.*,

$$Re = \frac{U_s \delta}{\nu} = const. \tag{2.18}$$

It will be shown later that this is an important constraint in the analysis of the twopoint equations.

Following the methodology outlined by George (1994), the growth rate of the layer can be determined by extending the similarity analysis to the equations that govern the individual Reynolds stresses. For example, using the standard high-Reynolds-number assumptions the equation for the Reynolds stresses $\overline{u_1u_1}$ is given by

$$\frac{\partial \overline{u_1^2}}{\partial t} = 2 \frac{\overline{p} \frac{\partial u_1}{\partial x_1}}{\rho \frac{\partial u_1}{\partial x_1}} - 2 \overline{u_1 u_2} \frac{\partial U_1}{\partial x_2} - \frac{\partial}{\partial x_2} \left(\overline{u_1^2 u_2} \right) - \epsilon_{u_1 u_1}, \tag{2.19}$$

where p is the fluctuating pressure, ρ is the density, and $\epsilon_{u_1u_1}$ is given by

$$\epsilon_{u_1 u_1} = 4\nu \overline{e_{1k} e_{1k}}.\tag{2.20}$$

It is hypothesized that a similarity solution exists for this equation where the new moments in equation 2.19 are given by

$$\overline{u_1^2} = K_{u_1}(t)k_{u_1}(\eta), \tag{2.21}$$

$$\frac{\overline{p}\,\partial u_1}{\rho\,\partial x_1} = \Pi_{u_1}(t)\pi_{u_1}(\eta),\tag{2.22}$$

$$\overline{u_1^2 u_2} = Tr_{u_1}(t) tr_{u_1}(\eta), \tag{2.23}$$

and

$$\epsilon_{u_1 u_1} = D_{u_1}(t) d_{u_1}(\eta). \tag{2.24}$$

The solutions for the other moments in this equation have already been defined.

Substituting these solutions into equation 2.19 yields

$$\left[\frac{dK_{u_1}}{dt}\right] k_{u_1} - \left[\frac{K_{u_1}}{\delta} \frac{d\delta}{dt}\right] \eta \frac{dk_{u_1}}{d\eta} = 2 \left[\Pi_{u_1}\right] \pi_{u_1} + 2 \left[\frac{R_s U_s}{\delta}\right] g \frac{df}{d\eta} - \left[\frac{T r_{u_1}}{\delta}\right] \frac{dt r_{u_1}}{d\eta} - \left[D_{u_1}\right] d_{u_1}, \tag{2.25}$$

where again the time-dependent portion of each term is contained in square brackets.

It is evident that equation 2.19 admits a similarity solution (of the hypothesized kind) when

$$\left[\frac{dK_{u_1}}{dt}\right] \propto \left[\frac{K_{u_1}}{\delta} \frac{d\delta}{dt}\right] \propto \left[\Pi_{u_1}\right] \propto \left[\frac{R_s U_s}{\delta}\right] \propto \left[\frac{T r_{u_1}}{\delta}\right] \propto \left[D_{u_1}\right]. \tag{2.26}$$

These constraints are only satisfied if the scale for the normal stress $\overline{u_1u_1}$ is chosen such that

$$K_{u_1} \propto U_s^2, \tag{2.27}$$

the scale for the transport terms is given by

$$Tr_{u_1} \propto U_s^2 \frac{d\delta}{dt},$$
 (2.28)

and the scales for the pressure-strain term and the dissipation term are chosen such that

$$\Pi_{u_1} \propto D_{u_1} \propto \frac{U_s^2}{\delta} \frac{d\delta}{dt}.$$
 (2.29)

The similarity analysis can also be extended the equations for the other Reynolds stresses $(\overline{u_2u_2}, \overline{u_3u_3}, \text{ and } \overline{u_1u_2})$ in a high-Reynolds-number wake. These are given by

$$\frac{\partial \overline{u_2^2}}{\partial t} = 2 \frac{\overline{p} \frac{\partial u_2}{\partial x_2}}{\rho \frac{\partial u_2}{\partial x_2}} - \frac{\partial}{\partial x_2} \left(\overline{u_2^3} + 2 \frac{\overline{pu_2}}{\rho} \right) - \epsilon_{u_2 u_2}, \tag{2.30}$$

$$\frac{\partial \overline{u_3^2}}{\partial t} = 2 \frac{\overline{p}}{\rho} \frac{\partial u_3}{\partial x_3} - \frac{\partial \overline{u_2 u_3^2}}{\partial x_2} - \epsilon_{u_3 u_3}, \tag{2.31}$$

and

$$\frac{\partial \overline{u_1 u_2}}{\partial t} = \frac{\overline{p} \left(\frac{\partial u_1}{\partial x_2} + \frac{\partial u_2}{\partial x_1} \right)}{\rho} - \frac{\partial}{\partial x_2} \left(\overline{u_1 u_2^2} + \frac{\overline{p u_1}}{\rho} \right) - \overline{u_2^2} \frac{\partial U}{\partial y}. \tag{2.32}$$

In addition, for an incompressible flow, the pressure-strain terms in the normal stress equations must satisfy

$$\frac{\overline{p}\frac{\partial u_1}{\rho \partial x_1} + \overline{p}\frac{\partial u_2}{\rho \partial x_2} + \overline{p}\frac{\partial u_3}{\rho \partial x_3} = 0$$
 (2.33)

so the pressure-strain terms act to redistribute the turbulent kinetic energy amongst the normal stresses.

Following the same approach as for the $\overline{u_1u_1}$ equation, it is hypothesized that the equations that govern the other Reynolds stresses admit similarity solutions where the solutions for the new single-point moments are given by

$$\overline{u_2^2} = K_{u_2}(t)k_{u_2}(\eta), \tag{2.34}$$

$$\overline{u_3^2} = K_{u_3}(t)k_{u_3}(\eta), \tag{2.35}$$

$$\frac{\overline{p}}{\rho} \frac{\partial u_2}{\partial x_2} = \Pi_{u_2}(t) \pi_{u_2}(\eta), \tag{2.36}$$

$$\frac{\overline{p}\,\overline{\partial u_3}}{\rho\,\overline{\partial x_3}} = \Pi_{u_3}(t)\pi_{u_3}(\eta),\tag{2.37}$$

$$\frac{\overline{p}\left(\frac{\partial u_1}{\partial x_2} + \frac{\partial u_2}{\partial x_1}\right)}{\overline{p}\left(\frac{\partial u_1}{\partial x_2} + \frac{\partial u_2}{\partial x_1}\right)} = \Pi_{u_1 u_2}(t)\pi_{u_1 u_2}(\eta), \tag{2.38}$$

$$\left(\overline{u_2^3} + 2\frac{\overline{pu_2}}{\rho}\right) = Tr_{u_2}(t)tr_{u_2}(\eta), \tag{2.39}$$

$$\overline{u_2 u_3^2} = Tr_{u_3}(t) tr_{u_3}(\eta), \tag{2.40}$$

$$\left(\overline{u_1 u_2^2} + \frac{\overline{pu_1}}{\rho}\right) = Tr_{u_1 u_2}(t) tr_{u_1 u_2}(\eta), \tag{2.41}$$

$$\epsilon_{u_2 u_2} = D_{u_2}(t) d_{u_2}(\eta), \tag{2.42}$$

and

$$\epsilon_{u_3 u_3} = D_{u_3}(t) d_{u_3}(\eta). \tag{2.43}$$

Substituting these solutions into equations 2.30 - 2.32, it can be shown these equations admit similarity solutions when

$$\left[\frac{dK_{u_2}}{dt}\right] \propto \left[\frac{K_{u_2}}{\delta} \frac{d\delta}{dt}\right] \propto \left[\Pi_{u_2}\right] \propto \left[\frac{Tr_{u_2}}{\delta}\right] \propto \left[D_{u_2}\right],\tag{2.44}$$

$$\left[\frac{dK_{u_3}}{dt}\right] \propto \left[\frac{K_{u_3}}{\delta} \frac{d\delta}{dt}\right] \propto \left[\Pi_{u_3}\right] \propto \left[\frac{Tr_{u_3}}{\delta}\right] \propto \left[D_{u_3}\right],\tag{2.45}$$

and

$$\left[\frac{dR_s}{dt}\right] \propto \left[\frac{R_s}{\delta} \frac{d\delta}{dt}\right] \propto \left[\Pi_{u_1 u_2}\right] \propto \left[\frac{Tr_{u_1 u_2}}{\delta}\right] \propto \left[\frac{K_{u_2} U_s}{\delta}\right] \propto \left[D_{u_1 u_2}\right].$$
(2.46)

In addition, substituting the solutions for the pressure-strain terms into equation 2.33 yields

$$[\Pi_{u_1}] \pi_{u_1} + [\Pi_{u_2}] \pi_{u_2} + [\Pi_{u_3}] \pi_{u_3} = 0. \tag{2.47}$$

This equation admits a similarity solution if the flux of energy leaving the $\overline{u_1^2}$ equation through the pressure-strain term is proportional to the flux entering the other two equations through the pressure-strain terms; *i.e.*,

$$[\Pi_{u_1}] \propto [\Pi_{u_2}] \propto [\Pi_{u_3}]. \tag{2.48}$$

Hence,

$$\frac{K_{u_1}}{\delta} \frac{d\delta}{dt} \propto \Pi_{u_1} \propto \frac{K_{u_2}}{\delta} \frac{d\delta}{dt} \propto \Pi_{u_2} \propto \frac{K_{u_3}}{\delta} \frac{d\delta}{dt} \propto \Pi_{u_3}. \tag{2.49}$$

Therefore, the single-point equations only admit similarity solution when

$$K_{u_1} \propto K_{u_2} \propto K_{u_3} \propto U_s^2. \tag{2.50}$$

The equation for the Reynolds stress $\overline{u_1u_2}$ can be utilized to determine the growth rate of the similarity length scale since this equation admits a similarity solution only when

$$\frac{R_s}{\delta} \frac{d\delta}{dt} \propto \frac{K_{u_2} U_s}{\delta} \tag{2.51}$$

Substituting equations 2.50 and 2.15 into this equation yields

$$\left(\frac{d\delta}{dt}\right)^2 \propto U_s^2 \propto \frac{1}{\delta^2}.\tag{2.52}$$

Therefore, the equations for the Reynolds stresses admit similarity solutions (of the hypothesized kind) when

$$\frac{d\delta^2}{dt} \propto const \tag{2.53}$$

or,

$$\delta \propto (t - t_0)^{1/2},\tag{2.54}$$

where t_0 is the virtual origin of the wake.

Once the scales for the Reynolds stresses have been determined, the scales for the other moments in the governing equations for the Reynolds stresses can be determined from equations 2.44, 2.45, and 2.46; *i.e.*,

$$Tr_{u_2} \propto U_s^2 \frac{d\delta}{dt},$$
 (2.55)

$$\Pi_{u_2} \propto D_{u_2} \propto \frac{U_s^2}{\delta} \frac{d\delta}{dt},$$
 (2.56)

$$Tr_{u_3} \propto U_s^2 \frac{d\delta}{dt},$$
 (2.57)

$$\Pi_{u_3} \propto D_{u_3} \propto \frac{U_s^2}{\delta} \frac{d\delta}{dt},$$
(2.58)

$$Tr_{u_1u_2} \propto U_s \left(\frac{d\delta}{dt}\right)^2,$$
 (2.59)

and

$$\Pi_{u_1 u_2} \propto D_{u_1 u_2} \propto \frac{U_s}{\delta} \left(\frac{d\delta}{dt}\right)^2.$$
 (2.60)

When interpreting these results it is useful to recall that

$$U_s \propto \frac{d\delta}{dt} \tag{2.61}$$

in this flow. Consequently, in the temporally evolving wake the similarity scale for all of the Reynolds stresses are proportional to each other. The is also true for the turbulent transport terms, the pressure strain terms, and the dissipation terms. However, the constants of proportionality for the members in each group may differ for different wakes (e.g. forced or unforced) due to the persistence of initial (or source) conditions.

The similarity scales for the single-point moments outlined above are consistent with the equations of motion, but there does not appear to be an unique choice for the scales that will make the resulting similarity equations independent of flow parameters. For example, if the scales for the moments are chosen such that

$$K_{u_1} = K_{u_2} = K_{u_3} = U_s^2 (2.62)$$

and

$$R_s = U_s \frac{d\delta}{dt},\tag{2.63}$$

while the constants of proportionality in equations 2.27-2.29 and 2.55 - 2.60 are taken to be unity, then it follows mean momentum equations reduce to

$$\int_{-\infty}^{\infty} f(\tilde{\eta})d\tilde{\eta} = \frac{M_0}{U_{\infty}U_s\delta}$$
 (2.64)

and

$$-\frac{d\eta f}{d\eta} = \frac{dg}{d\eta} \tag{2.65}$$

or,

$$g(\eta) = -\eta f(\eta) + \eta f(\eta)|_{\eta = \infty}. \tag{2.66}$$

The equations for the similarity profiles of the higher-order moments are given by

$$-2k_{u_1} - \eta \frac{dk_{u_1}}{d\eta} = 2\pi_{u_1} + 2g\frac{df}{d\eta} - \frac{dtr_{u_1}}{d\eta} - d_{u_1}, \qquad (2.67)$$

$$-2k_{u_2} - \eta \frac{dk_{u_2}}{d\eta} = 2\pi_{u_2} - \frac{dtr_{u_2}}{d\eta} - d_{u_2}, \tag{2.68}$$

$$-2k_{u_3} - \eta \frac{dk_{u_3}}{d\eta} = 2\pi_{u_3} - \frac{dtr_{u_3}}{d\eta} - d_{u_3}, \tag{2.69}$$

$$-2g - \eta \frac{dg}{d\eta} = \pi_{u_1 u_2} - \frac{dt r_{u_1 u_2}}{d\eta} + \left[\frac{1}{k_2^2}\right] k_v \frac{df}{d\eta} - d_{u_1 u_2}, \tag{2.70}$$

and

$$\pi_{u_1} + \pi_{u_2} + \pi_{u_3} = 0, (2.71)$$

where the parameter k_2 is given by

$$k_2 = \frac{1}{U_s} \frac{d\delta}{dt} = \frac{U_\infty}{2M_o} \frac{d\delta^2}{dt} \int_{-\infty}^{\infty} f(\tilde{\eta}) d\tilde{\eta}.$$
 (2.72)

This constant depends on both the initial mass deficit of the wake and the growth rate of the square of the wake thickness. At this point it may appear that the length and the velocity scales are free parameters that can be chosen to ensure that the value of this constant, k_2 , is the same for all flows (in which can one might argue that the resulting equation set may yield universal profiles). This is not true. If one wishes to argue that the profiles are universal, it is necessary to choose the length scale, δ , and the velocity scale, U_s , so that the mean velocity profile from different wakes collapse. If the constant k_2 is not the same for this choice of velocity and length scales, then the solutions from the equation set are dependent on the source conditions of the wake. It should be noted that the scale for the pressure-strain terms and the dissipation terms have been chosen such that this equation set reduces to this simplified form. Although the scales for these terms must be chosen proportional to the scales outlined here, the constant of proportionality for these terms may also depend on the source conditions of the wake. Thus, these terms may include an additional dependence on the source conditions that can not be deduced from the single-point analysis.

The location of the term k_2 in the set of equations is not unique. A different choice for the scales would have placed the constant in a different location in the set of equations. It is also important to note that the equations for the similarity profiles

form a coupled set of equations. Thus, the value of the constant k_2 will in general influence the solution to all of the equations unless it can be demonstrated that the equation set can be decoupled. Of course, this influence may be more significant for some of the similarity profiles than for others. It is evident from equation 2.66 that the similarity profile for the mean velocity and that for the Reynolds stress $\overline{u_1u_2}$ will be similarly affected since they can be related algebraically to each other. Hence, if the mean velocity profile is universal (as is the case for the spatially developing wake Wygnanski et al., 1986), then the profile for the Reynolds stress $\overline{u_1u_2}$ will also be universal when the scale defined in equation 2.63 is used to normalize the profiles (as it does in the spatially-evolving wake, v. George, 1989). However, the universality of the mean velocity and the Reynolds stress $\overline{u_1u_2}$ similarity profiles is an allowable outcome of the governing equations (if the profiles are properly scaled) not a predicted outcome of the similarity analysis.

2.4 Analysis of the Two-Point Correlations

2.4.1 The Two-Point Velocity Correlation Tensor

Applying a similarity hypothesis to the single-point moments is useful because it describes the evolution of the moments which are often of most interest in engineering problems. However, to gain more insight into the structure of the turbulence in the flow it is necessary to examine more complex statistical measures, such as the two-point velocity correlation tensor. The information in the two-point velocity correlation tensor is, of course, not sufficient to uniquely determine the structure of the turbulence in the flow, but it does provide some information about it. Thus,

it is useful to examine whether the equations of motion that govern the two-point velocity correlation tensor admit similarity solutions in order to demonstrate that the hypothesis that a similarity solution exists for the turbulent structure is consistent with the equations of motion up to the two-point equations.

In the temporally evolving wake, the governing equations for the correlation of the velocity at two arbitrary points in space and at the same point in time (v. Hinze, 1975) can be reduced to

$$\frac{\partial \overline{u_{i}u'_{j}}}{\partial t} + (U_{1} - U'_{1}) \frac{\partial \overline{u_{i}u'_{j}}}{\partial \varsigma} =$$

$$-\frac{1}{\rho} \left[\frac{\partial}{\partial \varsigma} \left(\overline{pu'_{j}} \delta_{i1} - \overline{p'u_{i}} \delta_{j1} \right) + \frac{\partial \overline{pu'_{j}}}{\partial x_{2}} \delta_{i2} + \frac{\partial \overline{p'u_{i}}}{\partial x'_{2}} \delta_{j2} + \frac{\partial}{\partial \gamma} \left(\overline{pu'_{j}} \delta_{i3} - \overline{p'u_{i}} \delta_{j3} \right) \right]$$

$$-\frac{\partial}{\partial \varsigma} \left(\overline{u_{1}u_{i}u'_{j}} - \overline{u'_{1}u_{i}u'_{j}} \right) - \frac{\partial \overline{u_{2}u_{i}u'_{j}}}{\partial x_{2}} - \frac{\partial \overline{u'_{2}u_{i}u'_{j}}}{\partial x'_{2}} - \frac{\partial}{\partial \gamma} \left(\overline{u_{3}u_{i}u'_{j}} - \overline{u'_{3}u_{i}u'_{j}} \right)$$

$$-\overline{u'_{j}u_{2}} \frac{\partial U_{1}}{\partial x_{2}} \delta_{i1} - \overline{u_{i}u'_{2}} \frac{\partial U'_{1}}{\partial x'_{2}} \delta_{j1} + \nu \left(2 \frac{\partial^{2}}{\partial \varsigma^{2}} + \frac{\partial^{2}}{\partial x'_{2}} + 2 \frac{\partial^{2}}{\partial x'_{2}} + 2 \frac{\partial^{2}}{\partial \gamma^{2}} \right) \overline{u_{i}u'_{j}}$$
(2.73)

where

$$\varsigma = x_1 - x_1' \tag{2.74}$$

and

$$\gamma = x_3 - x_3'. (2.75)$$

The primed variables in equations 2.73-2.75 are evaluated at an arbitrary point in the wake, while the unprimed variables are evaluated at a second point.

Following the methodology suggested by George (1989), it is hypothesized that similarity solutions exist for these equations where the two-point correlations can be written as the product of a time dependent scale and a function dependent on similarity variables; *i.e.*,

$$\overline{u_i(x_1, x_2, x_3, t)u_j'(x_1', x_2', x_3', t)} = Q^{i,j}(t)q_{i,j}(\xi, \eta, \eta', \zeta, *), \tag{2.76}$$

$$\overline{p(x_1, x_2, x_3, t)u_i'(x_1', x_2', x_3', t)} = P_1^{,j}(t)p_{,i}^1(\xi, \eta, \eta', \zeta, *), \tag{2.77}$$

$$\overline{p'(x_1', x_2', x_3', t)u_i(x_1, x_2, x_3, t)} = P_2^{i,}(t)p_{i,}^2(\xi, \eta, \eta', \zeta, *), \tag{2.78}$$

$$\overline{u_k u_i u_j'} = T_1^{ki,j}(t) t t_{ki,j}^1(\xi, \eta, \eta', \zeta, *), \tag{2.79}$$

and

$$\overline{u_i u_k' u_j'} = T_2^{i,jk}(t) t t_{i,jk}^2(\xi, \eta, \eta', \zeta, *), \tag{2.80}$$

where

$$\xi = \frac{\zeta}{\delta_1(t)} = \frac{x_1 - x_1'}{\delta_1(t)},\tag{2.81}$$

$$\eta = \frac{x_2}{\delta(t)}, \ \eta' = \frac{x_2'}{\delta(t)}, \tag{2.82}$$

and

$$\zeta = \frac{\gamma}{\delta_3(t)} = \frac{x_3 - x_3'}{\delta_3(t)}. (2.83)$$

The length scales used to define the similarity variables in the x_1 - and x_3 -directions in equations 2.81 and 2.83 are arbitrary at this point. The length scale used for the x_2 -direction is chosen equal to the to the length scale used in the single-point similarity analysis since the solutions for the two-point correlations and the single-point moments must be consistent in the limit when the separation distance between the points is zero. The star is included in the definition of the similarity solution to indicate that the functional form of these solutions may depend on the initial conditions (or source conditions) of the wake, such as the Reynolds number or type of boundary layers which initiate the flow.

The allowable choices for the scales in the hypothesized similarity solutions and the length scales in the definition of the similarity variables are determined by examining the governing equations. Substituting equations 2.76 - 2.80 and the hypothesized similarity solution for the mean flow given in equation 2.9 into equation 2.73 yields

$$\begin{bmatrix}
\frac{dQ^{i,j}}{dt}
\end{bmatrix} q_{i,j} - \begin{bmatrix}
\frac{Q^{i,j}}{\delta_1} \frac{d\delta_1}{dt}
\end{bmatrix} \xi \frac{\partial q_{i,j}}{\partial \xi} - \begin{bmatrix}
\frac{Q^{i,j}}{\delta} \frac{d\delta}{dt}
\end{bmatrix} \left(\eta \frac{\partial}{\partial \eta} + \eta' \frac{\partial}{\partial \eta'}\right) q_{i,j} - \begin{bmatrix}
\frac{Q^{i,j}}{\delta_3} \frac{d\delta_3}{dt}
\end{bmatrix} \zeta \frac{\partial q_{i,j}}{\partial \zeta} + \begin{bmatrix}
\frac{U_s(t)Q^{i,j}}{\delta_1}
\end{bmatrix} \{f(\eta') - f(\eta)\} \frac{\partial q_{i,j}}{\partial \xi} = -\frac{1}{\rho} \left(\begin{bmatrix}
\frac{P_1^{i,j}}{\delta_1}
\end{bmatrix} \frac{\partial P_{,j}^{i,j}}{\partial \xi} \delta_{i1} - \begin{bmatrix}
\frac{P_2^{i,j}}{\delta_1}
\end{bmatrix} \frac{\partial P_{i,j}^{2}}{\partial \xi} \delta_{j1} + \begin{bmatrix}
\frac{P_1^{i,j}}{\delta}
\end{bmatrix} \frac{\partial p_{,j}^{1}}{\partial \zeta} \delta_{i2} + \begin{bmatrix}
\frac{P_2^{i,j}}{\delta}
\end{bmatrix} \frac{\partial p_{i,j}^{2}}{\partial \zeta} \delta_{j2} + \begin{bmatrix}
\frac{P_1^{i,j}}{\delta_3}
\end{bmatrix} \frac{\partial p_{,j}^{1}}{\partial \zeta} \delta_{i3} - \begin{bmatrix}
\frac{P_2^{i,j}}{\delta_3}
\end{bmatrix} \frac{\partial p_{i,j}^{2}}{\partial \zeta} \delta_{j3} \right) - \begin{bmatrix}
\frac{T_1^{i,j,j}}{\delta_1}
\end{bmatrix} \frac{\partial tt_{1,j}^{1,j}}{\partial \xi} + \begin{bmatrix}
\frac{T_2^{i,1j}}{\delta_1}
\end{bmatrix} \frac{\partial tt_{i,1j}^{2,j}}{\partial \xi} - \begin{bmatrix}
\frac{T_1^{2i,j}}{\delta}
\end{bmatrix} \frac{\partial tt_{2i,j}^{1,j}}{\partial \eta} - \begin{bmatrix}
\frac{T_2^{i,2j}}{\delta}
\end{bmatrix} \frac{\partial tt_{2i,2j}^{2,j}}{\partial \eta'} - \begin{bmatrix}
\frac{T_1^{3i,j}}{\delta}
\end{bmatrix} \frac{\partial tt_{3i,j}^{2,j}}{\partial \zeta} + \begin{bmatrix}
\frac{T_2^{i,3j}}{\delta_3}
\end{bmatrix} \frac{\partial tt_{3i,j}^{2,j}}{\partial \zeta} + \begin{bmatrix}\frac{T_2^{i,3j}}{\delta_3}
\end{bmatrix} \frac{\partial t$$

The time-dependent portion of each term in equation 2.84 is contained in square brackets.

The equations admit similarity solutions if the time dependent portions of all of the terms in equation 2.84 are proportional; *i.e.*,

$$\begin{bmatrix} \frac{dQ^{i,j}}{dt} \end{bmatrix} \propto \begin{bmatrix} \frac{Q^{i,j}}{\delta_1} \frac{d\delta_1}{dt} \end{bmatrix} \propto \begin{bmatrix} \frac{Q^{i,j}}{\delta} \frac{d\delta}{dt} \end{bmatrix} \propto \begin{bmatrix} \frac{Q^{i,j}}{\delta_3} \frac{d\delta_3}{dt} \end{bmatrix} \propto \begin{bmatrix} \frac{U_s Q^{i,j}}{\delta} \end{bmatrix}$$

$$\propto \begin{bmatrix} \frac{P_1^{i,j}}{\delta_1} \end{bmatrix} \delta_{i1} \propto \begin{bmatrix} \frac{P_2^{i,j}}{\delta_1} \end{bmatrix} \delta_{j1} \propto \begin{bmatrix} \frac{P_1^{i,j}}{\delta} \end{bmatrix} \delta_{i2} \propto \begin{bmatrix} \frac{P_2^{i,j}}{\delta} \end{bmatrix} \delta_{j2} \propto \begin{bmatrix} \frac{P_1^{i,j}}{\delta_3} \end{bmatrix} \delta_{i3} \propto \begin{bmatrix} \frac{P_2^{i,j}}{\delta_3} \end{bmatrix} \delta_{j3}$$

$$\propto \begin{bmatrix} \frac{T_1^{1i,j}}{\delta_1} \end{bmatrix} \propto \begin{bmatrix} \frac{T_2^{i,1j}}{\delta_1} \end{bmatrix} \propto \begin{bmatrix} \frac{T_2^{2i,j}}{\delta} \end{bmatrix} \propto \begin{bmatrix} \frac{T_2^{2i,j}}{\delta} \end{bmatrix} \propto \begin{bmatrix} \frac{T_2^{3i,j}}{\delta_3} \end{bmatrix} \propto \begin{bmatrix} \frac{T_2^{3i,j}}{\delta_3} \end{bmatrix}$$

$$\propto \left\lceil \frac{Q^{2,j}U_s}{\delta} \right\rceil \delta_{i1} \propto \left\lceil \frac{Q^{i,2}U_s}{\delta} \right\rceil \delta_{j1} \propto \left\lceil \nu \frac{Q^{i,j}}{\delta_1^2} \right\rceil \propto \left\lceil \nu \frac{Q^{i,j}}{\delta^2} \right\rceil \propto \left\lceil \nu \frac{Q^{i,j}}{\delta_3^2} \right\rceil, \tag{2.85}$$

which, again, implies that all of the terms in the governing equations make the same relative contribution as the wake evolves.

For a finite-Reynolds-number flow, the viscous terms in equation 2.85 are only proportional if the three length scales are proportional; *i.e.*,

$$\delta_1^2 \propto \delta^2 \propto \delta_3^2 \propto (t - t_0). \tag{2.86}$$

It is important to note that this also implies that the virtual origin of the three length scales must occur at the same point.

In addition, the convective terms in equation 2.85 evolve in 'equilibrium' with the viscous terms only if

$$\left[\frac{U_s Q^{i,j}}{\delta} \right] \propto \left[\nu \frac{Q^{i,j}}{\delta^2} \right].$$
(2.87)

Therefore, the equations only admit similarity solutions when the Reynolds number of the flow, based on similarity variables, is a constant; *i.e.*,

$$\frac{U_s \delta}{\nu} \propto const, \tag{2.88}$$

which is the same as the constraint derived in the single-point similarity analysis. In the context of the two-point correlation tensor this constraint also has an important physical interpretation. In the definition of the similarity solution for the two-point correlations, the similarity coordinates were defined using a single length scale that was independent of the separation distance between the points. Thus, it was implicitly assumed that all of the relevant length scales in the flow grow in proportional as the flow evolves, an assumption that is appropriate for a constant-Reynolds-number

flow.

Since the similarity solution for the two-point velocity correlation tensor must be consistent with the solution for the single-point moments, it follows that the scale for the two-point velocity correlation tensor must satisfy

$$Q^{i,j} \propto U_s^2(t). \tag{2.89}$$

Of course, the constants of proportionality in equation 2.89 may differ for the different members of the correlation tensor and different initial (or source) conditions.

In addition, the scales for the other two-point correlations must satisfy

$$P_2^{i,} \propto P_2^{,j} \propto U_s^3 \tag{2.90}$$

and

$$T_1^{ki,j} \propto T_2^{i,kj} \propto Q^{i,j} U_s, \tag{2.91}$$

where again the constants of proportionality in these equations may also differ for the different components of each vector or tensor. (These scales are also consistent with those determined in the single-point analysis.)

Thus, the equations that govern the evolution of the two-point correlation tensor admit similarity solutions when the scales for the two-point correlations are consistent with the constraints outlined in equations 2.89, 2.90, and 2.91. For example, if the length scales for the three coordinate directions are chosen to be equal and the scales for the two-point correlations are defined to be

$$Q^{i,j} = U_s(t)^{b(i,j)} \frac{d\delta^{2-b(i,j)}}{dt},$$
(2.92)

$$T_1^{ki,j} = T_2^{i,kj} = Q^{i,j}U_s, (2.93)$$

and

$$P_2^{i,} = P_2^{,j} = U_s^3 (2.94)$$

(where b(i, j) is an exponent to allow for the fact that the scale for $\overline{u_1u_2}$ is dependent on the growth rate), then equations governing the similarity solutions for the twopoint correlations are given by

$$-k_{2}\left(2q_{i,j}+\left[\xi\frac{\partial}{\partial\xi}+\eta\frac{\partial}{\partial\eta}+\eta'\frac{\partial}{\partial\eta'}+\zeta\frac{\partial}{\partial\zeta}\right]q_{i,j}\right)+\left[f(\eta')-f(\eta)\right]\frac{\partial q_{i,j}}{\partial\xi}=$$

$$-\frac{1}{\rho}k_{2}^{[b(i,j)-2]}\left[\frac{\partial}{\partial\xi}\left(p_{,j}^{1}\delta_{i1}-p_{i,}^{2}\delta_{j1}\right)+\frac{\partial p_{,j}^{1}}{\partial\eta}\delta_{i2}+\frac{\partial p_{i,}^{2}}{\partial\eta'}\delta_{j2}++\frac{\partial}{\partial\zeta}\left(p_{,j}^{1}\delta_{i3}-p_{i,}^{2}\delta_{j3}\right)\right]$$

$$-\frac{\partial}{\partial\xi}\left(tt_{i1,j}^{1}-tt_{i,1j}^{2}\right)-\frac{\partial tt_{2i,j}^{1}}{\partial\eta}-\frac{\partial tt_{i,2j}^{2}}{\partial\eta'}-\frac{\partial}{\partial\zeta}\left(tt_{i3,j}^{1}-tt_{i,3j}^{2}\right)$$

$$-k_{2}^{b(1,j)-b(2,j)}q_{2,j}\frac{df}{d\eta}\delta_{i1}-k_{2}^{b(i,1)-b(i,2)}q_{i,2}\frac{df}{d\eta'}\delta_{j1}$$

$$-\left[\frac{1}{Re_{\delta}}\right]\left(2\frac{\partial^{2}}{\partial\xi^{2}}-\frac{\partial^{2}}{\partial\eta^{2}}-\frac{\partial^{2}}{\partial\eta'^{2}}+2\frac{\partial^{2}}{\partial\zeta^{2}}\right)q_{i,j},$$

$$(2.95)$$

where

$$k_2 = \left[\frac{\delta}{U_s}\right] \left[\frac{1}{\delta} \frac{d\delta}{dt}\right] = \left[\frac{U_\infty}{2M_o} \frac{d\delta^2}{dt} \int_{-\infty}^{\infty} f(\eta) d\eta\right]$$
(2.96)

The equations for the similarity profiles are dependent on two constants which may vary from flow to flow, Re_{δ} and k_2 . It is expected that the similarity solution for the full two-point correlation tensor is a function of Reynolds number, since the ratio of the characteristic length scales of the energy containing range and the dissipation range increases as the Reynolds number increases (v. Batchelor 1953). Consequently, the functional form of the similarity profiles for the correlation functions that are valid for all separation distances must vary as a function of the Reynolds number. The second constant, k_2 , is the same that occurred in the equations for the similarity

profiles of the single-point moments. This constant is the ratio of the scales for the time-dependent terms and the scales for the convective terms in the transport equations for the two-point correlation tensor. Thus, k_2 can be interpreted as the ratio of the mean convective time scale and a time scale which characterizes the spreading rate of the wake in the non-homogeneous direction.

2.4.2 Pressure-Velocity Correlation

It is well known that the equation governing the static pressure field in an incompressible fluid can be written as (c.f. Batchelor 1967)

$$\frac{1}{\rho} \nabla^2 \tilde{p} = -\frac{\partial \tilde{u}_k}{\partial x_l} \frac{\partial \tilde{u}_l}{\partial x_k},\tag{2.97}$$

where ∇^2 is the Laplacian operator and \tilde{u}_k and \tilde{p} are the instantaneous velocity vector and pressure. For free-shear flows, this equation can be integrated to yield (v. Batchelor, 1967)

$$\tilde{p} = -\frac{1}{4\pi} \int \frac{\partial \tilde{u}_k''}{\partial x_l''} \frac{\partial \tilde{u}_l''}{\partial x_k''} \frac{dx_1'' dx_2'' dx_3''}{[(x_m'' - x_m)(x_m'' - x_m)]^{1/2}},$$
(2.98)

where x_m'' is a dummy variable of integration.

Thus, the instantaneous fluctuating pressure, given by

$$\frac{p}{\rho} = \frac{\tilde{p}}{\rho} - \frac{\tilde{p}}{\rho},\tag{2.99}$$

can be written as

$$\frac{p}{\rho} = -\frac{1}{4\pi} \int \left[\frac{\partial U_k''}{\partial x_l''} \frac{\partial u_l''}{\partial x_k''} + \frac{\partial U_l''}{\partial x_k''} \frac{\partial u_k''}{\partial x_l''} \right] \frac{dx_1'' dx_2'' dx_3''}{[(x_m'' - x_m)(x_m'' - x_m)]^{1/2}}$$

$$-\frac{1}{4\pi} \int \frac{\partial^2}{\partial x_k'' \partial x_l''} \left[u_k'' u_l'' - \overline{u_k'' u_l''} \right] \frac{dx_1'' dx_2'' dx_3''}{\left[(x_m'' - x_m)(x_m'' - x_m) \right]^{1/2}} . \tag{2.100}$$

The equation for the two-point pressure-velocity correlation, $\overline{pu'_j}$, can be obtained by multiplying equation 2.100 by u'_j and averaging. Substituting the hypothesized similarity solutions for the mean velocity, the two-point velocity correlation, and the turbulent transfer terms into the resulting equation yields

$$\frac{\overline{pu_{j}'}}{\rho} = -\left[\frac{[U_{s}(t)Q^{2,j}]}{4\pi}\right] \left\{2\int \frac{\partial f(\eta'')}{\partial \eta''} \frac{\partial q_{2,j}(\xi'' + \xi, \eta'', \eta', \zeta'' + \zeta)}{\partial \xi''} \frac{d\xi''d\eta''d\zeta''}{\left[\xi''^{2} + (\eta'' - \eta)^{2} + \zeta''^{2}\right]^{1/2}} - \left[\frac{T_{1}^{kl,j}}{U_{s}Q^{2,j}}\right] \int \left[\delta_{k1}\frac{\partial}{\partial \xi''} + \delta_{k2}\frac{\partial}{\partial \eta''} + \delta_{k3}\frac{\partial}{\partial \zeta''}\right] \left[\delta_{l1}\frac{\partial}{\partial \xi''} + \delta_{l2}\frac{\partial}{\partial \eta''} + \delta_{l3}\frac{\partial}{\partial \zeta''}\right] t_{kl,j}(\xi'' + \xi, \eta'', \eta', \zeta'' + \zeta) \frac{d\xi''d\eta''d\zeta''}{\left[\xi''^{2} + (\eta'' - \eta)^{2} + \zeta''^{2}\right]^{1/2}} \right\},$$
(2.101)

where

$$\xi'' = \frac{x_1'' - x_1}{\delta},\tag{2.102}$$

$$\eta'' = \frac{x_2''}{\delta},\tag{2.103}$$

and

$$\zeta'' = \frac{x_3'' - x_3}{\delta}. (2.104)$$

Note, the term

$$\frac{T_1^{kl,j}}{U_s Q^{2,j}} \tag{2.105}$$

is independent of time, but it may be a function of the source conditions of the wake. Thus, the similarity profile of the pressure-velocity correlation (and hence the single-point pressure-strain terms) may implicitly depend on the source conditions of the flow.

This solution for the pressure-velocity correlation is consistent the solution obtained in the analysis of the governing equations for the two-point correlation tensor. This is an useful result, but it is expected since the equation for the instantaneous pressure is derived from the momentum equation and continuity equations.

2.4.3 Other Statistical Measures of The Flow

When a similarity solution exists for the two-point velocity correlation tensor, it is reasonable to expect that similarity solutions should exist for other statistical moments which can be determined from it. One set of moments that are of particular interest are the two-point velocity-gradient correlations since these moments can be used to determine the vorticity correlations and the rate of dissipation of turbulent kinetic energy per unit mass.

The two-point velocity gradient moments can, in general, be related to the twopoint velocity correlation tensor by

$$\frac{\overline{\partial u_i}}{\partial x_k} \frac{\partial u_j'}{\partial x_l'} = \frac{\partial^2 \overline{u_i u_j'}}{\partial x_k \partial x_l'}.$$
 (2.106)

It is straightforward to demonstrate that the two-point velocity-gradient correlations can be written in a similarity form when the two-point velocity correlation tensor has a similarity form; *i.e.*,

$$\frac{\overline{\partial u_i}}{\partial x_k} \frac{\partial u'_j}{\partial x'_l} \propto \left[\frac{Q^{i,j}}{\delta^2} \right] g_{i,k;j,l}(\xi, \eta, \eta', \zeta)$$
(2.107)

where $g_{i,k,j,l}$ is the similarity function for the two-point velocity gradient correlation tensor.

Using equation 2.107, the two-point vorticity correlation tensor can be written as

$$\overline{\omega_i \omega_l'} = \epsilon_{ijk} \epsilon_{lmn} \overline{\frac{\partial u_k}{\partial x_j} \frac{\partial u_n'}{\partial x_m'}} = \left[\frac{Q^{i,l}}{\delta^2} \right] h_{i,l}(\xi, \eta, \eta', \zeta, *)$$
(2.108)

where ϵ_{ijk} is the alternating unit tensor. In this case, it follows that the single point vorticity correlation tensor given by

$$\overline{\omega_i \omega_l} = \epsilon_{ijk} \epsilon_{lmn} \frac{\overline{\partial u_k}}{\partial x_j} \frac{\partial u_n}{\partial x_m} = \lim_{x_m' \to x_j} \epsilon_{ijk} \epsilon_{lmn} \frac{\overline{\partial u_k}}{\partial x_j} \frac{\partial u_n'}{\partial x_m'}, \tag{2.109}$$

can also be written in a similarity form given by

$$\overline{\omega_i \omega_l} = \epsilon_{ijk} \epsilon_{lmn} \frac{\overline{\partial u_k}}{\partial x_j} \frac{\partial u_n}{\partial x_m} = \left[\frac{Q^{i,l}}{\delta^2} \right] w_{i,l}(\eta, *)$$
 (2.110)

where $w_{i,l}$ is equal to $h_{i,l}$ in the limit of zero separation distance.

Analogously, the correlation of the fluctuating rate-of-strain tensor at two points in the flow given by (Batchelor 1953)

$$\overline{e_{ij}e'_{km}} = \frac{1}{4} \overline{\left(\frac{\partial u_i}{\partial x_j} + \frac{\partial u_j}{\partial x_i}\right) \left(\frac{\partial u'_k}{\partial x'_m} + \frac{\partial u'_m}{\partial x'_k}\right)}$$
(2.111)

can be written as

$$\overline{\left(\frac{\partial u_i}{\partial x_j} + \frac{\partial u_j}{\partial x_i}\right) \left(\frac{\partial u_k'}{\partial x_m'} + \frac{\partial u_m'}{\partial x_k'}\right)} \propto \left[\frac{Q^{i,j}}{\delta^2}\right] b_{ij,km}(\xi, \eta, \eta', \zeta, *)$$
(2.112)

Therefore, when the equations governing the evolution of the two-point velocity correlation tensor admit similarity solutions, the dissipation of turbulent kinetic

energy per unit mass given by

$$\epsilon = \lim_{x_k \to x_k'} 2\nu \overline{e_{ij}} e'_{ij} \tag{2.113}$$

can be written as

$$\epsilon = \left[\frac{\nu U_s^2}{\delta^2}\right] d(\eta, *) \tag{2.114}$$

This similarity solution is consistent with that obtained in the single-point analysis. This is expected, since the single-point equations are a subset of the more general equations which govern the two-point correlations. Hence, the equations governing the single-point Reynolds stresses must admit similarity solutions when the more general two-point equations do.

2.4.4 One-Dimensional Spectra Of the Velocity Field

The information in the turbulent field can be represented using one-dimensional spectra, which are Fourier transforms of the two-point velocity correlation tensor in the x_1 - and x_3 -directions. These representations of the turbulence contain the same information about the flow as the two-point velocity correlation tensor, since they are a Fourier transform pair. Consequently, the one-dimensional spectra of the turbulence should have a similarity solution when the two-point velocity correlation tensor has a similarity solution.

For example, the Fourier transform of the two point velocity correlation tensor in the x_1 direction (in the sense of generalized functions, v. Lumley 1970), F_{ij}^1 , is given by

$$F_{i,j}^{1}(k_{1}, x_{2}, x_{2}', \gamma) = \frac{1}{2\pi} \int_{-\infty}^{\infty} R_{i,j}(\varsigma, x_{2}, x_{2}', \gamma) e^{-ik_{1}\varsigma} d\varsigma, \qquad (2.115)$$

where $R_{i,j}$ is the two-point velocity correlation tensor and ς is the separation distance in the x_1 direction. Substituting the hypothesized similarity solution for $R_{i,j}$ (equation 2.76) into equation 2.115 and transforming yields

$$F_{i,j}^{1}(k_{1}, x_{2}, x_{2}, \gamma) = [Q_{i,j}\delta] \frac{1}{2\pi} \int_{-\infty}^{\infty} q_{i,j}(\xi, \eta, \eta', \zeta) e^{-i\tilde{k}_{1}\xi} d\xi, \qquad (2.116)$$

where \tilde{k}_1 , the similarity wavenumber, is the given by

$$\tilde{k}_1 = k_1 \delta. \tag{2.117}$$

Therefore, when the two-point velocity correlation tensor has a similarity solution, the one-dimensional spectral tensor $F_{i,j}^1$ can be written in a similarity form given by

$$F_{i,j}^{1}(k_{1}, x_{2}, x_{2}', \gamma) = [Q_{i,j}\delta] \tilde{F}_{i,j}^{1}(\tilde{k}_{1}, \eta, \eta', \zeta).$$
(2.118)

Similarly, when the two-point velocity correlation has a similarity solution, the Fourier transform in the x_3 -direction, $F_{i,j}^3$, given by

$$F_{i,j}^{3}(k_{1}, x_{2}, x_{2}', \gamma) = \frac{1}{2\pi} \int_{-\infty}^{\infty} R_{i,j}(\varsigma, x_{2}, x_{2}', \gamma) e^{-ik_{3}\gamma} d\gamma$$
 (2.119)

can be written as

$$F_{i,j}^{3}(\zeta, x_{2}, x_{2}', k_{3}) = [Q_{i,j}\delta] \frac{1}{2\pi} \int_{-\infty}^{\infty} q_{i,j}(\xi, \eta, \eta', \zeta) e^{-i\tilde{k}_{3}\zeta} d\zeta$$
$$= [Q^{i,j}\delta] \tilde{F}_{i,j}^{3}(\xi, \eta, \eta', \tilde{k}_{3}), \qquad (2.120)$$

where

$$\tilde{k}_3 = k_3 \delta. \tag{2.121}$$

This can be extended to the Fourier transform of any arbitrary two-point correlation that has a similarity solution. In general, the scale for the one-dimensional transform is simply the product of the scale for the two-point correlation and the length scale δ .

The similarity solutions for the one-dimensional spectra (eqn. 2.116 and 2.119) illustrate one of the interesting consequences of the two-point similarity hypothesis. The scaled one-dimensional spectra from different times in the evolution of the wake collapse when the one-dimensional spectra are written as a function of the similarity wavenumber \tilde{k}_1 or \tilde{k}_3 . Thus, the spectra in physical wavenumbers, k_1 or k_3 , must continuously shift to lower wavenumbers as the wake evolves in time. For example, if a peak occurs in the one-dimensional spectrum in similarity variables at \tilde{k}_1 , then this feature will occur at a decreasing value of k_1 (larger scale motion) as the flow evolves, since the shape of the spectrum in similarity variables is not a function of time.

2.5 Length and Velocity Scales

In the analysis of the equations that govern the two-point correlation tensor (v. section 2.4.1), it was argued that all of the physical length and velocity scales grow in proportion as the flow evolves. Using the information outlined in the previous sections, this assumption can be examined in detail; in particular, the integral length scales, the Taylor microscales, and the Kolmogorov length and velocity scales can be determined. It can easily be argued that the velocity scale for the energy containing eddies must be proportional to the velocity scale U_s from the similarity analysis of

the single-point Reynolds stress equations in section 2.3.1.

The integral scale of the turbulence is given by

$$L_{\alpha,\beta}^{k} = \frac{1}{\overline{u_{\alpha}u_{\beta}}} \int_{0}^{\infty} R_{\alpha,\beta}(x_{m}, x_{m}') dx_{k}, \qquad (2.122)$$

where

$$x_m = x_m' \qquad m \neq k . \tag{2.123}$$

Substituting the hypothesized similarity solution for the two-point velocity correlation tensor into the equation for the integral scale in the x_1 -direction yields

$$L^{1}_{\alpha,\beta} = [\delta] \frac{1}{k_{\alpha,\beta}(\eta)} \int_{0}^{\infty} q_{\alpha,\beta}(\xi,\eta,\eta,0) d\xi$$
 (2.124)

where $k_{\alpha,\beta}$ is the similarity solution for the single-point moment (which is equal to $q_{\alpha,\beta}$ in the limit of zero separation). Similarly, the integral length scale in the x_3 -direction can be written as

$$L_{\alpha,\beta}^{3} = [\delta] \frac{1}{k_{\alpha,\beta}} \int_{0}^{\infty} q_{\alpha,\beta}(0,\eta,\eta',\zeta) d\zeta$$
 (2.125)

and finally the integral scale in the x_2 -direction can be written as

$$L_{\alpha,\beta}^{2} = [\delta] \frac{1}{k_{\alpha,\beta}} \int_{0}^{\infty} q_{\alpha,\beta}(0,\eta,\eta',0) d(\eta'-\eta), \qquad (2.126)$$

The Taylor microscale of the turbulence can also be written in terms of the twopoint velocity correlation tensor; i.e.,

$$(\lambda_{\alpha,\beta}^k)^2 = -2\overline{u_\alpha u_\beta} \left(\frac{\partial^2 R_{\alpha,\beta}}{\partial x_k^2} \Big|_{x_k = x_k'} \right)^{-1}$$
(2.127)

Using the similarity solutions for the one-dimensional spectra in equations 2.118 and 2.120, the Taylor microscale in the x_1 - and x_3 -directions can be written as

$$\lambda_{\alpha,\beta}^{1} = [\delta] \left(-2 \frac{\int_{-\infty}^{\infty} \tilde{F}_{\alpha,\beta}^{1} d\tilde{k}}{\int_{-\infty}^{\infty} \tilde{k}_{1}^{2} \tilde{F}_{\alpha,\beta}^{1} d\tilde{k}} \right)^{1/2}$$

$$(2.128)$$

and

$$\lambda_{\alpha,\beta}^{3} = [\delta] \left(-2 \frac{\int_{-\infty}^{\infty} \tilde{F}_{\alpha,\beta}^{3} d\tilde{k}}{\int_{-\infty}^{\infty} \tilde{k}_{3}^{2} \tilde{F}_{\alpha,\beta}^{3} d\tilde{k}} \right)^{1/2}. \tag{2.129}$$

Further, substituting the similarity solution for the two point velocity correlation tensor (eq. 2.76) into equation 2.127, the Taylor microscales in the x_2 -direction can be written as

$$\lambda_{\alpha,\beta}^{2} = [\delta] \left(\frac{-2}{k_{\alpha,\beta}(\eta)} \left. \frac{\partial^{2} q_{\alpha,\beta}}{\partial \eta^{2}} \right|_{\eta=\eta'}^{-1} \right)^{1/2}$$
(2.130)

Finally, using the similarity solution for rate of dissipation of the kinetic energy per unit mass reported in equation 2.114, it is straightforward to demonstrate that the Kolmogorov length and velocity scale, η_k and u_k , given by

$$\eta_k = \left(\frac{\nu^3}{\epsilon}\right)^{1/4} \tag{2.131}$$

and

$$u_k = (\epsilon \nu)^{1/4} \tag{2.132}$$

grow in proportion to the similarity length and velocity scales; i.e.,

$$\eta_k \propto \epsilon^{-1/4} \propto (t-t)^{1/2} \propto \delta$$
 (2.133)

and

$$u_k \propto \epsilon^{1/4} \propto (t-t)^{-1/2} \propto U_s. \tag{2.134}$$

Therefore, when a similarity solution exists for the two-point velocity correlation tensor in this (constant-Reynolds-number) flow, the integral scales, the Taylor microscales, and the Kolmogorov length scale all grow in proportion to the similarity length scale δ , while the Kolmogorov velocity scale grows in proportion with U_s , the similarity velocity scale. The virtual origins of these length and velocity scales must, of course, all occur at the same location in the flow as the similarity length and velocity scale in order for them to be proportional.

2.6 Comparison of Theory to Data

The analysis outlined in the previous sections demonstrated that the two-point similarity hypothesis, if realized in practice/experiments, has significant implications for the statistical measurements in a temporally evolving wake; in particular, the one-dimensional velocity spectra of the turbulence (or the correlation tensor) and the length scales associated with the turbulence. In this section, the data bases from Direct Numerical Simulations of temporally evolving wakes, computed by Moser and Rogers (1994), are examined to determine if the simulated wakes evolve in a manner consistent with the two-point similarity hypothesis.

2.6.1 Simulations

The objective of the simulations was to model the evolution of temporally evolving wakes in an infinite environment which is statistically homogeneous in the x_1 - and

 x_3 - directions. It is, of course, not possible to carry out a simulation of a wake that is infinite in extent, so it was necessary to approximate this flow by a flow in a box that was periodic in the homogeneous directions. The length of the box in the x_1 - and x_3 -directions is $50\delta_d$ and $12.5\delta_d$ respectively (where δ_d is the displacement thickness eqn. 2.1). Only those scales of the turbulence that are 'much' smaller than the length of the box in these directions should be an effective model in an infinite environment. Of course, one of the important questions in these simulations is how much is 'much'. One reasonable technique to address this question is to compare the statistical measures of the wake with those one might expect to find in an infinite wake. In this sense the two-point similarity hypothesis is useful because it provides predictions for the possible functional form of the statistics in an infinite wake. Hence, the comparison of the predictions of the theory and the data serves a dual purpose, since it tests both the similarity hypothesis and the supposition that the simulation in a finite box resembles the flow in an infinite environment. Agreement between the predictions of the theory and the data from the simulations adds credence to both hypotheses.

The simulated portion of non-homogeneous x_2 -direction is also of bounded extent in these simulations, but a mapping technique (Spalart *et al.* 1991) is used to expand the grid in this direction over the infinite domain in the x_2 -direction This technique concentrates most of the points near the middle of the grid where the wake is evolving.

The initial conditions for the simulation of the temporally evolving wake were generated using two realizations from a turbulent boundary layer simulation (Spalart 1988) with a Reynolds number, based on momentum thickness, of 670. Two different realizations of the boundary layer were utilized to form the initial conditions for the

wakes in order to ensure that the simulations did not have an artificial symmetry at the centerline of the wake. Thus, the initial conditions for the simulations are analogous to the flow behind a flat plate of zero thickness at a zero angle of attack. The initial Reynolds number of the wake based on the displacement thickness of the wake, δ_d , given by

$$Re = \frac{-\int_{-\infty}^{\infty} (U - U_{\infty}) dy}{\nu} = \frac{(U_{\infty} - U_c(t_0))\delta_d}{\nu},$$
 (2.135)

is equal to 2000 for these simulations.

Moser and Rogers (1994) carried out simulations of temporally evolving wakes using three different sets of initial conditions. In the first case, the initial conditions generated from the turbulent boundary layer were used to simulate an 'unforced' wake. In order to examine the influence of two-dimensional forcing and two-dimensional roller structures in the wake on the evolution of the temporally evolving wake, two other simulations were carried out with initial conditions that incorporated 'forcing' or amplification of the two-dimensional modes in the wake. In these cases, all of the disturbances with the wavenumber k_3 (the wavenumber in the x_3 direction) equal to zero were amplified. These two simulations are analogous to the forced wakes studied by Wygnanski et al. (1986) which were forced using a flap at the end of a plate. Note that Wygnanski et al. forced the wake using a single frequency, while Moser and Rogers (1994) amplified all of the two-dimensional modes in the wakes, thereby simulating a broad-band forcing. In the first 'forced' wake, Moser and Rogers simulated a 'midly forced' wake by multiplying the amplitude of the two-dimensional modes in the initial conditions by a factor of five. In the second, 'strongly forced' wake (that will not be considered here), the two-dimensional mode amplitudes are multiplied by a factor of twenty. (Note, in both of these case the w velocity portion of these disturbances are not amplified so the amplification of the energy is less than 5² and 20².) Since only data from the 'mildly forced' wake is used in the comparison of the prediction of the similarity theory and the data, the term 'forced wake' will be utilized to refer to the 'mildly forced' wake, while the term 'unforced wake' will refer to the simulation that was initiated without amplified initial conditions.

2.6.2 Evolution of the Reynolds Number and Similarity Length Scale

The similarity analysis demonstrated that the Reynolds number of the flow based on the similarity variables must be constant for a similarity solution to exist; *i.e.*,

$$Re_{\delta} = \frac{U_s \delta}{\nu} = const,$$
 (2.136)

The evolution of this Reynolds number, where U_s is equal to the centerline mean velocity deficit and δ is the distance between the two half-deficit points in the wake (both chosen to collapse the mean-velocity profiles), as a function of non-dimensional time, τ , given by

$$\tau = \frac{t(U_{\infty} - U_{cl}(t_o))}{\delta_d},\tag{2.137}$$

is illustrated in figure 2.3 for both the unforced and forced wakes. It is evident that both of the simulations evolve with an approximately constant Reynolds number for a finite amount of time after an initial transient. The slight decrease of the Reynolds number from the constant value near the end of both simulations is most likely due to the finite box size.

The similarity analysis also requires that

$$\frac{d\delta^2}{d\tau} \propto const. \tag{2.138}$$

The variation of δ^2 normalized by the square of the displacement thickness, δ_d^2 , for both simulations are illustrated in figure 2.4. In both cases, there is a region of approximately linear growth of the square of the length scale.

Note, the results for the 'strongly' forced wake simulation are not consistent with either of these predictions for any extended period of time during the simulation. Consequently, the results from this simulation are not considered here.

The similarity hypothesis for the two-point velocity correlation tensor is tested using full-field realizations from each simulation at four different times. The locations of these times are shown in figures 2.3 and 2.4 by the diamonds on the curves. All of these points fall in the region where the simulations approximately satisfy the Reynolds-number and length-scale constraints imposed by the similarity analysis.

2.6.3 Single-Point Moments

For the unforced wake, the single-point moments reported by Moser and Rogers (1994) are in good agreement with the single-point similarity hypothesis. The scaled normal Reynolds stresses are illustrated in figures 2.5 - 2.7. The data from the forced wake (Moser and Rogers 1994) also exhibits fair agreement with the similarity hypothesis, although there are trends in the scaled normal Reynolds stresses illustrated in figures 2.8 - 2.10 which are inconsistent with the similarity hypothesis. In particular, the value the $\overline{u_2u_2}$ decays more slowly than the similarity hypothesis predicts.

Moser and Rogers (1994) were unable to find a set of scales for the Reynolds stresses which would reduce the measured profiles in the unforced and forced to a single set of profiles that is valid for both simulations, indicating that the two wakes are not in the same universal state. This result is in agreement with the experimental results reported by Wygnanski et al. (1986) for the spatially developing wake, and the theoretical arguments of George (1989). Consequently, no attempt will be made to find universal functions that describe the two-point information in both wakes. Instead, the data from each simulation is examined to determine if the evolution of the individual wakes is consistent with the predictions of the two-point similarity hypothesis.

2.6.4 Computation of One-Dimensional Spectra

Since the simulations were carried out in a finite box, the Fourier spectra computed from the wake data bases in both the x_1 - and x_3 -directions are discrete Fourier series with a fixed set of wavenumbers. For example, the two-point velocity correlation can be represented as a Fourier series given by

$$R_{ij}(r_1, x_2, 0, t) = \sum_{n = -\infty}^{\infty} \hat{F}_{ij}^{1n}(x_2, 0, t)e^{ik_1^n r_1}$$
(2.139)

where the coefficients of the Fourier series are given by

$$\hat{F}_{ij}^{1n}(x_2, 0, t) = \frac{1}{l_{x_1}} \int_{-l_{x_1}/2}^{l_{x_1}/2} R_{ij}(r_1, x_2, 0, t) e^{-ik_1^n r_1} dr_1$$
(2.140)

and the discrete wavenumbers, k_1^n , are given by

$$k_1^n = \frac{2n\pi}{l_{x_1}}, \quad n \in I.$$
 (2.141)

Clearly, the one-dimensional spectra determined from the simulations can not shift continuously in wave number space as the flow evolves in time as required by the two-point similarity hypothesis, so it is evident that the simulation of the wake in a box cannot satisfy the two-point similarity hypothesis exactly. This is not unexpected since the wake in the finite box does not exactly model a temporally evolving wake in an infinite environment.

The definitions of the Fourier transform pair given in equations 2.139 and 2.140 are not consistent with the Fourier transform defined previously for the infinite domain; i.e., as $l_{x_1} \to \infty$. Since it is argued that the flow in the box should resemble the flow in an infinite environment, it is more appropriate to utilize a definition of the Fourier series that is consistent with the Fourier transform in an infinite domain. This Fourier transform pair is given by

$$R_{11}(r_1, x_2, 0, t) = \sum_{m = -\infty}^{\infty} F_{ij}^{1m} e^{ik_1^m r_1} \Delta k$$
 (2.142)

and

$$F_{ij}^{1m} = \frac{1}{l_{x_1} \Delta k} \int_{-l_{x_1}/2}^{l_{x_1}/2} R_{ij}(r_1, x_2, 0, t) e^{-ik_1^n r_1} dr_1, \qquad (2.143)$$

where Δk is the step size between the discrete wavenumbers given by

$$\Delta k = \frac{2\pi}{l_{x_1}}.\tag{2.144}$$

This definition of the Fourier transform pair is consistent with the definition for the infinite domain in the limit $l_{x_1} \to \infty$ in the sense of generalized functions (v. Lumley 1970).

The one-dimensional spectra computed from the wake simulation data bases (used to examine the two-point similarity hypothesis) are reported in the form defined in

equation 2.143. These spectra are presented as half-line spectra so the areas under the positive half of the spectra are equal to the corresponding single-point moments; e.g.,

$$\overline{u_1 u_1}(x_2, t) = R_{1,1}(0, x_2, 0, t) = \sum_{n=0}^{(\tilde{N}-1)/2} F_{11}^{1n}(k_1^n, x_2, t) \Delta k_1, \tag{2.145}$$

where \tilde{N} is the number of discrete Fourier modes in the simulation.

In order to provide a better estimate of the average value of the spectra in the flow, the one-dimensional spectra calculated from the simulation are spatially averaged over the homogeneous direction that was not transformed (e.g., the computed value of the one-dimensional spectra in the x_1 direction are spatially averaged in the x_3 direction). No other smoothing has been carried out on the one-dimensional spectra.

Of course, the full-field realizations of the wake provide few independent realizations of the large-scale motions in the wake, so the one-dimensional spectra in the low-wavenumber region may not be statistically accurate estimates of the ensemble averaged spectra. The relative error that occurs in the spectra computed from an single trace of data is unity, so the relative error which occurs in the averaged spectra at any wavenumber is approximately $1/\sqrt{N}$ (George, 1978), where N is the number of independent samples of the spectra used to compute the average. For the low-wavenumber region of the spectra, only those spectra computed from positions which are at least a distance of 3 integral length scales apart can be treated as approximately independent (George 1978).

In both simulations, the box size in the x_1 -direction is approximately 10 times

the integral length scale of the $\overline{u_1u_1'}$ correlation in this direction at the center of the wake, while the box size in the x_3 -direction is approximately 5 times the integral scale of the $\overline{u_1u_1'}$ correlation in this direction at the center of the wake. It is reasonable to expect that the integral scales for the other components and other positions in the wake are of the same order. Hence, the data bases from the simulations do not provide a large number of independent realizations of the low-wavenumber spectra. Of course, the small-scale motions will become approximately independent over a much smaller distance, so the data bases should provide a much better estimate of the high-wavenumber region of the spectra.

2.6.5 One-Dimensional Spectra of the Fluctuating Velocity

The unscaled one-dimensional spectra of the u_1 - and the u_2 -fluctuating velocity components in the x_1 -direction at the centerline of the unforced wake are illustrated in figure 2.11; the same spectra for the forced wake are illustrated in figure 2.12. These figures illustrate that the high-wavenumber regions of each set of spectra have the same basic shape and shifts down and to the left in agreement with the predictions of the similarity hypothesis. The individual spectra in each group are distinct in this region and should provide a test for the scaling determined from the two-point similarity analysis. In contrast, the low-wavenumber regions of the spectra exhibit behavior that is inconsistent with the similarity hypothesis. This is particularly true for the one-dimensional spectra in the forced wake. This is expected because the forcing introduced into the initial conditions of the forced wake simulation creates two-dimensional modes that are affected by the periodic boundary conditions in the box. Figures 2.13 and 2.14 illustrate the spectra of the u_1 - and u_2 -fluctuating velocity

62

for various positions across the forced wake in the non-homogeneous x_2 -direction at one time in the evolution of the wake. It is evident that peaks in the spectra occur at the same wavenumber at different locations across the wake, indicating that forcing has introduced motions that influence the development of the entire wake. Hence, it is not expected that the similarity hypothesis will collapse the spectra in the low-wavenumber region in the forced wake. In the unforced wake simulation, the spectra F_{22}^1 also exhibits peaks at the same wavenumber at different locations in the wake (not shown here), but the effect is not as significant as in the forced wake.

The scaled one-dimensional spectra of the three normal stresses in the x_1 direction for the unforced wake are illustrated in figures 2.15, 2.16, and 2.17. These figures include spectra from three different positions in the wake: the centerline of the wake, $\eta = 0.0$; the half-deficit point, $\eta = 0.5$; and twice the distance to the half-deficit point, $\eta = 1.0$. In these figures, the spectra at the centerline and at $\eta = 1.0$ have been plotted on the same scale, while the spectra computed at $\eta = 0.5$ have been shifted upward by an order of magnitude. The spectra of the normal stresses are scaled by $U_s^2\delta$, which is consistent with the scale predicted by the similarity analysis. The collapse in the low-wavenumber region of the spectra is not that good, in particularly the peaks which occur in the F_{22}^1 spectra at the same wavenumber in physical variables occur at different positions in similarity variables. In all cases, there is excellent collapse of the data for wavenumbers \tilde{k}_1 where $\tilde{k}_1/\Delta \tilde{k}_1$ is greater than 15-20. In the largest wavenumber region of the spectra there is also some disagreement in the spectra due to the 'turn up' of the spectra. This 'turn up' of the spectra occurs because the computational grid is not fully capable of resolving the smallest scales of motion, causing the energy to pile up in the highest wavenumbers.

In these simulations all of the scales of motion in the flow grow as the flow evolves so the effective resolution of the fixed computational grid increases in time. As a result, the 'turn up' of the spectra is reduced as the simulation evolves. In cases such as this, where the resolution of the grid increases with time, it is conventional to modify the computational grid to a coarser grid during the simulation in order to conserve computer resources. After a regrid, the resolution is significantly reduced so the 'turn up' of the spectra in the high-wavenumber region increases. For the unforced wake simulation the first three realizations used to examine the two-point similarity hypothesis were computed on one grid, while the final realization was computed on a second grid. Therefore, the 'turn up' in the spectra should reduce over the first three spectra and jump up on the final spectra – as, in fact, it does in figures 2.15-2.17.

The corresponding spectra of the normal stresses in the x_1 -direction for the forced wake are illustrated in figures 2.18, 2.19, and 2.20. In these figures, all but the low-wavenumber region of the spectra also collapse, in good agreement with the predictions of the similarity hypothesis. In the forced wake simulation, the first two realizations were computed on one grid, while the second two realizations were computed on a second grid, leading to the decrease and increase of the 'turn up' in the highest-wavenumber region of the spectra seen in the figures. The lack of collapse in the low-wavenumber region of the spectra in these figures is expected because of the poor statistical convergence and the influence of the two dimensional forcing which was added to the initial conditions.

The one-dimensional spectra of the normal stresses in the x_3 -direction at the same locations in the unforced wake are illustrated in figures 2.21, 2.22, and 2.23. The

64

collapse of the data in these spectra is, for the most part, better than the collapse that occurs in the one-dimensional spectra in the x_1 -direction because the computational domain is much longer in the x_1 -direction that the x_3 -direction providing more independent realizations of the spectra. Note, the collapse of the data at the outer position $\eta = 1.0$ is not quite as good as that for the inner positions.

The corresponding one-dimensional spectra of the turbulence in the forced wake simulation are illustrated in figures 2.24, 2.25, and 2.26. The collapse of the data for the forced wake is also good, except for the data at $\eta = 1.0$. There are several possible explanations for the poor collapse of the data: Firstly, the regrid that occurred between the second and third realizations may have effected the high-wavenumber region, since the spectra from the two times collapse and the data from the second two times collapse. This does not explain all of the lack of collapse, though, since the spectra at the points closer to the centerline are not affected as significantly. Secondly, the flow in the outer portion of the wake is highly intermittent. Thus, the one-dimensional spectra in this region can effectively be thought of as a weighted sum of the one-dimensional spectra from three different regimes: the turbulent regime, the potential flow regime, and the interface regime. If the data base does not provide enough realizations from all three of these regions in the right ratios then the spectra in these regions may not collapse. Finally, this data could simply be indicating that the small scale motions in the flow are not evolving in a manner that is consistent with the similarity hypothesis, but the excellent agreement at the inner positions in the wake suggests that other reasons are behind the discrepancy.

The one-dimensional spectra of the Reynolds stress $\overline{u_1u_2}$ also provide an useful test

of the two-point similarity theory. The unscaled magnitudes of the one-dimensional spectra in the x_1 -direction at the centerline of the unforced wake are illustrated in 2.27. Each spectrum in this figure has been plotted twice. The lower set of curves are the actual magnitudes of the different spectra at all wavenumbers while, the second set of curves has the same information shifted upward including only every 7^th or $8^{t}h$ point from the data (the same symbols were used for each spectra in the two groups). This second group shows that the higher wavenumber region of the spectra shift downward and toward lower wavenumbers as the flow evolves, as predicted by the similarity hypothesis. The scaled one-dimensional spectra of the Reynolds stress in the x_1 -direction at the centerline of the unforced wake are illustrated in figure 2.28, while these spectra for the forced wake are illustrated in figure 2.29. The spectra have been plotted in two groups again as they were in figure 2.27. Although there is a significant amount of variability in the magnitude of the one-dimensional spectra, $|F_{12}^1|$, it is apparent from figures 2.28 and 2.29 that the similarity scale determined from the two point similarity hypothesis does collapse the magnitude of the one-dimensional spectra at the centerline of the wake. The magnitude of the one-dimensional spectra $|F_{12}^1|$ scaled by $U_s^2\delta$ at two other points in the unforced wake, $\eta=0.5$ and $\eta=1.0$, are illustrated in figure 2.30, while the spectra from the forced wake are illustrated in figure 2.31. It both cases the scaling determined from the similarity analysis collapses the data at these two points, although again the collapse in the data is not as good at $\eta = 1.0$. The one-dimensional spectra of the Reynolds stress $\overline{u_1u_2}$ in the x_3 -direction of the unforced wake in figure 2.32 also collapse when plotted in the similarity variables. (Note, that the larger x_1 -domain used in the spatial average causes the k_3 spectra to be smoother than the k_1 spectra.)

Overall, the evolution of the one-dimensional spectra of the dominant Reynolds stresses in the simulations of a temporally evolving, turbulent, plane wake are in good agreement with the prediction of the two-point similarity hypothesis. There are some discrepancies between the measured data and the predictions of the theory, particularly in the low-wavenumber region and for the positions farther out in the wake. It is likely that these discrepancies can be attributed to either the limited sample of the large-scale eddies in the simulation or the impact of the artificially imposed periodic boundary conditions, particularly in the forced wake.

2.6.6 Taylor Microscales

Although the one-dimensional spectra collapse when they are scaled in the manner determined from the similarity analysis, it is also useful to examine if the characteristic length scales determined from the one-dimensional spectra are proportional to the the similarity length scale δ as required by the similarity analysis (v. section 2.5). In this regard, the integral scale of the turbulence is not useful because it is inherently biased to the largest scales of motions which may be affected by the finite dimensions of the box. (Note, the same is true in isotropic and homogeneous shear turbulence, v. George 1992 and George and Gibson 1992). In contrast, the Taylor microscale, which can also be computed from the one-dimensional velocity spectra (eqn. 2.128 or 2.129), is characteristic of smaller motions in the flow and should evolve like those in an infinite wake.

The ratios of the Taylor microscales in the x_1 - and x_3 -directions and the similarity length scale δ at several different positions in the unforced wake flow are illustrated in

figures 2.33 and 2.34. There is some variability in the ratios of the Taylor microscales and the similarity length scale, but overall the ratios are approximately constant as predicted in the similarity analysis. Some of the data, such as the Taylor microscale for $\overline{u_3u_3}$ in the x_1 -direction at the centerline (\triangleright in fig. 2.33), exhibit downward trends suggesting that the virtual origin for these Taylor microscale may be different than the virtual origin of the similarity length scale δ .

The ratios of the Taylor microscales and the similarity length scale in the forced wake are illustrated in figures 2.35 and 2.36. There are several cases, particularly the length scales in the x_1 -direction, where the Taylor microscale grows slower than that of the similarity length scale, but for the most part the ratios are approximately constant.

The variations of the ratios from a constant value, if statistically true, indicate that the evolution of the simulations are not exactly compatible with the predictions of the two-point similarity hypothesis at this point in the simulations. It is not clear whether this phenomenon is be caused by the finite dimensions of the periodic box or an incomplete evolution towards the asymptotic solution. The trends in the data do not seem to be due to the 'turn up' of the spectra at the highest wavenumbers since there is not a consistent trend exhibited in all of the microscales.

The Taylor microscales farther out in both wakes (particularly the forced wake) flows (e.g., $\eta = 1.0$) grow slower than the similarity length scale and in several cases the Taylor microscales are approximately constant. The lack of agreement between

the data at these position and the predictions of the theory may be due to the intermittent character of the turbulence far from the wake centerline.

2.6.7 Velocity Correlation in the Non-Homogeneous Direction

The correlations of the velocity between two points separated in the x_2 -direction (but not in the x_1 - or x_3 -directions) were computed for both wake simulations. These correlations were obtained by spatially averaging in both the x_1 - and x_3 -directions. (Note, the computed correlations have statistical convergence problems similar to those outlined for the spectra, particularly for the large-scale motions.) In order to compare the predictions of the similarity hypothesis with the data, the two-point correlation functions have been normalized by U_s^2 and written as a function of the similarity variable η .

The scaled auto-correlation of u_1 about the centerline of the unforced wake are illustrated in figure 2.37, while the scaled auto-correlations about the points $\eta=\pm 0.5$ are illustrated in figure 2.38. The collapse of the data is fairly good over most of the separation distance, although it is clear that the estimates of the correlations suffer from a limited statistical sample because they are not symmetrical about the centerline of the wake. Much of the discrepancy between the data and the prediction of the theory occurs around the peak of the auto-correlation, the value of the single point moment at the position of the fixed probe.

One difficulty with examining the two-point velocity correlation is that the largescale motions (for which there are few realizations that may be affected by the periodic boundary conditions) influence the value of the correlation for all separation distances. Thus, it is more useful to examine a statistical measures, such as the second-order structure functions given by

$$\overline{(u_{\alpha} - u_{\beta}')^2} = \overline{u_{\alpha}u_{\alpha}} + \overline{u_{\beta}'u_{\beta}'} - 2\overline{u_{\alpha}u_{\beta}'}, \tag{2.146}$$

that are better measures of the motions whose size is on the order of the separation distance between the points. These structure functions can be written as a similarity solution when the two-point velocity correlation tensor has a similarity solution, so this moment can be utilized to compare the predictions of the similarity hypothesis and the data from the small-scale motions in the simulations. Figures 2.39 and 2.40 show the u_1 component of this moment at the centerline and the half-deficit points, $\eta = \pm 0.5$, of the unforced wake. In both cases, the collapse of the data is good except for large separation distances, as expected.

The scaled structure functions for the u_2 velocity component about the points $\eta = 0.0$ and $\eta = \pm 0.5$ in the unforced wake are illustrated in figures 2.41 and 2.42, while the structure functions for the u_3 component about the same points are illustrated in figures 2.43 and 2.44. There is good agreement with prediction of the theory for all but the large separation distances (where there is significant scatter in the data due to the insufficient statistical sample).

The structure function is not an effective tool for examining the cross-correlation of the u_1 and u_2 fluctuating velocities because the single point moments that appear in the expanded definition of the structure function are not the same as in the two-point

correlation. For example,

$$\overline{(u_1 - u_2')^2} = \overline{u_1 u_1} + \overline{u_2' u_2'} - 2\overline{u_1 u_2'}.$$
(2.147)

Consequently, this function is biased by any discrepancy the in the single-point moments, so here the two-point correlation are examined, recognizing that there may be an inherent discrepancies due to the influence of the large-scale motions.

The cross-correlations of the u_1 and u_2 fluctuating velocities about $\eta=0$ and $\eta=\pm 0.5$ are illustrated in figures 2.45, 2.46, 2.47, and 2.48. In figures 2.45 and 2.46 the velocity component u_1 is being measured at the fixed position and u_2 is measured at the moving position, while in figures 2.47 and 2.48 the opposite is true. The collapse in the data is better for the $\overline{u_1u_2}$ correlation than for the $\overline{u_1'u_2}$ correlation. The scatter in the value of $\overline{u_1'u_2}$ at the centerline of the wake is due to poor statistical convergence of a moment which is nearly (or is) zero. The curves at the points, $\eta=\pm 0.5$, indicate that the magnitude of the correlation in the wake is decreasing slower than predicted in the similarity hypothesis. This discrepancy is not unexpected because the large-scale motions are the primary contributors to the cross-correlations $\overline{u_1'u_2}$ and $\overline{u_1u_2'}$.

The structure functions for the fluctuating velocity components at the centerline, $\eta = 0$, and the half-deficit points, $\eta = \pm 0.5$, in the forced wake are illustrated in figures 2.49- 2.54. There is good agreement between the predictions of the theory and the data from the forced wake for the smaller separation distances, although it is evident that the statistics are not fully converged. The scatter in the data and the discrepancies between the theory and the data (particularly in the u_2 component) for large separation distances are greater than in the unforced wake. The large scatter in

the data is to be expected since the asymmetries in the initial conditions that were amplified by the forcing propagate through the simulation can not be averaged out with the limited sample provided by the data base.

2.7 Analysis of the Two-Point, Two-Time Correlations

Although there is not sufficient data to examine the two-point, two-time correlation, it is interesting to examine if the similarity analysis can be extended to the governing equations for these correlations (i.e., the correlation of $u_i(x_1, x_2, x_3, t)$ and $u'_j(x'_1, x'_2, x'_3, t')$). The governing equations for these correlations in the temporally evolving wake are given by

$$\frac{\partial \overline{u_i u'_j}}{\partial t} + U_1 \frac{\partial \overline{u_i u'_j}}{\partial x_1} = -\frac{1}{\rho} \frac{\partial \overline{p u'_j}}{\partial x_i} - \frac{\partial \overline{u_i u_k u'_j}}{\partial x_k} - \overline{u'_j u_2} \frac{\partial U_1}{\partial x_2} \delta_{i1} + \nu \left(\frac{\partial^2}{\partial \beta^2} + \frac{\partial^2}{\partial x_2^2} + \frac{\partial^2}{\partial \zeta^2} \right) \overline{u_i u'_j}$$
(2.148)

and

$$\frac{\partial \overline{u_i u'_j}}{\partial t'} + U'_1 \frac{\partial \overline{u_i u'_j}}{\partial x'_1} = -\frac{1}{\rho} \frac{\partial \overline{p' u_i}}{\partial x'_j} - \frac{\partial \overline{u_i u'_k u'_j}}{\partial x'_k} - \overline{u_i u'_2} \frac{\partial U'_1}{\partial x'_2} \delta_{j2}
+ \nu \left(\frac{\partial^2}{\partial \beta^2} + \frac{\partial^2}{\partial x'_2^2} + \frac{\partial^2}{\partial \zeta^2} \right) \overline{u_i u'_j} .$$
(2.149)

These equations have been simplified by noting that the only non-zero mean velocity component, U_1 , is a function of x_2 and t only.

The objective of the similarity analysis is to determine if these equations admit solutions in which the two-point, two-time correlation tensor can be written as a product of a scale function and a similarity function that is independent of the two times relative to the virtual origin of the flow. Since the flow is non-stationary in the present time coordinate system, this requires the definition of a new time coordinate system. Thus, it is hypothesized that there is a transformed time coordinate, \tilde{t} , in which the scaled two-point, two-time correlations are only a function of the separation time, τ , given by

$$\tau(t, t') = \tilde{t} - \tilde{t}'. \tag{2.150}$$

The allowable choices for this transformed coordinate system are determined by examining the equations of motion.

The similarity coordinates in the x_2 -direction are given by

$$\eta = \frac{x_2}{\delta(t)} \tag{2.151}$$

and

$$\eta' = \frac{x_2'}{\delta(t')},\tag{2.152}$$

which are consistent with the definitions in the previous analyses.

It is not as straightforward to define the similarity coordinates in the homogeneous x_1 - and x_3 -directions. In the previous analysis of the two-point, single-time correlation, the similarity coordinates were determined by scaling the separation distances in these coordinate directions by the single similarity length scale, $\delta(t)$; *i.e.*,

$$\xi = \frac{x_1 - x_1'}{\delta}.\tag{2.153}$$

It is not immediately evident how to extend this definition of the similarity variable to the present case where there are two different similarity length scales, $\delta(t)$ and

 $\delta(t')$, that can be used to scale the separation distance. One choice might be to scale the homogeneous coordinate by the similarity length scale; *i.e.*,

$$\tilde{x}_1 = \frac{x_1}{\delta} \tag{2.154}$$

This choice of scaling, however, does not appear to be consistent with the requirement that the flow is homogeneous in the physical system, since it imposes an origin onto the statistical measures in this coordinate direction. Consequently, the solution will be non-homogeneous in this new coordinate system, since

$$x_1 - x_1' = \tilde{x}_1 \delta(t) - \tilde{x}_1' \delta(t'). \tag{2.155}$$

This definition offers no advantage because it increases the number of independent variables necessary to define the solution (i.e., the correlation would be a function of both \tilde{x}_1 and \tilde{x}'_1).

Another choice is to scale the separation distances in the homogeneous directions by some product of the similarity length scales, such as

$$\frac{x_1 - x_1'}{\delta(t)^n \delta(t')^m}. (2.156)$$

This choice of similarity variables is included in a more general choice of similarity variables; that being the definition of two similarity variables for each homogeneous direction given by

$$\xi = \frac{x_1 - x_1'}{\delta} \tag{2.157}$$

$$\xi' = \frac{x_1 - x_1'}{\delta'} \tag{2.158}$$

$$\zeta = \frac{x_3 - x_3'}{\delta} \tag{2.159}$$

$$\zeta' = \frac{x_3 - x_3'}{\delta'} \tag{2.160}$$

where the notation δ' is used as a short hand notation for $\delta(t')$. This definition of the similarity variables also appears to increase the number of independent variables required to define the similarity solution, but, as it will be shown later, this is not the case because the two similarity variables used for each direction can be related by the separation distance in the similarity time coordinate, τ .

Thus, it is hypothesized that equations 2.148 and 2.149 admit to similarity solutions where the two point correlations are given by

$$\overline{u_i u_j'} = Q^{i,j}(t, t') q_{i,j}(\xi, \xi', \eta, \eta', \zeta, \zeta', \tau), \tag{2.161}$$

$$\overline{pu'_{i}} = \Pi_{1}^{j}(t, t')\pi_{i}^{1}(\xi, \xi', \eta, \eta', \zeta, \zeta', \tau), \tag{2.162}$$

$$\overline{u_i u_k u'_j} = T_1^{ik,j}(t, t') t t_{ik,j}^1(\xi, \xi', \eta, \eta', \zeta, \zeta', \tau), \tag{2.163}$$

$$\overline{p'u_i} = \Pi_2^i(t, t')\pi_i^2(\xi, \xi', \eta, \eta', \zeta, \zeta', \tau), \tag{2.164}$$

and

$$\overline{u_i u_k' u_j'} = T_2^{i,kj}(t,t') t t_{i,kj}^2(\xi, \xi', \eta, \eta', \zeta, \zeta', \tau).$$
(2.165)

The use of the mixed coordinate system t, t', and τ is included to facilitate comparison with the solutions for the two-point, single-time correlation.

Equations 2.148 and 2.149 do not admit similarity solutions of the hypothesized kind as the equations are presently written because there are two different mean convection velocity scales in the equations, U_s and U_{∞} , that are not proportional.² These equation may admit similarity solution if it is possible to eliminate one of these velocity scales from the problem. This can be accomplished by examining the flow

²These two convection velocity introduce two time scales into the problem which are not proportional.

in a reference frame translating at the freestream velocity U_{∞} , in which the mean velocity, \tilde{U}_1 , is given by

$$\tilde{U}_1 = U_1 - U_\infty = U_s(t)f(\eta).$$
 (2.166)

In this case the mean velocity only introduces one velocity scale.³

Substituting the hypothesized similarity solutions into the governing equations (eqn. 2.148 and 2.149) yields

$$\left[\frac{\partial Q^{i,j}}{\partial t}\right] q_{i,j} - \left[\frac{Q^{i,j}}{\delta} \frac{d\delta}{dt}\right] \left(\xi \frac{\partial q_{i,j}}{\partial \xi} + \eta \frac{\partial q_{i,j}}{\partial \eta} + \zeta \frac{\partial q_{i,j}}{\partial \zeta}\right) + \left[Q^{i,j} \frac{\partial \tau}{\partial t}\right] \frac{\partial q_{i,j}}{\partial \tau} \\
+ \left[\frac{U_s Q^{i,j}}{\delta}\right] f(\eta) \frac{\partial q_{i,j}}{\partial \xi} + \left[\frac{U_s Q^{i,j}}{\delta'}\right] f(\eta) \frac{\partial q_{i,j}}{\partial \xi'} = -\frac{1}{\rho} \left(\left[\frac{\Pi_1^j}{\delta}\right] \frac{\partial \pi_j^1}{\partial \xi} + \left[\frac{\Pi_1^j}{\delta'}\right] \frac{\partial \pi_j^1}{\partial \xi'}\right) \delta_{i1} \\
-\frac{1}{\rho} \left[\frac{\Pi_1^j}{\delta}\right] \frac{\partial \pi_j^1}{\partial \eta} \delta_{i2} - \frac{1}{\rho} \left(\left[\frac{\Pi_1^j}{\delta}\right] \frac{\partial \pi_j^1}{\partial \zeta} + \left[\frac{\Pi_1^j}{\delta'}\right] \frac{\partial \pi_j^1}{\partial \zeta'}\right) \delta_{i3} - \left[\frac{T_1^{i1,j}}{\delta}\right] \frac{\partial tt_{i1,j}^1}{\partial \xi} - \left[\frac{T_1^{i1,j}}{\delta'}\right] \frac{\partial tt_{i1,j}^1}{\partial \xi'} \\
- \left[\frac{T_1^{i2,j}}{\delta}\right] \frac{\partial tt_{i2,j}^1}{\partial \eta} - \left[\frac{T_1^{i3,j}}{\delta}\right] \frac{\partial tt_{i3,j}^1}{\partial \zeta} - \left[\frac{T_1^{i3,j}}{\delta'}\right] \frac{\partial tt_{i1,j}^1}{\partial \zeta'} - \left[\frac{Q^{2,j}U_s}{\delta}\right] q_{2,j} \frac{df}{d\eta} \Big|_{\eta=\eta} \delta_{i1} \\
+ \left[\frac{\nu Q^{i,j}}{\delta^2}\right] \left(\frac{\partial^2}{\partial \xi^2} + \frac{\partial^2}{\partial \eta^2} + \frac{\partial^2}{\partial \zeta^2}\right) q_{i,j} + \left[\frac{\nu Q^{i,j}}{\delta'^2}\right] \left(\frac{\partial^2}{\partial \xi'^2} + \frac{\partial^2}{\partial \zeta'^2}\right) q_{i,j} f \qquad (2.167)$$

and

$$\begin{split} \left[\frac{\partial Q^{i,j}}{\partial t'}\right]q_{i,j} - \left[\frac{Q^{i,j}}{\delta'}\frac{d\delta'}{dt'}\right] \left(\xi'\frac{\partial q_{i,j}}{\partial \xi'} + \eta'\frac{\partial q_{i,j}}{\partial \eta'} + \zeta'\frac{\partial q_{i,j}}{\partial \zeta'}\right) + \left[Q^{i,j}\frac{\partial \tau}{\partial t'}\right] \frac{\partial q_{i,j}}{\partial \tau} \\ - \left[\frac{U'_sQ^{i,j}}{\delta}\right]f(\eta')\frac{\partial q_{i,j}}{\partial \xi} - \left[\frac{U'_sQ^{i,j}}{\delta'}\right]f(\eta')\frac{\partial q_{i,j}}{\partial \xi'} = +\frac{1}{\rho}\left(\left[\frac{\Pi_2^i}{\delta}\right]\frac{\partial \pi_i^2}{\partial \xi} + \left[\frac{\Pi_2^i}{\delta'}\right]\frac{\partial \pi_2^i}{\partial \xi'}\right)\delta_{j1} \\ - \frac{1}{\rho}\left[\frac{\Pi_2^i}{\delta'}\right]\frac{\partial \pi_i^2}{\partial \eta'}\delta_{j2} + \frac{1}{\rho}\left(\left[\frac{\Pi_2^i}{\delta}\right]\frac{\partial \pi_i^2}{\partial \zeta} + \left[\frac{\Pi_2^i}{\delta'}\right]\frac{\partial \pi_i^2}{\partial \zeta'}\right)\delta_{j3} + \left[\frac{T_2^{i,1j}}{\delta}\right]\frac{\partial tt_{i,1j}^2}{\partial \xi} + \left[\frac{T_2^{i,1j}}{\delta'}\right]\frac{\partial tt_{i,1j}^2}{\partial \xi'} \\ - \left[\frac{T_2^{i,2j}}{\delta'}\right]\frac{\partial tt_{i,2j}^2}{\partial \eta'} + \left[\frac{T_2^{i,3j}}{\delta}\right]\frac{\partial tt_{i,3j}^2}{\partial \zeta} + \left[\frac{T_2^{i,3j}}{\delta'}\right]\frac{\partial tt_{i,3j}^2}{\partial \zeta'} - \left[\frac{Q^{i,2}U'_s}{\delta'}\right]q_{i,2}\frac{df}{d\eta}\bigg|_{\eta=\eta'}\delta_{j1} \end{split}$$

³The flow in this coordinate system is effectively the temporal version of a plane jet going the opposite direction, which is one of the interesting features of temporally evolving flows.

$$+ \left[\frac{\nu Q^{i,j}}{\delta^2} \right] \left(\frac{\partial^2}{\partial \xi^2} + \frac{\partial^2}{\partial \zeta^2} \right) q_{i,j} + \left[\frac{\nu Q^{i,j}}{\delta'^2} \right] \left(\frac{\partial^2}{\partial \xi'^2} + \frac{\partial^2}{\partial \eta'^2} + \frac{\partial^2}{\partial \zeta'^2} \right) q_{i,j}, \tag{2.168}$$

where the portion of each term that is a function of the position of the two points in time is included in square brackets.

In order to demonstrate that these equations admit similarity solutions, it is necessary to demonstrate that they reduce to a form that is a function of the similarity variables only. Therefore, the ratio of the terms in square brackets must be a function of τ only.

Initially, it is useful to obtain the allowable choices for the variable τ . Since the ratio of the second and third terms in each equation must be a function of τ only, it follows that

$$Q^{i,j} \frac{\partial \tau}{\partial t} \left(\frac{Q^{i,j}}{\delta} \frac{d\delta}{dt} \right)^{-1} \propto g_1(\tau)$$
 (2.169)

and

$$Q^{i,j} \frac{\partial \tau}{\partial t'} \left(\frac{Q^{i,j}}{\delta'} \frac{d\delta'}{dt'} \right)^{-1} \propto g_2(\tau). \tag{2.170}$$

These conditions are satisfied if

$$\frac{1}{g_1(\tau)} \frac{\partial \tau}{\partial t} \propto \frac{1}{\delta} \frac{d\delta}{dt} \propto t^{-1} \tag{2.171}$$

and

$$\frac{1}{g_2(\tau)} \frac{\partial \tau}{\partial t'} \propto \frac{1}{\delta'} \frac{d\delta'}{dt'} \propto t'^{-1}, \tag{2.172}$$

where the origin of the time coordinate system has been placed at the virtual origin of the wake. These conditions are satisfied if

$$\tau \propto \ln(t) + c_1(t') \tag{2.173}$$

and

$$\tau \propto \ln(t') + c_2(t) \tag{2.174}$$

where $g_1(\tau)$ and $g_2(\tau)$ are constant. Thus, one choice for the transformed time coordinate system that satisfies these conditions is given by

$$\tilde{t} = \ln(t/t_s) \tag{2.175}$$

 $(t_s \text{ is included for dimensional reasons})$, in which case the separation distance in the transformed coordinate system is given by

$$\tau = \tilde{t} - \tilde{t}' = \ln(t/t'). \tag{2.176}$$

This definition of the similarity time scale can also be obtained using physical arguments. The similarity analysis of the equations that govern the single-time correlations illustrated that there are at least three characteristic time scales in this problem; a convection time scale given by

$$\delta/U_s, \tag{2.177}$$

a time scale which characterizes the growth of the layer due to the turbulent diffusion given by

$$\left(\frac{1}{\delta}\frac{d\delta}{dt}\right)^{-1},\tag{2.178}$$

and a viscous diffusion time scale given by

$$\delta^2/\nu. \tag{2.179}$$

All of these time scales are proportional to the location of the point in time relative to the virtual origin; i.e., t (where the virtual origin of the wake is, again, chosen to

coincide with the origin of the time coordinate system). Evidently, the characteristic time scales of the physical mechanisms in the wake increase as the flow evolves.

If the statistics of events separated by a small distance in time at one point in the wakes evolution are to be compared to the statistics between two points at a later point in the evolution, it is important to recognize that the events are occurring more slowly at the later point in time. Thus, it is reasonable to choose the sets of points so that the separation distances between the points at the two different times are the same when they are normalized by the local time scale. In the limit of zero separation distance, these are given by

$$d\tilde{t} = \frac{dt}{t}. (2.180)$$

Integrating this yields

$$\tilde{t} - \tilde{t}' = \ln(t/t'),\tag{2.181}$$

which is the time scale derived from the similarity analysis. Thus, the transformed time scale is one where each incremental change in time is normalized by the local physical time scale of the flow, yielding a time scale that is effectively synchronous with the flow dynamics.

It also follows that

$$\frac{t}{t'} = e^{\tau} \tag{2.182}$$

or

$$\frac{\delta}{\delta'} = \left(\frac{t}{t'}\right)^{1/2} = e^{\tau/2}.\tag{2.183}$$

Thus, for this choice of τ , ξ and ξ' are related by

$$\xi = \frac{x_1 - x_1'}{\delta(t)} = \frac{x_1 - x_1'}{\delta(t')} \frac{\delta(t')}{\delta(t)} = \xi' e^{-\tau/2}$$
(2.184)

and ζ is related to ζ' by

$$\zeta = \frac{x_3 - x_3'}{\delta(t)} = \frac{x_3 - x_3'}{\delta(t')} \frac{\delta(t')}{\delta(t)} = \zeta' e^{-\tau/2}.$$
 (2.185)

Therefore, the two different similarity variables utilized to represent the information in each homogeneous direction are not independent, but are related by the independent similarity variable τ , as previously suggested.

The scales for the two-point velocity correlation tensor can also be deduced from the constraints in equations 2.167 and 2.168. One choice for the scales can be determined by requiring

$$\frac{\partial Q^{i,j}}{\partial t} \propto \frac{Q^{i,j}}{t},\tag{2.186}$$

so that

$$Q^{i,j} = c_3(t')t^{d_1}. (2.187)$$

Similarly, requiring

$$\frac{\partial Q^{i,j}}{\partial t'} \propto \frac{Q^{i,j}}{t'} \tag{2.188}$$

implies that

$$Q^{i,j} = c_4(t)t'^{d_2}. (2.189)$$

Further, in the limit when the separation distance between the two points is zero the scale must be consistent with the scale for the single-time correlation. Thus, it follows that a choice for $Q^{i,j}$ is given by

$$Q^{i,j} \propto U_s^n(t)U_s^{2-n}(t'). \tag{2.190}$$

A reasonable choice is to set n = 1, so that the scale is equally weighted on the

velocity scale at each point.4

It is straightforward to demonstrate that equations 2.148 and 2.149 reduce to equations that are functions of similarity variables if the scales for the other two-point correlations are given by

$$\Pi_1^j \propto U_s Q^{i,j} \propto U_s^2 U_s', \tag{2.191}$$

$$\Pi_2^i \propto U_s' Q^{i,j} \propto U_s'^2 U_s, \tag{2.192}$$

$$T_1^{ik,j} \propto U_s Q^{i,j} \propto U_s^2 U_s', \tag{2.193}$$

and

$$T_{i,kj}^2 \propto U_s' Q^{i,j} \propto U_s'^2 U_s, \tag{2.194}$$

which are consistent with the scales for the two-point, single-time similarity solutions.

Therefore, the similarity analysis can be extended to governing equations for the two-point, two-time velocity correlation tensor. The governing equations for the similarity profiles of the two-point, two-time correlations are dependent on the ratio of the viscous, convection, and spreading rate time scales, so the functional form of these profiles may also depend on the source conditions of the wake (if the ratio of these time scales vary for different source conditions). The analysis can also be extended to demonstrate that the two-point, two-time velocity-gradient correlation tensor can be expressed in similarity form when the two-point, two-time velocity correlation can.

⁴Note, that this choice for the similarity scale is not unique since this scale could be multiplied by any function of τ and still satisfy the requirement that the ratio of the terms in square brackets in equations 2.167 and 2.168 are only a function of τ . Of course, the functions would then appear in the governing equations for the similarity solutions.

2.8 Analysis of a Scalar Field

The similarity analysis of the governing equations can also be extended to other phenomena in the flow, such as the evolution of a passive scalar field. In this analysis, the evolution of two different types of passive scalar fields in the wake are considered: First, a two-stream (or binary) passive scalar field; *i.e.*, a field in which the mean value of the passive scalar field on the two sides of the wake differ. Physically, this corresponds to the wake behind a splitter plate separating two, equal-velocity streams, each containing a different amount of a scalar (v. figure 2.55). The second is a scalar field where the mean value of the passive scalar on both sides of the wake is equal, but a surplus or deficit of the scalar exists in the wake (v. figure 2.56). Physically, this corresponds to a wake produced behind a hot/cold plane body or the wake produced by a plane body injecting a scalar into the wake.

2.8.1 Single-Point Moments: The Two-Stream Field

In this section, the similarity analysis is applied to a two-stream (or binary) passive scalar field in a temporally developing, high-Peclet-number wake. Following this, the similarity analysis is extended to the scalar-deficit field.

Using the standard high-Peclet-number assumptions, the equation governing the mean value of the passive scalar in the temporally evolving wake reduces to

$$\frac{\partial\Theta}{\partial t} = -\frac{\partial\overline{u_2\theta}}{\partial x_2},\tag{2.195}$$

where Θ is the mean value of a passive scalar and θ is the instantaneous fluctuating value of this passive scalar.

For the two-stream geometry, it is hypothesized that this equation has a similarity solution where

$$\Theta - \Theta_1 = S_c(t)s_c(\eta_\theta), \tag{2.196}$$

$$\overline{u_2\theta} = R_{u_2\theta}(t)r_{u_2\theta}(\eta_\theta), \tag{2.197}$$

 η_{θ} , the similarity coordinate for the passive scalar field is given by

$$\eta_{\theta} = \frac{x_2}{\delta_{\theta}},\tag{2.198}$$

and Θ_1 is the mean value of the passive scalar in the flow as $x_2 \to -\infty$. The solution for the mean value of the scalar must also satisfy the boundary condition as $x_2 \to \infty$ in this two-stream geometry, namely

$$\lim_{x_2 \to \infty} \Theta(x_2) = \Theta_2 \tag{2.199}$$

Therefore,

$$S_c(t) \propto \Theta_2 - \Theta_1 = const.$$
 (2.200)

It is conventional to choose

$$S_c(t) = \Theta_2 - \Theta_1 \tag{2.201}$$

so $s_c(\eta_\theta)$ is a function bounded by 0 and 1.

Substituting the hypothesized similarity solutions into equation 2.195 yields

$$-\left[\frac{S_c}{\delta_\theta} \frac{d\delta_\theta}{dt}\right] \eta_\theta \frac{ds_c}{d\eta_\theta} = -\left[\frac{R_{u_2\theta}}{\delta_\theta}\right] \frac{dr_{u_2\theta}}{d\eta_\theta}$$
 (2.202)

Thus, equation 2.195 admits a similarity solution when

$$\left[\frac{Sc}{\delta_{\theta}}\frac{d\delta_{\theta}}{dt}\right] \propto \left[\frac{R_{v\theta}}{\delta_{\theta}}\right]$$
(2.203)

or,

$$R_{v\theta} \propto Sc \frac{d\delta_{\theta}}{dt} \propto \Delta\Theta \frac{d\delta_{\theta}}{dt}$$
 (2.204)

Note, the growth rate of the scalar field is not yet determined. The equations for the higher-order moments must be examined to determine the growth rate of the similarity length scale for the scalar field.

Using the standard high-Peclet-number assumptions, the equation for the fluctuating scalar variance can be reduced to

$$\frac{\partial \overline{\theta^2}}{\partial t} = -\frac{\partial \overline{u_2 \theta^2}}{\partial x_2} - 2\overline{u_2 \theta} \frac{\partial \Theta}{\partial x_2} - \epsilon_{\theta \theta}, \qquad (2.205)$$

where $\epsilon_{\theta\theta}$ is given by

$$\epsilon_{\theta\theta} = 2\alpha \frac{\partial \theta}{\partial x_k} \frac{\partial \theta}{\partial x_k} \tag{2.206}$$

and α is the molecular diffusivity of the scalar.

The hypothesized similarity solutions for the new moments in equation 2.205 are given by

$$\overline{\theta^2} = V_{\theta\theta}(t)v_{\theta\theta}(\eta_{\theta}), \tag{2.207}$$

$$\overline{u_2\theta^2} = Tr_\theta(t)tr_\theta(\eta_\theta), \tag{2.208}$$

and

$$\epsilon_{\theta\theta} = D_{\theta}(t)d_{\theta}(\eta_{\theta}). \tag{2.209}$$

Substituting these solutions into the equation for the scalar variance yields

$$\left[\frac{dV_{\theta\theta}}{dt}\right]v_{\theta\theta} - \left[\frac{V_{\theta\theta}}{\delta_{\theta}}\frac{d\delta_{\theta}}{dt}\right]\eta_{\theta}\frac{dv_{\theta\theta}}{d\eta_{\theta}} = -\left[\frac{Tr_{\theta}}{\delta_{\theta}}\right]\frac{dtr_{\theta}}{d\eta_{\theta}}$$

$$-2\left[\frac{R_{u_2\theta}S_c}{\delta_{\theta}}\right]r_{u_2\theta}\frac{ds_c}{d\eta_{\theta}} - [D_{\theta}]d_{\theta}. \tag{2.210}$$

The first term in the equation is included to allow for the possibility that the scale for the scalar variance is a function of time. If this scale is not a function of time, then this term is zero and does not provide a constraint in the similarity analysis.

Equation 2.205 admits a similarity solution (of the hypothesized kind) when

$$\left[\frac{dV_{\theta\theta}}{dt}\right] \propto \left[\frac{V_{\theta\theta}}{\delta_{\theta}}\frac{d\delta_{\theta}}{dt}\right] \propto \left[\frac{Tr_{\theta}}{\delta_{\theta}}\right] \propto \left[\frac{R_{u_2\theta}Sc}{\delta_{\theta}}\right] \propto [D_{\theta}].$$
(2.211)

The second and fourth terms in equation 2.211 can be utilized to deduce the scale for the variance since these terms are proportional only when

$$V_{\theta\theta} \propto (Sc)^2 \propto (\Delta\Theta)^2.$$
 (2.212)

Therefore, the scale for the scalar variance is independent of time. Consequently, the first term in equation 2.211 is not included in the rest of the analysis for this geometry.

It can be shown that the other constraints in equation 2.211 are satisfied when

$$Tr_{\theta} \propto Sc^2 \frac{d\delta_{\theta}}{dt} \propto (\Delta\Theta)^2 \frac{d\delta_{\theta}}{dt}$$
 (2.213)

and

$$D_{\theta} \propto \frac{Sc^2}{\delta_{\theta}} \frac{d\delta_{\theta}}{dt} \propto \frac{(\Delta\Theta)^2}{\delta_{\theta}} \frac{d\delta_{\theta}}{dt}.$$
 (2.214)

It is also instructive to examine the transport equation for the turbulent scalar flux, $\overline{u_2\theta}$. Using the standard high-Reynolds/Peclet-number assumptions, the governing equation reduces to

$$\frac{\partial \overline{u_2 \theta}}{\partial t} = + \frac{\overline{p} \frac{\partial \theta}{\partial x_2}}{\rho \frac{\partial \theta}{\partial x_2}} - \frac{\partial \Theta}{\partial x_2} - \frac{\partial}{\partial x_2} \left(\overline{u_2^2 \theta} + \frac{\overline{p \theta}}{\rho} \right)$$
(2.215)

The hypothesized similarity solutions for the new moments in equation 2.215 are given by

$$\left(\overline{u_2^2\theta} + \frac{\overline{p\theta}}{\rho}\right) = Tr_{u_2\theta}(t)tr_{u_2\theta}(\eta_\theta)$$
 (2.216)

and

$$\frac{\overline{p}}{\rho} \frac{\partial \theta}{\partial x_2} = \Pi_{u_2\theta}(t) \pi_{u_2\theta}(\eta_\theta).$$
(2.217)

Substituting these solutions into equation 2.215 yields

$$\left[\frac{dR_{u_2\theta}}{dt}\right] r_{u_2\theta} - \left[\frac{R_{u_2\theta}}{\delta_{\theta}} \frac{d\delta_{\theta}}{dt}\right] \eta_{\theta} \frac{dr_{u_2\theta}}{d\eta_{\theta}} = + \left[\Pi_{u_2\theta}\right] \pi_{u_2\theta}
- \left[\frac{Tr_{u_2\theta}}{\delta_{\theta}}\right] \frac{dtr_{u_2\theta}}{d\eta_{\theta}} - \left[\frac{K_{u_2}S_c}{\delta_{\theta}}\right] k_{u_2}(\eta) \frac{ds_c}{d\eta_{\theta}},$$
(2.218)

where the similarity solution for the turbulent stress $\overline{u_2^2}$ from the analysis of the velocity field (eqn. 2.34) has been substituted into equation 2.215. The equation for the turbulent scalar flux admits a similarity solution only when

$$\left[\frac{dR_{u_2\theta}}{dt}\right] \propto \left[\frac{R_{u_2\theta}}{\delta_{\theta}}\frac{d\delta_{\theta}}{dt}\right] \propto \left[\Pi_{u_2\theta}\right] \propto \left[\frac{Tr_{u_2\theta}}{\delta_{\theta}}\right] \propto \left[\frac{K_{u_2}S_c}{\delta_{\theta}}\right].$$
(2.219)

The second and fifth terms in equation 2.219 are proportional only when

$$\left(\frac{d\delta_{\theta}}{dt}\right)^2 \propto U_s^2 \propto (t - t_0)^{-1}.$$
(2.220)

Therefore,

$$\delta_{\theta} \propto (t - t_o)^{1/2},\tag{2.221}$$

where t_o is the location of the virtual origin of the velocity field in the wake. Thus, the equations for the passive scalar field admit similarity solutions only when the growth rate of the similarity length scale for the scalar field is proportional to the similarity length scale for the velocity field. This is a reasonable outcome since the turbulent velocity field is the primary transport mechanism for the scalar field in a high-Pecletnumber flow. Further, the equations governing the scalar field only admit similarity solutions when the virtual origin of the scalar field occurs at the same location as the virtual origin of the velocity field.

It can be shown that the other constraints in equation 2.219 are satisfied when

$$T_{u_2\theta} \propto S_c \left(\frac{d\delta_{\theta}}{dt}\right)^2$$
 (2.222)

and

$$\Pi_{u_2\theta} \propto \frac{S_c}{\delta_{\theta}} \left(\frac{d\delta_{\theta}}{dt}\right)^2.$$
 (2.223)

Thus, the equations that governing the mean scalar field, the scalar variance, and the turbulent flux, $\overline{u_2\theta}$, for the two-stream scalar field in the temporally developing wake admit similarity solutions. For example, if the constants of proportionality in the definition of the similarity scales in equations 2.204, 2.212 - 2.214, 2.222, and 2.223 are taken as unity, it follows that the governing equation for the similarity solutions are given by

$$-\eta_{\theta} \frac{ds_c}{d\eta_{\theta}} = -\frac{dr_{u_2\theta}}{d\eta_{\theta}},\tag{2.224}$$

$$-\eta_{\theta} \frac{dv_{\theta\theta}}{d\eta_{\theta}} = -\frac{dtr_{\theta}}{d\eta_{\theta}} - 2r_{u_{2}\theta} \frac{ds_{c}}{d\eta_{\theta}} - d_{\theta}, \qquad (2.225)$$

and

$$-r_{u_2\theta} - \eta_\theta \frac{dr_{u_2\theta}}{d\eta_\theta} = \pi_{u_2\theta} - \frac{dtr_{u_2\theta}}{d\eta_\theta} - \frac{1}{k_2''^2} k_{u_2}(\eta) \frac{ds_c}{d\eta_\theta}, \tag{2.226}$$

where

$$k_2' = \frac{1}{U_s} \frac{d\delta_{\theta}}{dt} = \frac{U_{\infty}}{2M_0} \frac{\delta}{\delta_{\theta}} \frac{d\delta_{\theta}^2}{dt} \int_{-\infty}^{\infty} f(\tilde{\eta}) d\tilde{\eta}$$
 (2.227)

is a constant that may depend on the source conditions of the flow. Thus, the similarity profiles for the single-point measures of the scalar field, in general, depend on the initial conditions of the disturbances in the scalar field. The solution for the scalar field is also coupled to the similarity solution for the velocity field, so the similarity solution for the scalar field may also be dependent on the source conditions of the velocity field.

2.8.2 Analysis of Scalar-Deficit Flow

This analysis of the scalar field in a temporally evolving plane wake can easily be extended to a second geometry in which there is a scalar-deficit or surplus in the wake. The analysis for all of the higher-order moments is the same as the analysis laid out for the previous geometry. The only difference between the two problems is the scale for the mean value of the scalar. Thus, all that is necessary to extend the analysis to this second geometry is to carry out the similarity analysis for the equations that governs the mean scalar field in this geometry.

Using the standard high-Peclet-number assumptions, the equation for the mean

value of the scalar (in deficit or surplus form) can be reduced to

$$\frac{\partial(\Theta_{\infty} - \Theta)}{\partial t} = \frac{\partial \overline{u_2 \theta}}{\partial x_2},\tag{2.228}$$

where Θ_{∞} is the value of the scalar in the free stream.

When there is negligible free-stream turbulence, this equation can be integrated to yield

$$\frac{\partial}{\partial t} \int_{-\infty}^{\infty} (\Theta_{\infty} - \Theta) \, dx_2 = 0 \tag{2.229}$$

It is hypothesized that these equations for the scalar-deficit field admit similarity solutions where

$$\Theta_{\infty} - \Theta = S_c(t)s_c(\eta_{\theta}) \tag{2.230}$$

and

$$\overline{u_2\theta} = R_{u_2\theta}(t)r_{u_2\theta}(\eta_\theta). \tag{2.231}$$

These solutions are consistent with the equations for the mean scalar field if

$$\left[\frac{dS_c}{dt}\right] \propto \left[\frac{S_c}{\delta_\theta} \frac{d\delta_\theta}{dt}\right] \propto \left[\frac{R_{u_2\theta}}{\delta_\theta}\right]$$
(2.232)

and

$$S_c \delta_{\theta} \propto const,$$
 (2.233)

or

$$Sc \propto \frac{1}{\delta_{\theta}}$$
 (2.234)

and

$$R_{u_2\theta} \propto S_c \frac{d\delta_{\theta}}{dt},$$
 (2.235)

which are analogous to the conditions derived for the velocity field.

This similarity analysis can also be extended to the higher-order moments, although, of course, the scale for the mean scalar field S_c is now time dependent, so that all of the other moments which depend on this scale (including the scale for the scalar variance) are time dependent.

2.9 Analysis of the Two-Point Scalar Correlation

The analysis of the scalar field can be extended to the two-point correlation of the passive scalar field. In the previous sections examined two different scalar fields. A two-stream mixing field and a scalar field with a mean deficit (or surplus). The analyses of the governing equation for the two-point scalar correlation for these two cases are very similar, so it is convenient to examine them simultaneously.

For the temporally evolving wake, the governing equation for the two-point scalar correlation reduces to

$$\frac{\partial \overline{\theta} \overline{\theta'}}{\partial t} + (U_1 - U_1') \frac{\partial \overline{\theta} \overline{\theta'}}{\partial \zeta} =$$

$$-\frac{\partial}{\partial \zeta} \left(\overline{u_1 \theta \theta'} - \overline{u_1' \theta \theta'} \right) - \frac{\partial \overline{u_2 \theta \theta'}}{\partial x_2} - \frac{\partial \overline{u_2' \theta \theta'}}{\partial x_2} - \frac{\partial}{\partial \gamma} \left(\overline{u_3 \theta \theta'} - \overline{u_3' \theta \theta'} \right)$$

$$-\overline{\theta' u_2} \frac{\partial \Theta}{\partial x_2} - \overline{\theta u_2'} \frac{\partial \overline{\Theta'}}{\partial x_2'} + \alpha \left(2 \frac{\partial^2}{\partial \zeta^2} + \frac{\partial^2}{\partial x_2^2} + \frac{\partial^2}{\partial x_2'^2} + 2 \frac{\partial^2}{\partial \gamma} \right) \overline{\theta \theta'}, \tag{2.236}$$

where the primed and unprimed variables have the same meaning as in the previous sections.

The similarity analysis of the two-point scalar correlation is carried out in exactly the same manner as the analysis of the two-point velocity correlation tensor. In this case, it is hypothesized that a similarity solution exists for this equation where the two-point correlations are given by

$$\overline{\theta\theta'} = \chi(t)\varphi(\xi_{\theta}, \eta_{\theta}, \eta_{\theta}', \zeta_{\theta}), \tag{2.237}$$

$$\overline{\theta u_2'} = R_1^{\theta}(t) r_{\theta}^1(\xi_{\theta}, \eta_{\theta}, \eta_{\theta}', \zeta_{\theta}), \tag{2.238}$$

$$\overline{\theta' u_2} = R_2^{\theta}(t) r_{\theta}^2(\xi_{\theta}, \eta_{\theta}, \eta_{\theta}', \zeta_{\theta}), \tag{2.239}$$

$$\overline{u_k \theta \theta'} = S_1^{\theta k}(t) s_{\theta k}^1(\xi_\theta, \eta_\theta, \eta'_\theta, \zeta_\theta), \tag{2.240}$$

and

$$\overline{u_k'\theta\theta'} = S_2^{\theta k}(t) s_{\theta k}^2(\xi_\theta, \eta_\theta, \eta_\theta', \zeta_\theta), \tag{2.241}$$

where

$$\xi_{\theta} = \frac{x_1 - x_1'}{\delta_{\theta}},\tag{2.242}$$

$$\eta_{\theta} = \frac{x_2}{\delta_{\theta}}, \eta_{\theta}' = \frac{x_2'}{\delta_{\theta}}, \tag{2.243}$$

and

$$\zeta_{\theta} = \frac{x_3 - x_3'}{\delta_{\theta}}.\tag{2.244}$$

Substituting these solutions for the two-point correlations, the mean scalar field for the two-stream geometry (eqn. 2.196), and the mean velocity field (eqn. 2.9) into equation 2.236 yields

$$\left[\frac{d\chi}{dt}\right]\varphi - \left[\frac{\chi}{\delta_{\theta}}\frac{d\delta_{\theta}}{dt}\right]\left(\xi_{\theta}\frac{\partial}{\partial\xi_{\theta}} + \eta_{\theta}\frac{\partial}{\partial\eta_{\theta}} + \eta_{\theta}'\frac{\partial}{\partial\eta_{\theta}'} + \zeta_{\theta}\frac{\partial}{\partial\zeta_{\theta}}\right)\varphi$$

$$+ \left[\frac{U_s \chi}{\delta_{\theta}} \right] \left\{ f(\eta') - f(\eta) \right\} \frac{\partial \varphi}{\partial \xi_{\theta}} = - \left[\frac{R_1^{\theta} S_c}{\delta_{\theta}} \right] r_{\theta}^{1} \frac{ds_c}{d\eta'} - \left[\frac{R_2^{\theta} S_c}{\delta_{\theta}} \right] r_{\theta}^{2} \frac{ds_c}{d\eta'}$$

$$- \left[\frac{S_1^{\theta 1}}{\delta_{\theta}} \right] \frac{\partial s_{\theta 1}^{1}}{\partial \xi_{\theta}} + \left[\frac{S_2^{\theta 1}}{\delta_{\theta}} \right] \frac{\partial s_{\theta 1}^{1}}{\partial \xi_{\theta}} - \left[\frac{S_1^{\theta 2}}{\delta_{\theta}} \right] \frac{\partial s_{\theta 2}^{1}}{\partial \eta_{\theta}} - \left[\frac{S_2^{\theta 2}}{\delta_{\theta}} \right] \frac{\partial s_{\theta 2}^{1}}{\partial \eta'_{\theta}} - \left[\frac{S_1^{\theta 3}}{\delta_{\theta}} \right] \frac{\partial s_{\theta 3}^{1}}{\partial \zeta_{\theta}} + \left[\frac{S_2^{\theta 3}}{\delta_{\theta}} \right] \frac{\partial s_{\theta 3}^{1}}{\partial \zeta_{\theta}}$$

$$+ \left[\frac{\alpha \chi}{\delta_{\theta}^{2}} \right] \left(2 \frac{\partial^{2}}{\partial \xi_{\theta}^{2}} + \frac{\partial^{2}}{\partial \eta_{\theta}^{2}} + \frac{\partial^{2}}{\partial \gamma_{\theta}^{2}} + \frac{\partial^{2}}{\partial \zeta_{\theta}^{2}} \right) \varphi$$

$$(2.245)$$

(where the time dependent portion of each term in this equation is contained in square brackets). The first term in the equation is present only when the scale χ is a function of time. The equation for the scalar-deficit geometry is the same as this except the sign in front of the last two terms on the second line are positive instead of negative.

Thus, for both the two-stream and the scalar-deficit fields, the governing equation for the two-point scalar correlation admits a similarity solution when

$$\frac{d\chi}{dt} \propto \frac{\chi}{\delta_{\theta}} \frac{d\delta_{\theta}}{dt} \propto \frac{U_s \chi}{\delta_{\theta}} \propto \frac{R_{\theta}^1 S_c}{\delta_{\theta}} \propto \frac{R_{\theta}^2 S_c}{\delta_{\theta}}$$

$$\propto \frac{S_1^{\theta k}}{\delta_{\theta}} \propto \frac{S_2^{\theta k}}{\delta_{\theta}} \propto \frac{\alpha \chi}{\delta_{\theta}^2}.$$
(2.246)

It is evident from the relationships in equation 2.246 that the convective terms are only proportional to the diffusive terms if

$$\frac{U_s \chi}{\delta_\theta} \propto \frac{\alpha \chi}{\delta_\theta^2} \to \frac{U_s \delta_\theta}{\alpha} = const, \qquad (2.247)$$

analogous to the constant-Reynolds-number constraint derived in the analysis of the velocity field. This is a reasonable result since similarity solutions for the scalar field were formulated with the implicit assumption that all of the characteristic length

scales of the flow grow in proportion, an idea that is consistent with a constant-Peclet-number flow.

In the limit when the separation distance between the points approaches zero, the two-point correlation tensor must be equal to the variance of the fluctuating scalar field. Thus, for both geometries the scales for the two-point correlations must be chosen such that

$$\chi \propto S_c^2, \tag{2.248}$$

$$R_{\theta}^2 \propto R_{\theta}^1 \propto \chi,$$
 (2.249)

and

$$S_1^{\theta k} \propto S_2^{\theta k} \propto \chi U_s. \tag{2.250}$$

Of course, the constants of proportionality in these equations may be dependent on the source conditions of the flow.

Thus, the equation that governs the evolution of the two-point scalar correlation for both the mean scalar-deficit and the two-stream scalar field in the temporally evolving wake flow admits a similarity solution. It is also straightforward to demonstrate that the two-point scalar gradient moments can also be written in a similarity form when the two-point scalar correlation can. In this case, the scalar dissipation can be written in a similarity form that is consistent with the solution required by the single point similarity analysis.

Following the methodology outlined for the two-point velocity correlation, it can also be demonstrated that the one-dimensional spectra of the scalar field in the homogeneous directions have a similarity form when the two-point scalar correlation tensor has a similarity solution. Further, the length scales determined from these spectra (or the two-point correlation tensor), such as the integral scale and the Taylor microscale, are proportional to the similarity length scale, δ_{θ} or δ .

2.10 Comparison of Theory to Data: Scalar Field

2.10.1 Simulation: Scalar Field

The evolution of a two-stream scalar field in the temporally-developing wake was also computed by Moser and Rogers (1994) in their simulations of the wake. The mean value of the scalar was unity on one side of the wake, while the value of the scalar field was zero on the other side of the wake. The Prandtl number of the simulations was equal to 0.7. The initial conditions for the scalar field were generated using a hyberbolic tangent curve for the mean value of the scalar.

2.10.2 One-Dimensional Spectra of the Scalar Field

The one-dimensional spectra of the scalar field in the temporally-evolving wake simulation can be utilized to test predictions of the similarity hypothesis for the two-stream geometry. The one-dimensional spectra computed from simulations are presented as approximations to the one-dimensional spectra of a flow, in an infinite field, analogous to the one-dimensional spectra for the velocity field (v. sec. 2.6.4).

The unscaled one-dimensional scalar spectrum in the- x_1 direction at the centerline of the unforced wake is illustrated in figure 2.57. The one-dimensional spectra have a

similar shape in the high-wave-number region and shift down and to the left with time as predicted by the similarity hypothesis, indicating that the spectra may collapse when they are scaled with similarity variables. The difference in the unscaled one-dimensional spectra of the scalar field is not as large as the difference that occurred in the unscaled velocity spectra because the scale for the one-dimensional spectra is smaller. Hence, collapse of these spectra may not provide as rigorous a test of the similarity hypothesis as the velocity spectra.

The scaled one-dimensional spectra in the x_1 direction of the scalar field at the centerline of the wake, $\eta=0$, and the half-deficit point in the unforced wake, $\eta=0.5$, are shown in figure 2.58, while the one-dimensional spectra in the x_3 directions are illustrated in figure 2.59. (Data from points farther out in the flow are not considered because the fluctuating scalar field becomes highly intermittent in this region and the data base does not provide sufficient realizations.) The similarity length scale for the velocity field has been used to scale the one-dimensional spectra in this case. This is appropriate, since the similarity length scale for the scalar field must be proportional with the similarity length scale for the velocity field when the governing equation for two-point correlation of the scalar admits a similarity solution. The spectra in these figures indicate that the data from the centerline of the wake and the half-deficit point for all but the lowest wavenumbers (the large-scale motions) are in agreement with the predictions of the similarity hypothesis. A similar result can also be seen in the one-dimensional scalar spectra in the forced wake illustrated in figures 2.60 and 2.61.

2.10.3 Taylor Microscales of the Scalar Field

The Taylor microscales of the scalar field in the x_1 and x_3 can also be used to test whether the similarity hypothesis accurately predicts the evolution of the scalar field in the wake. The hypothesis predicts that these length scale grow in proportion to the similarity length scale.

The ratios of the Taylor microscales and the similarity length scale in the unforced wake are illustrated in figures 2.62 and 2.63, while the ratios in the forced wake are shown in figures 2.64 and 2.65. All of these figures show the ratios for three different positions in the wake; $\eta = 0.0$, $\eta = 0.25$, and $\eta = 0.5$. The ratios are approximately constant, as predicted by the similarity theory although the data is not in perfect agreement with the theory. This is not unexpected since the data from the velocity field that mixes the scalar field are not in perfect agreement with the theory.

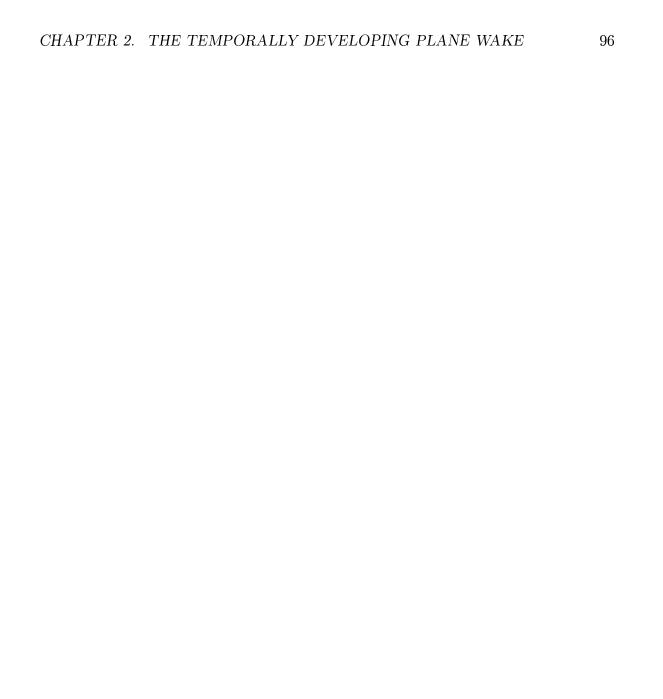


Figure 2.1: Instantaneous realization of the temporally evolving wake simulation – vorticity contours

Figure 2.2: Geometry of the temporally evolving wake flow



Figure 2.3: Evolution of Reynolds number in the temporally developing wake simulations – diamonds indicate points where the data is utilized to examine the two point similarity hypothesis

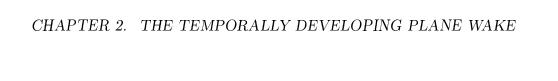


Figure 2.4: Evolution of the similarity length scale in the temporally evolving wake simulations – δ is the distance between the half-deficit points in the wake

Figure 2.5: Scaled value of $\overline{u_1u_1}$ in the unforced wake.

Figure 2.6: Scaled value of $\overline{u_2u_2}$ in the unforced wake.

Figure 2.7: Scaled value of $\overline{u_3u_3}$ in the unforced wake.

Figure 2.8: Scaled value of $\overline{u_1u_1}$ in the forced wake.

Figure 2.9: Scaled value of $\overline{u_2u_2}$ in the forced wake.

Figure 2.10: Scaled value of $\overline{u_3u_3}$ in the forced wake.

Figure 2.11: One-dimensional spectra in the unforced wake at $x_2/\delta=0.$

Figure 2.12: One-dimensional spectra in the forced wake at $x_2/\delta=0.$

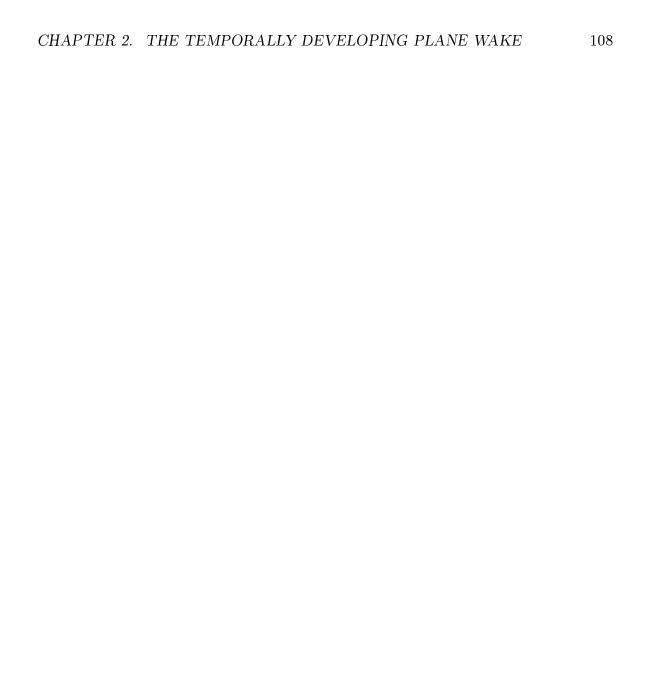


Figure 2.13: One-dimensional spectra of $\overline{u_1u_1}$ at different x_2 -positions in the forced wake.

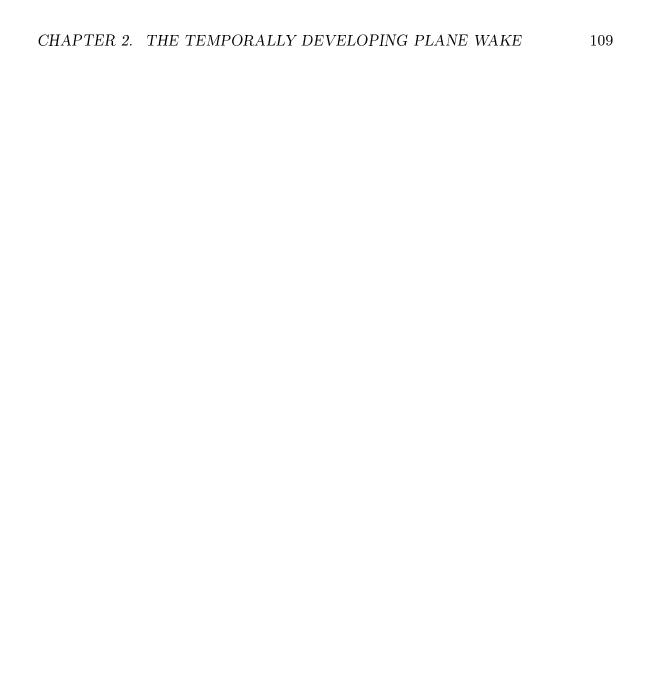


Figure 2.14: One-dimensional spectra of $\overline{u_2u_2}$ at different x_2 -positions in the forced wake.

Figure 2.15: Scaled one-dimensional spectra F_{11}^1 in the unforced wake – at $\eta=0.0$, $\eta=0.5$, and $\eta=1.0$. Spectra from $\eta=0.5$ are shifted up by an order of magnitude.

Figure 2.16: Scaled one-dimensional spectra F_{22}^1 in the unforced wake – at $\eta=0.0$, $\eta=0.5$, and $\eta=1.0$. Spectra from $\eta=0.5$ are shifted up by an order of magnitude.

Figure 2.17: Scaled one-dimensional spectra F_{33}^1 in the unforced wake – at $\eta=0.0$, $\eta=0.5$, and $\eta=1.0$. Spectra from $\eta=0.5$ are shifted up by an order of magnitude.

Figure 2.18: Scaled one-dimensional spectra F_{11}^1 in the forced wake – at $\eta=0.0$, $\eta=0.5$, and $\eta=1.0$. Spectra from $\eta=0.5$ are shifted up by an order of magnitude.

Figure 2.19: Scaled one-dimensional spectra F_{22}^1 in the forced wake— at $\eta=0.0$, $\eta=0.5$, and $\eta=1.0$. Spectra from $\eta=0.5$ are shifted up by an order of magnitude.

Figure 2.20: Scaled one-dimensional spectra F_{33}^1 in the forced wake – at $\eta=0.0$, $\eta=0.5$, and $\eta=1.0$. Spectra from $\eta=0.5$ are shifted up by an order of magnitude.

Figure 2.21: Scaled one-dimensional spectra F_{11}^3 in the unforced wake – at $\eta=0.0$, $\eta=0.5$, and $\eta=1.0$. Spectra from $\eta=0.5$ are shifted up by an order of magnitude.

Figure 2.22: Scaled one-dimensional spectra F_{22}^3 in the unforced wake – at $\eta=0.0$, $\eta=0.5$, and $\eta=1.0$. Spectra from $\eta=0.5$ are shifted up by an order of magnitude.

Figure 2.23: Scaled one-dimensional spectra F_{33}^3 in the unforced wake – at $\eta=0.0$, $\eta=0.5$, and $\eta=1.0$. Spectra from $\eta=0.5$ are shifted up by an order of magnitude.

Figure 2.24: Scaled one-dimensional spectra F_{11}^3 in the forced wake – at $\eta=0.0$, $\eta=0.5$, and $\eta=1.0$. Spectra from $\eta=0.5$ are shifted up by an order of magnitude.

Figure 2.25: Scaled one-dimensional spectra F_{22}^3 in the forced wake— at $\eta=0.0$, $\eta=0.5$, and $\eta=1.0$. Spectra from $\eta=0.5$ are shifted up by an order of magnitude.

Figure 2.26: Scaled one-dimensional spectra F_{33}^3 in the forced wake – at $\eta=0.0$, $\eta=0.5$, and $\eta=1.0$. Spectra from $\eta=0.5$ are shifted up by an order of magnitude.

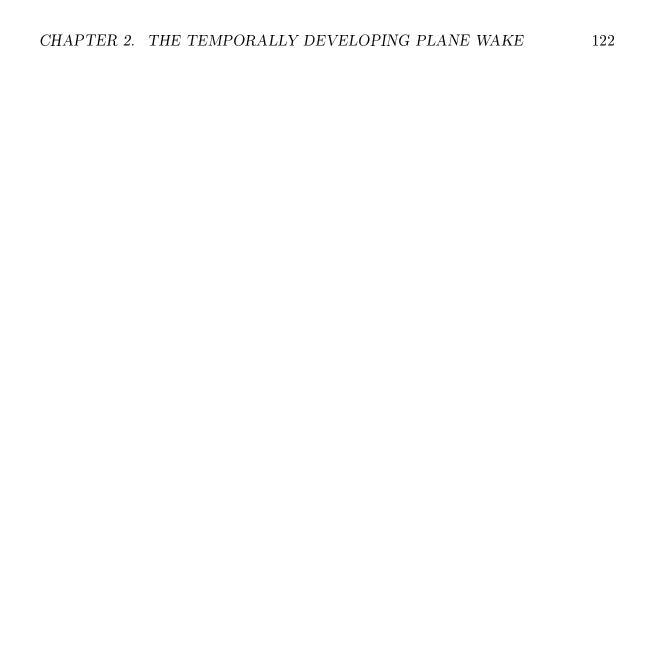


Figure 2.27: Magnitude of one-dimensional spectra F_{12}^1 at $\eta{=}0.0$ in the unforced wake.



Figure 2.28: Scaled magnitude of the spectra F_{12}^1 at $\eta=0.0$ in the unforced wake.



Figure 2.29: Scaled magnitude of the spectra F_{12}^1 at $\eta=0.0$ in the forced wake.



Figure 2.30: Scaled magnitude of the spectra F_{12}^1 at $\eta=0.5$ and $\eta=1.0$ in the unforced wake.



Figure 2.31: Scaled magnitude of the spectra F_{12}^1 at $\eta=0.5$ and $\eta=1.0$ in the forced wake.



Figure 2.32: Scaled magnitude of the spectra F_{12}^3 at $\eta=0.0$ and $\eta=0.5$ in the unforced wake.

Figure 2.33: Taylor microscales in the x_1 -direction in the unforced wake.

Figure 2.34: Taylor microscales in the x_3 -direction in the unforced wake.

Figure 2.35: Taylor microscales in the x_1 -direction in the forced wake.

Figure 2.36: Taylor microscales in the x_3 -direction in the forced wake.

Figure 2.37: Scaled autocorrelation of $\overline{u_1u_1'}$ about $\eta=0.0$; unforced wake.

Figure 2.38: Scaled autocorrelation of $\overline{u_1u_1'}$ about $\eta=\pm 0.5$; unforced wake.

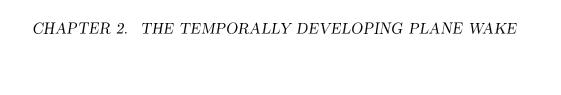


Figure 2.39: Structure function of the u_1 component at $\eta = 0.0$ in the unforced wake.



Figure 2.40: Structure function of the u_1 component at $\eta=\pm 0.5$ in the unforced wake.



Figure 2.41: Structure function of the u_2 component at $\eta=0.0$ in the unforced wake.



Figure 2.42: Structure function of the u_2 component at $\eta=\pm 0.5$ in the unforced wake.

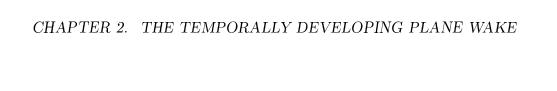


Figure 2.43: Structure function of the u_3 component at $\eta=0.0$ in the unforced wake.



Figure 2.44: Structure function of the u_3 component at $\eta=\pm 0.5$ in the unforced wake.



Figure 2.45: Scaled autocorrelation of $\overline{u_1u_2'}$ about $\eta=0.0$ in the unforced wake.



Figure 2.46: Scaled autocorrelation of $\overline{u_1u_2'}$ about $\eta=\pm 0.5$ in the unforced wake.



Figure 2.47: Scaled autocorrelation of $\overline{u_2u_1'}$ about $\eta=0.0$ in the unforced wake.



Figure 2.48: Scaled autocorrelation of $\overline{u_2u_1'}$ about $\eta=\pm 0.5$ in the unforced wake.



Figure 2.49: Structure function of the u_1 component at $\eta = 0.0$ in the forced wake.

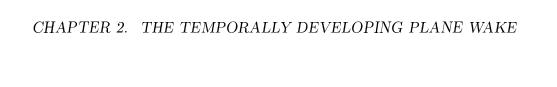


Figure 2.50: Structure function of the u_1 component at $\eta=\pm 0.5$ in the forced wake.



Figure 2.51: Structure function of the u_2 component at $\eta=0.0$ in the forced wake.



Figure 2.52: Structure function of the u_2 component at $\eta=\pm 0.5$ in the forced wake.



Figure 2.53: Structure function of the u_3 component at $\eta=0.0$ in the forced wake.



Figure 2.54: Structure function of the u_3 component at $\eta=\pm 0.5$ in the forced wake.

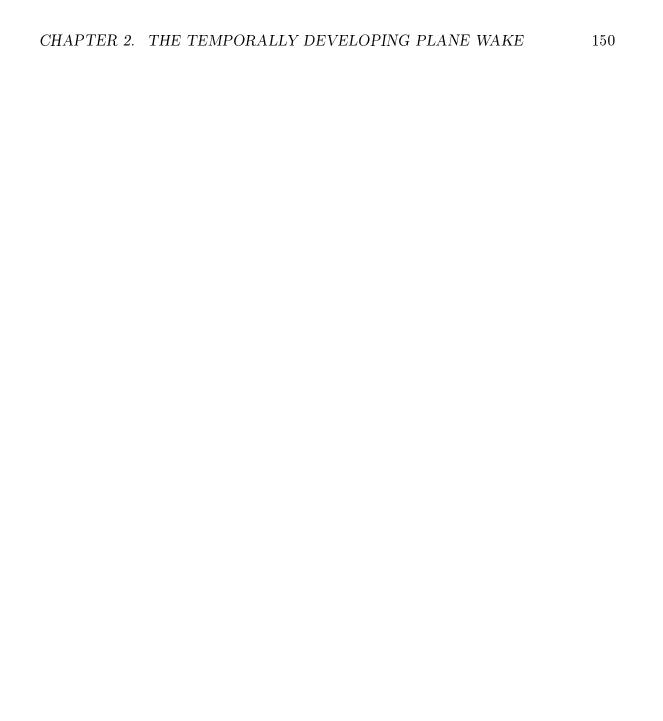


Figure 2.55: Geometry of the two-stream scalar field in the temporally developing wake.

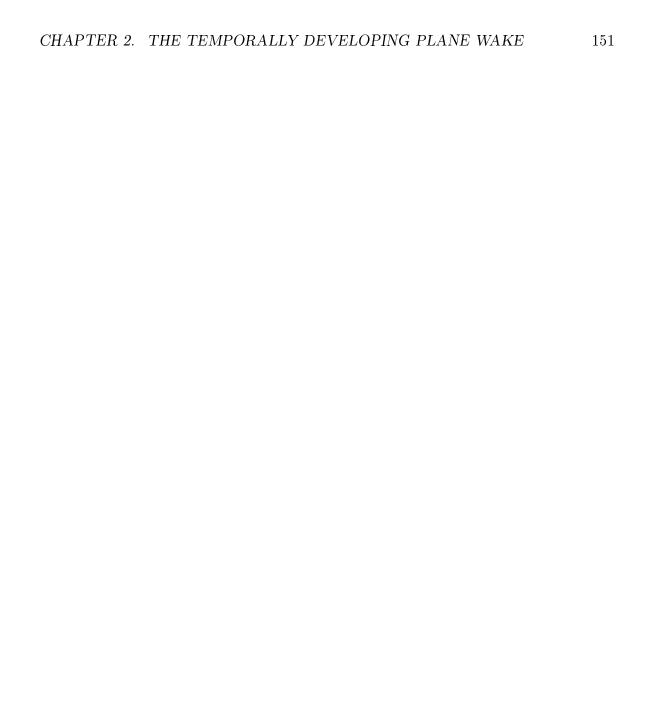


Figure 2.56: Geometry of the scalar-deficit field in the temporally developing wake.



Figure 2.57: One-dimensional scalar spectra $F_{\theta\theta}^1$ at η =0.0 in the unforced wake.

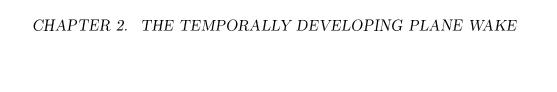


Figure 2.58: Scaled one-dimensional spectra $F^1_{\theta\theta}$ at $\eta{=}0.0$ and η =0.5 in the unforced wake.

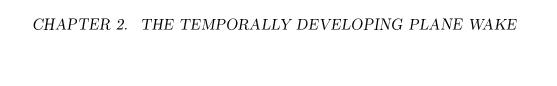


Figure 2.59: Scaled one-dimensional spectra $F_{\theta\theta}^3$ at $\eta{=}0.0$ and $\eta=0.5$ in the unforced wake.

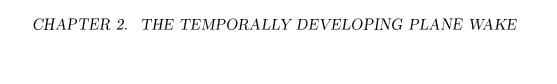


Figure 2.60: Scaled one-dimensional spectra $F_{\theta\theta}^1$ at $\eta{=}0.0$ and η =0.5 in the forced wake.



Figure 2.61: Scaled one-dimensional spectra $F_{\theta\theta}^3$ at $\eta{=}0.0$ and η =0.5 in the forced wake.



Figure 2.62: Taylor microscales of the scalar field in the x_1 -direction in the unforced wake.



Figure 2.63: Taylor microscales of the scalar field in the x_3 -direction in the unforced wake.

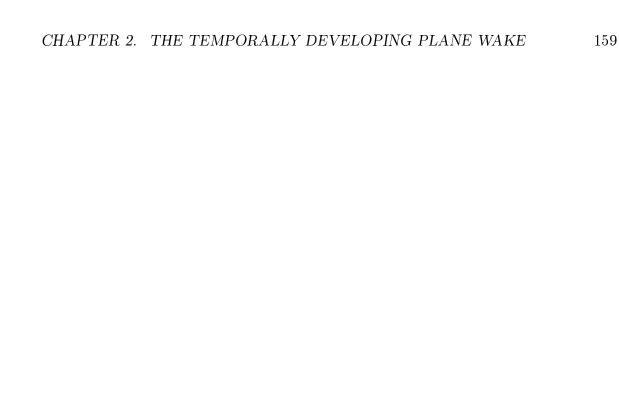


Figure 2.64: Taylor microscales of the scalar field in the x_1 -direction in the forced wake.

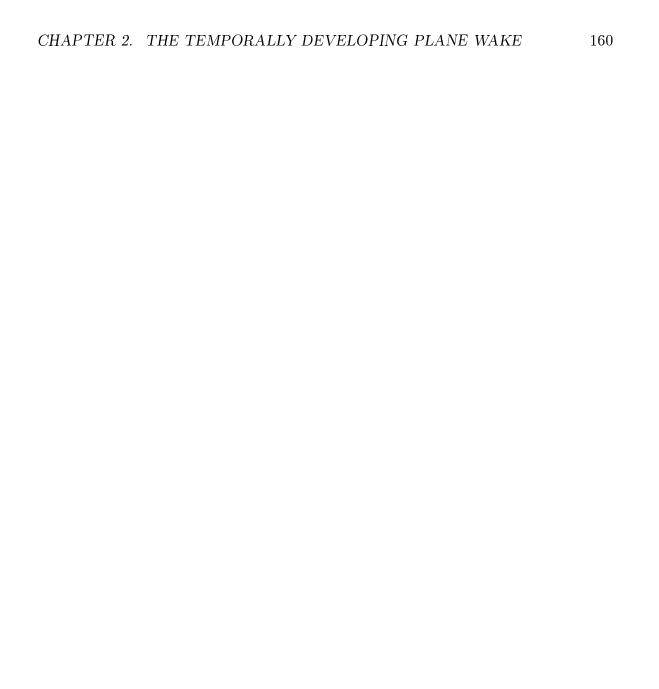


Figure 2.65: Taylor microscales of the scalar field in the x_3 -direction in the forced wake.

Chapter 3

A Constant-Reynolds-Number,
Spatially Developing Flow With a
Constant Growth Rate: The
Axisymmetric Jet

The spatially evolving, axisymmetric jet is an important flow in fluid mechanics because it is prevalent in many applications. Much of the research on this flow has been carried out in the near field of the jet (e.g., Glauser et al. 1995, Cohen and Wygnanski 1987, Sreenivasan 1983, or Zaman and Hussain 1980) since this is the region of the jet where much of the gross mixing and the production of aerodynamic noise occurs. The evolution of the flow in this region is highly dependent on the initial conditions of the jet as the velocity profile makes the transition from a velocity profile at the jet exit to the velocity profile for the fully developed jet.

As the flow evolves downstream, the jet reaches a region where the velocity profiles become similar. George (1989) demonstrated that the equations that govern the evolution of the mean velocity and the turbulent kinetic energy admit similarity solutions that are dependent on the initial conditions of the jet. (The similarity analysis applied to the individual Reynolds stress equations is included in appendix A.) The experimental measurements of Hussein *et al.* (1994) and Panchepakesan and Lumley (1993) are in excellent agreement prediction of the similarity hypothesis. In this section, the similarity analysis is extended to the equations that govern the evolution of the two-point velocity correlation tensor.

3.1 Similarity Analysis of the Two-Point Velocity Correlation Tensor

The equations that govern the evolution of the velocity correlation at two arbitrary points in space and a single time for an axisymmetric jet are given by (the analogous equation in Cartesian coordinates is reported in Hinze 1975)

$$U_{k} \frac{1}{h^{k}} \frac{\partial \overline{u_{i}u'_{j}}}{\partial x_{k}} + U'_{k} \frac{1}{h^{k\prime}} \frac{\partial \overline{u_{i}u'_{j}}}{\partial x'_{k}} + \frac{U_{2}\overline{u_{3}u'_{j}}}{x_{2}} \delta_{i3} \frac{U'_{2}\overline{u_{i}u'_{3}}}{x'_{2}} \delta_{j3} =$$

$$-\frac{1}{\rho} \frac{1}{h^{i}} \frac{\partial \overline{pu'_{j}}}{\partial x_{i}} - \frac{1}{\rho} \frac{1}{h^{j\prime}} \frac{\partial \overline{p'u_{i}}}{\partial x'_{j}} - \frac{1}{h^{k}} \frac{\partial \overline{u_{k}u_{i}u'_{j}}}{\partial x_{k}} - \frac{1}{h^{k\prime}} \frac{\partial \overline{u'_{k}u_{i}u'_{j}}}{\partial x'_{k}}$$

$$-\frac{\overline{u_{2}u_{i}u'_{j}}}{x_{2}} - \frac{\overline{u'_{2}u_{i}u'_{j}}}{x'_{2}} + \frac{\overline{u'_{3}u'_{j}}}{x_{2}} \delta_{i2} + \frac{\overline{u'_{3}u'_{i}}}{x'_{2}} \delta_{j2} - \frac{\overline{u_{2}u_{3}u'_{j}}}{x_{2}} \delta_{i3} - \frac{\overline{u'_{2}u_{i}u'_{3}}}{x'_{2}} \delta_{j3}$$

$$-\overline{u'_{j}u_{k}} \frac{\partial U_{i}}{\partial x_{k}} - \overline{u_{i}u'_{k}} \frac{\partial U'_{j}}{\partial x'_{k}} + \nu \nabla^{2} \overline{u_{i}u'_{j}} + \nu \nabla^{\prime 2} \overline{u_{i}u'_{j}}$$

$$-\nu \left(\frac{\overline{u_{2}u'_{j}}}{x_{2}^{2}} + \frac{2}{x_{2}^{2}} \frac{\partial \overline{u_{3}u'_{j}}}{\partial x_{3}} \right) \delta_{i2} - \nu \left(\frac{\overline{u_{i}u'_{2}}}{x_{2}^{2\prime}} + \frac{2}{x_{2}^{\prime 2}} \frac{\partial \overline{u_{i}u'_{3}}}{\partial x'_{3}} \right) \delta_{j2}$$

$$-\nu \left(\frac{\overline{u_3 u_j'}}{x_2^2} - \frac{2}{x_2^2} \frac{\partial \overline{u_2 u_j'}}{\partial x_3} \right) \delta_{i3} - \nu \left(\frac{\overline{u_i u_3'}}{x_2^{2'}} - \frac{2}{x_2'^2} \frac{\partial \overline{u_i u_2'}}{\partial x_3'} \right) \delta_{j3}, \tag{3.1}$$

where the prime and unprimed variables in in equation 3.1 have the same meaning as in the previous sections (v. figure 3.1), while $h^j = (1, 1, x_2)$ is the metric of the coordinate system. The value of the superscript on the metric, j, has the same value as the index of the differential coordinate next to the metric.

The objective of this analysis is to determine whether these equations admit similarity solutions for an arbitrary choice of the two points in this non-homogeneous flow. In order to answer this question, the two-point correlations in equation 3.1 are written in a form where the functional dependence is the product of two parts (analogous to the similarity solutions for the single-point equations). The first part is a scale function that depends on the position of the two points relative to the origin of the jet, while the second part is a function of the separation vector between the points and independent of the position of the two points relative to the origin of the jet. This hypothesized set of solutions are then substituted into equation 3.1 to determine if they are in fact consistent with this equation.

In this case, the scale for the similarity solution is a function of the position both points downstream of the jet origin. It must, of course, reduce to the appropriate scale for the single-point moments in the limit when the separation distance between the point is zero.

When considering the second portion of the similarity solution that is a function of the separation distance between the two points, it is important to note that the characteristic length scales of the turbulent field in the jet grow as the jet evolves downstream. In analysis of the single-point equations this is accounted for by scaling the distance in radial direction by the length scale δ . The analysis of the single-point moments also indicates that the Reynolds number of the jet based on similarity variables, $Re = U_s \delta/\nu$, is constant for the axisymmetric jet. Thus, it is reasonable to expect that all of the physical length scales of the flow, such as the integral length scales and the Kolmogorov length scale, grow in proportion as the flow evolves downstream. In this case, all of the length scales in the problem can be normalized by a single length scale. Of course, the solution for all of the statistical moments in the jet may depend on the ratio of the other length scales and the single length scale chosen to normalize the problem, but these ratios should remain constant for any particular jet.

In order to rescale the separation distances and remove the influence of the length scale growth, a new coordinate system is defined by normalizing the differential lengths of the physical coordinate system by the local length scale; *i.e.*,

$$d\xi \propto \frac{dx_1}{\delta(x_1)},\tag{3.2}$$

$$d\eta \propto \frac{dx_2}{\delta(x_1)},\tag{3.3}$$

and

$$\eta dx_3 \propto \frac{x_2 dx_3}{\delta(x_1)}.$$
(3.4)

The transformed coordinate system in the x_2 -direction is η , the same coordinate used in the single-point analysis. In addition, since the length in the azimuthal direction is contained in the metric x_2 , the coordinate x_3 is the same in both the physical and the transformed coordinate system. When the growth of the length scale δ is linear, the transformed coordinate in the mean flow direction is given by

$$\xi = \ln\left(\frac{x_1 - x_1^v}{l}\right),\tag{3.5}$$

where l is a constant with units of length (included for dimensional reasons) and x_1^v is the location of the virtual origin of the jet. This transformation converts the streamwise coordinate in the jet from a semi-infinite coordinate, x_1 , into a coordinate ξ that is infinite in extent.

For functions that depend on two different positions in this new coordinate, say ξ and ξ' , it is useful to define two new coordinates given by

$$\varpi = \xi + \xi' \tag{3.6}$$

and

$$v = \xi - \xi' = \ln\left(\frac{x_1 - x_1^v}{x_1' - x_1^v}\right). \tag{3.7}$$

Since the second portion of the hypothesized similarity solution must be independent of the position of the two points relative to the jet origin in the transformed coordinate (by definition), it follows that this portion of the similarity solution must be a function of the variable v.

Thus, the hypothesized solutions for the two-point correlations are given by

$$\overline{u_i u_i'} = Q^{i,j}(x_1, x_1') q_{i,j}(v, \eta, \eta', \theta), \tag{3.8}$$

$$\overline{u_k u_i u_j'} = T_1^{ki,j}(x_1, x_1') t_{ki,j}^1(v, \eta, \eta', \theta), \tag{3.9}$$

$$\overline{u_k'u_iu_j'} = T_2^{i,kj}(x_1, x_1')t_{i,kj}^2(v, \eta, \eta', \theta), \tag{3.10}$$

$$\overline{pu_{i}'} = \Pi_{1}^{j}(x_{1}, x_{1}')\pi_{i}^{1}(v, \eta, \eta', \theta), \tag{3.11}$$

and

$$\overline{p'u_i} = \Pi_2^i(x_1, x_1') \pi_i^2(v, \eta, \eta', \theta). \tag{3.12}$$

The mixed coordinate notation in these equations (i.e. x_1 , x'_1 , and v) is included to facilitate the comparison between the scales for the two-point correlation and the relevant scales for the single-point moments (since $Q^{i,j}$, $T_1^{ki,j}$, and $T_2^{i,kj}$ must reduce to the scale for the appropriate single-point moments in the limit of zero separation distance).

Substituting these solutions, the similarity solution for the mean velocity profile given by

$$U_1(x_1, x_2) = U_s(x_1) f(\eta), \tag{3.13}$$

and the solution for $U_2(x_1, x_2)$ (v. App. A) into the equations for the two-point correlation tensor (eqn. 3.1) yields

$$\left[U_s(x_1) \frac{\partial Q^{i,j}}{\partial x_1} \right] f(\eta) q_{i,j} + \left[\frac{Q^{i,j}U_s(x_1)}{x_1} \right] \left\{ f(\eta) \frac{\partial q_{i,j}}{\partial v} - \left(\frac{\partial q_{i,j}}{\partial \eta} + \frac{q_{3,j}}{\eta} \delta_{i3} \right) \frac{1}{\eta} \int_0^{\eta} \tilde{\eta} f(\tilde{\eta}) d\tilde{\eta} \right. \\ \left. + f(\eta) q_{3,j} \delta_{i3} \right\} + \left[U_s(x_1') \frac{\partial Q^{i,j}}{\partial x_1'} \right] f(\eta') q_{i,j} + \\ \left[\frac{Q^{i,j}U_s(x_1')}{x_1'} \right] \left\{ - f(\eta') \frac{\partial q_{i,j}}{\partial v} - \left(\frac{\partial q_{i,j}}{\partial \eta'} + \frac{q_{i,3}}{\eta'} \delta_{j3} \right) \frac{1}{\eta'} \int_0^{\eta'} \tilde{\eta} f(\tilde{\eta}) d\tilde{\eta} + f(\eta') q_{i,3} \delta_{j3} \right\} = \\ - \frac{1}{\rho} \left\{ \left[\frac{\partial \Pi_1^j}{\partial x_1} \right] \pi_1^j \delta_{i1} + \left[\frac{\Pi_1^j}{x_1} \right] \left(- \eta \frac{\partial \pi_1^j}{\partial \eta} + \frac{\partial \pi_1^j}{\partial v} \right) \delta_{i1} - \left[\frac{\Pi_1^j}{\delta(x_1)} \right] \left(\frac{\partial \pi_1^j}{\partial \eta} \delta_{i2} + \frac{1}{\eta} \frac{\partial \pi_1^j}{\partial \theta} \delta_{i3} \right) \right\} \\ - \frac{1}{\rho} \left\{ \left[\frac{\partial \Pi_2^i}{\partial x_1'} \right] \pi_i^2 \delta_{j1} + \left[\frac{\Pi_1^i}{x_1'} \right] \left(- \eta' \frac{\partial \pi_i^2}{\partial \eta'} - \frac{\partial \pi_i^2}{\partial v} \right) \delta_{j1} - \left[\frac{\Pi_2^i}{\delta(x_1')} \right] \left(\frac{\partial \pi_i^2}{\partial \eta'} \delta_{j2} - \frac{1}{\eta'} \frac{\partial \pi_i^2}{\partial \theta} \delta_{j3} \right) \right\} \\ - \left[\frac{\partial T_1^{1i,j}}{\partial x_1} \right] t_{1i,j}^1 + \left[\frac{T_1^{1i,j}}{x_1} \right] \left(+ \eta \frac{\partial t_{1i,j}^1}{\partial \eta} - \frac{\partial t_{1i,j}^1}{\partial v} \right) - \left[\frac{T_1^{2i,j}}{\delta(x_1)} \right] \frac{1}{\eta} \frac{\partial \eta' t_{2i,j}^2}{\partial \eta} - \left[\frac{T_1^{2i,j}}{\delta(x_1')} \right] \frac{1}{\eta'} \frac{\partial t_{3i,j}^2}{\partial \eta'} + \left[\frac{T_2^{2i,j}}{\delta(x_1')} \right] \frac{1}{\eta'} \frac{\partial t_{2i,j}^2}{\partial \eta'} \\ + \left[\frac{T_1^{33,j}}{\delta(x_1')} \right] \frac{t_{13,j}^1}{\eta} \delta_{i2} - \left[\frac{T_1^{23,j}}{\delta(x_1)} \right] \frac{t_{23,j}^1}{\eta} \delta_{i3} + \left[\frac{T_2^{2i,33}}{\delta(x_1')} \right] \frac{t_{23,3}^2}{\eta'} \delta_{j2} - \left[\frac{T_2^{2i,23}}{\delta(x_1')} \right] \frac{t_{23,3}^2}{\eta'} \delta_{j3}$$

$$-\left\{-\left[\frac{Q^{1,j}U_s(x_1)}{x_1}\right]q_{1,j}\left(f(\eta)+\eta\frac{df}{d\eta}\right)+\left[\frac{Q^{2,j}U_s(x_1)}{\delta(x_1)}\right]q_{2,j}\frac{df}{d\eta}\right\}\delta_{i1}+\right.$$

$$\left\{\left[\frac{Q^{1,j}U_s(x_1)}{x_1}\frac{d\delta}{dx_1}\right]q_{1,j}\left(\eta f(\eta)+\eta^2\frac{df}{d\eta}\right)-\left[\frac{Q^{2,j}U_s(x_1)}{x_1}\right]q_{2,j}\left(\eta\frac{df}{d\eta}+\frac{1}{\eta^2}\int\limits_0^{\eta}\tilde{\eta}fd\tilde{\eta}\right)\right\}\delta_{i2}$$

$$-\left\{-\left[\frac{Q^{i,1}U_s(x_1')}{x_1'}\right]q_{i,1}\left(f(\eta')+\eta'\frac{df}{d\eta'}\right)+\left[\frac{Q^{i,2}U_s(x_1')}{\delta(x_1')}\right]q_{i,2}\frac{df}{d\eta'}\right\}\delta_{j1}+\right.$$

$$\left\{\left[\frac{Q^{i,1}U_s(x_1')}{x_1'}\frac{d\delta}{dx_1'}\right]q_{i,1}\left(\eta'f(\eta')+\eta'^2\frac{df}{d\eta'}\right)-\left[\frac{Q^{i,2}U_s(x_1')}{x_1'}\right]q_{i,2}\left(\eta'\frac{df}{d\eta'}+\frac{1}{\eta'^2}\int\limits_0^{\eta'}\tilde{\eta}fd\tilde{\eta}\right)\right\}\delta_{j2}$$

$$+\nu\left\{\left[\frac{\partial^2Q^{i,j}}{\partial x_1^2}\right]q_{i,j}+\left[\frac{2Q^{i,j}}{x_1^2}-\frac{2}{x_1}\frac{\partial Q^{i,j}}{\partial x_1}\right]\eta\frac{\partial q_{i,j}}{\partial \eta}+\left[\frac{2}{x_1}\frac{\partial Q^{i,j}}{\partial x_1}-\frac{Q^{i,j}}{x_1^2}\right]\frac{\partial q_{i,j}}{\partial v}-\left[\frac{2Q^{i,j}}{x_1^2}\right]\eta\frac{\partial^2 q_{i,j}}{\partial \eta\partial v}$$

$$+\left[\frac{Q^{i,j}}{x_1^2}\right]\left(\eta^2\frac{\partial^2 q_{i,j}}{\partial \eta^2}+\frac{\partial^2 q_{i,j}}{\partial v^2}\right)+\left[\frac{Q^{i,j}}{\delta^2(x_1)}\right]\left(\frac{1}{\eta}\frac{\partial}{\eta}\eta\frac{\partial q_{i,j}}{\partial \eta}+\frac{1}{\eta^2}\frac{\partial^2 q_{i,j}}{\partial \theta^2}\right)\right\}$$

$$-\nu\left\{\left[\frac{Q^{2,i,j}}{\delta^2(x_1)}\right]\frac{q_{2,j}}{\eta^2}+\left[\frac{2Q^{3,j}}{\delta^2(x_1)}\right]\frac{\partial q_{3,j}}{\eta^2}\right\}\delta_{i2}-\nu\left\{\left[\frac{Q^{3,j}}{\delta^2(x_1)}\right]\frac{q_{3,j}}{\eta^2}-\left[\frac{2Q^{2,j}}{\delta^2(x_1)}\right]\frac{1}{\eta^2}\frac{\partial q_{2,j}}{\partial \theta}\right\}\delta_{i3}$$

$$+\nu\left\{\left[\frac{\partial^2Q^{i,j}}{\partial x_1'^2}\right]q_{i,j}+\left[\frac{2Q^{i,j}}{x_1'^2}-\frac{2}{x_1'}\frac{\partial Q^{i,j}}{\partial x_1'}\right]\eta'\frac{\partial q_{i,j}}{\partial \eta'}-\left[\frac{2}{x_1'}\frac{\partial Q^{i,j}}{\partial x_1'}-\frac{Q^{i,j}}{x_1'^2}\right]\frac{\partial q_{i,j}}{\partial v}+\left[\frac{2Q^{i,j}}{x_1'^2}\right]\eta'\frac{\partial^2 q_{i,j}}{\partial \eta'\partial v}$$

$$+\frac{Q^{i,j}}{x_1'^2}\left(\eta^2\frac{\partial^2 q_{i,j}}{\partial \eta'^2}+\frac{\partial^2 q_{i,j}}{\partial v^2}\right)+\left[\frac{Q^{i,j}}{\delta^2(x_1')}\right]\left(\frac{1}{\eta'}\frac{\partial}{\eta'\eta'}\frac{\partial q_{i,j}}{\partial \eta'}+\frac{1}{\eta'^2}\frac{\partial^2 q_{i,j}}{\partial \theta^2}\right)\right\}$$

$$-\nu\left\{\left[\frac{Q^{i,2}}{\partial^2(x_1')}\right]\frac{q_{i,2}}{\eta^2}-\left[\frac{2Q^{i,3}}{\delta^2(x_1')}\right]\frac{1}{\eta'^2}\frac{\partial q_{i,3}}}{\partial \theta^2}\right\}\delta_{j2}-\nu\left\{\left[\frac{Q^{i,3}}{\delta^2(x_1')}\right]\frac{q_{i,3}}{\eta'^2}+\left[\frac{2Q^{i,2}}{\delta^2(x_1')}\right]\frac{1}{\eta'^2}\frac{\partial q_{i,2}}{\partial \theta^2}\right\}\delta_{j3}$$

$$(3.14)$$

This expression has been simplified by defining the origin of the coordinate system in physical space to be at the virtual origin of the jet and using the relationships

$$\frac{1}{\delta} \frac{d\delta}{dx_1} = \frac{1}{x_1} \tag{3.15}$$

and

$$\frac{1}{U_s} \frac{dU_s}{dx_1} = \frac{-1}{x_1},\tag{3.16}$$

which are valid for this flow (since the growth rate and Reynolds number are constant).

The portion of each term in equation 3.14 that is dependent on the position of the two points relative to the virtual origin of the flow is included in square brackets. Equation 3.14 can be reduced to an equations in terms of the similarity variables if it is possible to choose the scale functions $(Q^{i,j} \ etc.)$ so the ratio of the terms in the square brackets are only a function of v, the separation distance between the points in the transformed coordinate system.

A close examination of equation 3.14 reveals that the functions in the square brackets can be easily divided into two groups. The terms in each of these groups are proportional if the terms satisfy constraints analogous to the constraints outlined for the single-point equations. The constraints for the first group are given by

$$\left[U_{s}(x_{1})\frac{\partial Q^{i,j}}{\partial x_{1}}\right] \propto \left[\frac{Q^{i,j}U_{s}(x_{1})}{x_{1}}\right] \propto \left\{\left[\frac{\partial \Pi_{1}^{j}}{\partial x_{1}}\right] \propto \left[\frac{\Pi_{1}^{j}}{x_{1}}\right]\right\} \delta_{i1}$$

$$\propto \left[\frac{\Pi_{1}^{j}}{\delta(x_{1})}\right] \left(\delta_{i2} + \delta_{i3}\right) \propto \left[\frac{\partial T_{1}^{1i,j}}{\partial x_{1}}\right] \propto \left[\frac{T_{1}^{1i,j}}{x_{1}}\right] \propto \left[\frac{T_{1}^{2i,j}}{\delta(x_{1})}\right] \propto \left[\frac{T_{1}^{3i,j}}{\delta(x_{1})}\right] \propto \left[\frac{Q^{2,j}U_{s}(x_{1})}{\delta(x_{1})}\right] \delta_{i1} \propto \left\{\left[\frac{Q^{1,j}U_{s}(x_{1})}{x_{1}}\frac{d\delta}{dx_{1}}\right] \propto \left[\frac{Q^{2,j}U_{s}(x_{1})}{x_{1}}\right]\right\} \delta_{i2} \propto \nu \left\{\left[\frac{\partial^{2}Q^{i,j}}{\partial x_{1}^{2}}\right] \propto \left[\frac{2Q^{i,j}}{x_{1}^{2}}\right] \propto \left[\frac{Q^{i,j}}{\delta^{2}(x_{1})}\right]\right\} \delta_{i2} \propto \nu \left\{\left[\frac{Q^{3,j}}{\delta^{2}(x_{1})}\right]\right\} \delta_{i3} \qquad (3.17)$$

and the constraints for the second group are given by

$$\left[U_{s}(x_{1}')\frac{\partial Q^{i,j}}{\partial x_{1}'}\right] \propto \left[\frac{Q^{i,j}U_{s}(x_{1}')}{x_{1}'}\right] \propto \left\{\left[\frac{\partial \Pi_{2}^{i}}{\partial x_{1}'}\right] \propto \left[\frac{\Pi_{2}^{i}}{x_{1}'}\right]\right\} \delta_{j1} \propto$$

$$\left[\frac{\Pi_{2}^{i}}{\delta(x_{1}')}\right] (\delta_{j2} + \delta_{j3}) \propto \left[\frac{\partial T_{2}^{i,1j}}{\partial x_{1}'}\right] \propto \left[\frac{T_{2}^{i,1j}}{x_{1}'}\right] \propto \left[\frac{T_{2}^{i,2j}}{\delta(x_{1}')}\right] \propto \left[\frac{T_{2}^{i,3j}}{\delta(x_{1}')}\right] \propto$$

$$\left\{\left[\frac{Q^{1,j}U_{s}(x_{1}')}{x_{1}'}\right] \propto \left[\frac{Q^{i,2}U_{s}(x_{1}')}{\delta(x_{1}')}\right]\right\} \delta_{j1} \propto \left\{\left[\frac{Q^{i,1}U_{s}(x_{1}')}{x_{1}'}\frac{d\delta}{dx_{1}}\right] \propto \left[\frac{Q^{i,2}U_{s}(x_{1}')}{x_{1}'}\right]\right\} \delta_{j2} \propto$$

$$\nu \left\{ \left[\frac{\partial^{2} Q^{i,j}}{\partial x_{1}^{\prime 2}} \right] \propto \left[\frac{2Q^{i,j}}{x_{1}^{\prime 2}} \right] \propto \left[\frac{2}{x_{1}^{\prime}} \frac{\partial Q^{i,j}}{\partial x_{1}^{\prime}} \right] \propto \left[\frac{Q^{i,j}}{\delta^{2}(x_{1}^{\prime})} \right] \right\} \propto$$

$$\nu \left\{ \left[\frac{Q^{i,2}}{\delta^{2}(x_{1}^{\prime})} \right] \propto \left[\frac{Q^{i,3}}{\delta^{2}(x_{1}^{\prime})} \right] \right\} \delta_{j2} \propto \left\{ \left[\frac{Q^{i,3}}{\delta^{2}(x_{1}^{\prime})} \right] \propto \left[\frac{Q^{i,2}}{\delta^{2}(x_{1}^{\prime})} \right] \right\} \delta_{j3}. \tag{3.18}$$

Examining the first two terms in equations 3.17 and 3.18 (and the consistency condition for zero separation) leads to the choice of the scale for the two-point velocity correlation tensor, $Q^{i,j}$, given by

$$Q^{i,j} = U_s(x_1)U_s(x_1')\frac{d\delta}{dx_1}^{b(i,j)},$$
(3.19)

where b(i, j) is a numerical power which may be a function of the value of i and j. The function b(i, j) must be chosen so the scales for the two-point velocity correlation tensor are consistent with the scales chosen for the single-point moments. However, neither the two-point nor the single-point analyses yield sufficient information to uniquely determine the values of b(i, j).

Once the scale $Q^{i,j}$ is chosen, all of the other scales can be determined. These are given by

$$T_1^{1i,j} \propto U_s(x_1)Q^{i,j},$$
 (3.20)

$$T_1^{2i,j} \propto T_1^{3i,j} \propto U_s(x_1) Q^{i,j} \frac{d\delta}{dx_1},$$
 (3.21)

$$T_2^{i,1j} \propto U_s(x_1')Q^{i,j},$$
 (3.22)

$$T_2^{i,2j} \propto T_2^{i,3j} \propto U_s(x_1') Q^{i,j} \frac{d\delta}{dx_1},$$
 (3.23)

$$\Pi_1^j \propto U_s(x_1)Q^{i,j},\tag{3.24}$$

and

$$\Pi_2^i \propto U_s(x_1')Q^{i,j},\tag{3.25}$$

where growth rate terms are included in the scales when the equations indicate they are appropriate.

The scales for the viscous terms in equation 3.14 are only proportional to each other if the growth rate of the jet is constant (for the current choice of transformed streamwise coordinate)¹ In addition, the viscous terms in each group of constraints are only proportional to the convective terms if

$$\frac{U_s(x_1)Q^{i,j}}{x_1} \propto \nu \frac{Q^{i,j}}{x_1^2} \tag{3.26}$$

or

$$\frac{U_s(x_1)x_1}{\nu} \propto \frac{U_s\delta}{\nu} \propto const \tag{3.27}$$

since the growth rate of the jet is a constant. Thus, the Reynolds number of the jet based on the similarity variables must be a constant in order for the full equations to admit similarity solutions.

It is straightforward to demonstrate that both groups of constraints in equations 3.17 and 3.18 are satisfied when the scales are chosen as defined in equations 3.19-3.25. In addition, the ratio of the terms from the two groups in equation 3.17 and 3.18 is given by

$$\frac{Q^{i,j}U_s(x_1)}{x_1} \frac{x_1'}{Q^{i,j}U_s(x_1')} \propto \frac{x_1'^2}{x_1^2} = e^{-2v}, \tag{3.28}$$

which is a function of only v, as required. Therefore, when the scales are chosen as in equations 3.19-3.25, it follows that the governing equations for the two-point velocity

¹The transformed coordinate in the x_1 direction could have been chosen differently, say $v^n = (d\delta/dx)^{-1} \ln(x_1/x_1')$, which would have made all of the viscous terms proportional, but all of the convective terms in this formulation would only be proportional if the growth rate of the jet were constant. Thus, for either coordinate system the growth rate of the jet would need to be constant.

correlation tensor admit similarity solutions.

For example, if the scales for $Q^{i,j}$ are defined as

$$Q^{3,3} = Q^{2,2} = Q^{1,1} \left(\frac{d\delta}{dx_1}\right)^2 = U_s(x_1) U_s(x_1') \left(\frac{d\delta}{dx_1}\right)^2, \tag{3.29}$$

$$Q^{3,2} = Q^{2,3} = U_s(x_1)U_s(x_1') \left(\frac{d\delta}{dx_1}\right)^2, \tag{3.30}$$

and

$$Q^{1,2} = Q^{2,1} = Q^{3,1} = Q^{1,3} = U_s(x_1)U_s(x_1')\frac{d\delta}{dx_1},$$
(3.31)

the constants of proportionality in equations 3.20-3.23 are taken as unity, and the scales for the pressure-velocity correlations are defined as

$$\Pi_1^j = U_s^2(x_1)U_s(x_1') \tag{3.32}$$

and

$$\Pi_2^i = U_s(x_1)U_s^2(x_1'), \tag{3.33}$$

then it follows that equation 3.14 can be rewritten as

$$\begin{split} e^{-v} \left[-f(\eta)q_{i,j} + f(\eta)\frac{\partial q_{i,j}}{\partial v} - \left(\frac{\partial q_{i,j}}{\partial \eta} + \frac{q_{3,j}}{\eta}\delta_{i3}\right) \frac{1}{\eta} \int_{0}^{\eta} \tilde{\eta}f(\tilde{\eta})d\tilde{\eta} + f(\eta)q_{3,j}\delta_{i3} \right] \\ e^{v} \left[-f(\eta')q_{i,j} - f(\eta')\frac{\partial q_{i,j}}{\partial v} - \left(\frac{\partial q_{i,j}}{\partial \eta'} + \frac{q_{i,3}}{\eta'}\delta_{j3}\right) \frac{1}{\eta'} \int_{0}^{\eta'} \tilde{\eta}f(\tilde{\eta})d\tilde{\eta} + f(\eta')q_{i,3}\delta_{j3} \right] = \\ + \frac{e^{-v}}{\rho} \left(\frac{d\delta}{dx_{1}}\right)^{-b(i,j)} \left\{ \left[2\pi_{j}^{1} + \eta \frac{\partial p_{j}^{1}}{\partial \eta} - \frac{\partial p_{j}^{1}}{\partial v} \right] \delta_{i1} - \left(\frac{d\delta}{dx_{1}}\right)^{-1} \left[\frac{\partial \pi_{j}^{1}}{\partial \eta}\delta_{i2} + \frac{1}{\eta} \frac{\partial \pi_{j}^{1}}{\partial \theta}\delta_{i3} \right] \right\} \\ + \frac{e^{v}}{\rho} \left(\frac{d\delta}{dx_{1}}\right)^{-b(i,j)} \left\{ \left[2\pi_{i}^{2} + \eta \frac{\partial p_{i}^{2}}{\partial \eta'} + \frac{\partial p_{j}^{1}}{\partial v} \right] \delta_{j1} - \left(\frac{d\delta}{dx_{1}}\right)^{-1} \left[\frac{\partial \pi_{i}^{2}}{\partial \eta'}\delta_{j2} - \frac{1}{\eta'} \frac{\partial \pi_{i}^{2}}{\partial \theta}\delta_{j3} \right] \right\} \\ + e^{-v} \left[2t_{1i,j}^{1} + \eta \frac{\partial t_{1i,j}^{1}}{\partial \eta} - \frac{\partial t_{1i,j}^{1}}{\partial v} - \frac{1}{\eta} \frac{\partial \eta t_{2i,j}^{1}}{\partial \eta} - \frac{1}{\eta} \frac{\partial t_{3i,j}^{1}}{\partial \theta} + \frac{t_{33,j}^{1}}{\eta} \delta_{i2} - \frac{t_{23,j}^{1}}{\eta} \delta_{i3} \right] \end{split}$$

$$+e^{v}\left[2t_{i,1j}^{2}+\eta'\frac{\partial t_{i,1j}^{2}}{\partial\eta'}+\frac{\partial t_{i,1j}^{2}}{\partial\upsilon}-\frac{1}{\eta'}\frac{\partial\eta't_{i,2j}^{2}}{\partial\eta'}+\frac{1}{\eta'}\frac{\partial t_{i,3j}^{2}}{\partial\theta}+\frac{t_{i,33}^{2}}{\eta'}\delta_{j2}-\frac{t_{i,23}^{1}}{\eta'}\delta_{j3}\right]$$

$$+e^{-v}\left[\left\{q_{1,j}\left(f(\eta)+\eta\frac{df}{d\eta}\right)-q_{2,j}\frac{df}{d\eta}\right\}\delta_{i1}+\left\{q_{1,j}\left(\eta f(\eta)+\eta^{2}\frac{df}{d\eta}\right)-q_{2,j}\frac{df}{d\eta}\right\}\delta_{i1}+\left\{q_{i,j}\left(\eta f(\eta)+\eta^{2}\frac{df}{d\eta'}\right)-q_{i,2}\frac{df}{d\eta'}\right\}\delta_{j1}\right]$$

$$+\left\{q_{i,1}\left(\eta' f(\eta')+\eta'^{2}\frac{df}{d\eta'}\right)-q_{i,2}\left(\eta'\frac{df}{d\eta'}+\frac{1}{\eta'^{2}}\int_{0}^{\eta'}\tilde{\eta}fd\tilde{\eta}\right)\right\}\delta_{j2}\right]$$

$$e^{-v}\left[\frac{1}{Re_{\delta}}\frac{d\delta}{dx_{1}}\right]\left[2q_{i,j}+4\eta\frac{\partial q_{i,j}}{\partial\eta}-3\frac{\partial q_{i,j}}{\partial\upsilon}-2\eta\frac{\partial^{2}q_{i,j}}{\partial\eta\partial\upsilon}+\eta^{2}\frac{\partial^{2}q_{i,j}}{\partial\eta^{2}}+\frac{\partial^{2}q_{i,j}}{\partial\upsilon^{2}}\right]$$

$$e^{-v}\left[\frac{1}{Re_{\delta}}\left(\frac{d\delta}{dx_{1}}\right)^{-1}\right]\left\{\frac{1}{\eta}\frac{\partial}{\partial\eta}\eta\frac{\partial q_{i,j}}{\partial\eta}+\frac{1}{\eta^{2}}\frac{\partial^{2}q_{i,j}}{\partial\theta^{2}}-\left(\frac{q_{2,j}}{\eta^{2}}+2\frac{1}{\eta^{2}}\frac{\partial q_{3,j}}{\partial\theta}\right)\delta_{i2}\right\}$$

$$-\left(\frac{q_{3,j}}{\eta^{2}}-2\frac{1}{\eta^{2}}\frac{\partial q_{2,j}}{\partial\theta}\right)\delta_{i3}\right\}$$

$$e^{v}\left[\frac{1}{Re_{\delta}}\left(\frac{d\delta}{dx_{1}}\right)^{-1}\right]\left\{\frac{1}{\eta'}\frac{\partial}{\partial\eta'}\eta'\frac{\partial q_{i,j}}{\partial\eta'}+\frac{1}{\eta'^{2}}\frac{\partial^{2}q_{i,j}}{\partial\theta^{2}}-\left(\frac{q_{i,2}}{\eta'^{2}}-2\frac{1}{\eta'^{2}}\frac{\partial q_{i,j}}{\partial\eta'^{2}}+\frac{\partial^{2}q_{i,j}}{\partial\upsilon^{2}}\right)\delta_{i2}\right\}$$

$$-\left(\frac{q_{i,3}}{\eta'^{2}}+2\frac{1}{\eta'^{2}}\frac{\partial q_{i,j}}{\partial\theta^{2}}-\left(\frac{q_{i,2}}{\eta'^{2}}-2\frac{1}{\eta'^{2}}\frac{\partial q_{i,j}}{\partial\theta}\right)\delta_{i2}\right\}$$

$$-\left(\frac{q_{i,3}}{\eta'^{2}}+2\frac{1}{\eta'^{2}}\frac{\partial^{2}q_{i,j}}{\partial\theta^{2}}-\left(\frac{q_{i,2}}{\eta'^{2}}-2\frac{1}{\eta'^{2}}\frac{\partial q_{i,3}}{\partial\theta}\right)\delta_{i2}$$

$$-\left(\frac{q_{i,3}}{\eta'^{2}}+2\frac{1}{\eta'^{2}}\frac{\partial^{2}q_{i,j}}{\partial\theta^{2}}-\left(\frac{q_{i,2}}{\eta'^{2}}-2\frac{1}{\eta'^{2}}\frac{\partial q_{i,3}}{\partial\theta}\right)\delta_{i2}\right\}$$

If this equation has a non-trivial solution, then the equations for the two-point velocity correlation tensor admit similarity solutions.

With some additional effort it can be shown that these solutions maintain two important properties: First the correlation is Hermitian; *i.e.*,

$$\overline{u_i u_j^{\prime *}} = \overline{u_i u_j^{\prime *}}^* \tag{3.35}$$

Second, the solution has the appropriate reflective properties in the azimuthal direction; i.e.,

$$Q^{i,j}(x_1, x_1')q_{i,j}(\eta, \eta', \theta, v) = Q^{i,j}(x_1, x_1')q_{i,j}(\eta, \eta', -\theta, v) \begin{cases} i \cap j \neq 3 \\ i \cap j = 3 \end{cases}$$
(3.36)

and

$$Q^{i,j}(x_1, x_1')q_{i,j}(\eta, \eta^p r, \theta, v) = -Q^{i,j}(x_1, x_1')q_{i,j}(\eta, \eta', -\theta, v) \begin{cases} i \cup j = 3 \\ \text{but not both.} \end{cases}$$
(3.37)

The similarity analysis of the two-point equations was carried out using a virtual origin to replace the flow exit, so the similarity solution defined by equation 3.34 must be viewed as a possible asymptotic state of the turbulence in a jet. However, this does not necessarily imply that an unique asymptotic state exists for all axisymmetric jets. Some of the coefficients in equation 3.34 have an explicit dependence on both the growth rate and the Reynolds number of the jet. There is no obvious technique to eliminate both of these factors from the equations for the similarity profiles,² so the solutions may be dependent on source conditions of the jet, to the extent that the source conditions affect the value of Reynolds number and the growth rate of the jet.

²It is important to note that the choice for the length and velocity scale are not totally arbitrary if one wishes to demonstrate that the similarity state for the jet is universal. It is necessary to choose the length and velocity scale such that they collapse mean velocity profile for different jets. For example, the length scale of the jet can be interpreted as the growth rate of the half-mean velocity point in the jet.

3.2 The Pressure Field

Since the two-point velocity information is now available in similarity form, it is also possible to examine the pressure field generated in the self-similar region to verify if it yields a pressure-velocity correlation consistent with the hypothesized similarity solution. For an incompressible free-shear flow, it is possible to demonstrate that the instantaneous fluctuating pressure field (i.e., the instantaneous pressure minus the mean pressure) is related to the velocity field (excluding the singularity at the virtual origin of the flow) by the expression (v., Townsend, 1956 for the expression in Cartesian coordinates)

$$\frac{p}{\rho} = -\frac{1}{4\pi} \int \int \left\{ \frac{2}{h^{l''}} \frac{\partial U_k''}{\partial x_l''} \frac{1}{h^{k''}} \frac{\partial u_l''}{\partial x_k''} + 2 \frac{U_2'' u_2''}{x_2''^2} + 2 \frac{U_2''}{x_2''^2} \frac{\partial u_3''}{\partial x_3''} \right\}
= \frac{x_2'' dx_3'' dx_2'' dx_1''}{\left\{ x_2^2 + x_2''^2 - 2x_2 x_2'' \cos(x_3 - x_3'') + (x_1 - x_1'')^2 \right\}^{1/2}}
- \frac{1}{4\pi} \int \int \int \left\{ \frac{1}{h^{l''}} \frac{1}{h^{k''}} \frac{\partial}{\partial x_l''} \frac{\partial}{\partial x_k''} \left(u_k'' u_l'' - \overline{u_k'' u_l''} \right) \right\}
+ \frac{2}{x_2''} \frac{1}{h^{k''}} \frac{\partial}{\partial x_k''} \left(u_2'' u_k'' - \overline{u_2'' u_k''} \right) - \frac{1}{x_2''} \frac{\partial}{\partial x_2''} \left(u_3'' u_3'' - \overline{u_3'' u_3''} \right) \right\}
= \frac{x_2'' dx_3'' dx_2'' dx_1''}{\left\{ x_2^2 + x_2''^2 - 2x_2 x_2'' \cos(x_3 - x_3'') + (x_1 - x_1'')^2 \right\}^{1/2}}, \tag{3.38}$$

where the integration is carried out over the domain excluding the virtual origin (for example, using a cut along the $-x_1$ axis). The fluctuating pressure field also includes a contribution from the surface around the singularity.

The contribution of the pressure determined from the flow in the volume in equation 3.38 to the pressure velocity correlation is given by

$$\frac{\overline{pu_k'}}{\rho} = -\frac{1}{4\pi} \int \int \int \left\{ \frac{2}{h^{l\prime\prime}} \frac{\partial U_k''}{\partial x_l''} \frac{1}{h^{k\prime\prime}} \frac{\partial \overline{u_j' u_l''}}{\partial x_k''} + 2 \frac{U_2'' \overline{u_j' u_2''}}{x_2''^2} + 2 \frac{U_2''}{x_2''^2} \frac{\partial \overline{u_j' u_3''}}{\partial x_3''} \right\}$$

$$\frac{x_2'' \, dx_3'' \, dx_2'' \, dx_1''}{\left\{x_2^2 + x_2''^2 - 2x_2 x_2'' \cos(x_3 - x_3'') + (x_1 - x_1'')^2\right\}^{1/2}}$$

$$\frac{1}{4\pi} \int \int \int \left\{ \frac{1}{h^{ll'}} \frac{\partial}{\partial x_l''} \frac{1}{h^{kl''}} \frac{\partial}{\partial x_k''} \frac{u_j' u_k'' u_l''}{u_j' u_k'' u_l''} + \frac{2}{x_2''} \frac{1}{h^{kl''}} \frac{\partial}{\partial x_k''} \frac{u_j' u_2'' u_k''}{u_j' u_2'' u_k''} \right.$$

$$\left. - \frac{1}{x_2''} \frac{\partial}{\partial_3^3 \prime \prime} \left(\overline{u_j' u_3'' u_3''} \right) \right\} \frac{x_2'' \, dx_3'' \, dx_2'' \, dx_3''}{\left\{x_2^2 + x_2''^2 - 2x_2 x_2'' \cos(x_3 - x_3'') + (x_1 - x_1^{pp})^2\right\}^{1/2}}$$
(3.39)

where the integration is again carried out over a volume excluding the singularity at the virtual origin. This domain can be split into two regions: The region described by the similarity variables which includes the flow on the positive side of the x_1 -axis (taking the virtual origin at the origin of the coordinate system with the jet flowing in the positive direction). And, the region behind the virtual origin that cannot be described by the similarity coordinate system because it becomes singular at the virtual origin of the jet.

The contribution of the self-similar region to the pressure-velocity correlation can be determined by substituting the hypothesized solution for the two-point correlation tensor defined in equation 3.19 into equation 3.39. For example, the similarity form of $\overline{u'_i u''_k}$ given by

$$\overline{u_j'u_k''} = Q_{j,k}(x_1', x_1'')q_{j,k}(\eta', \eta'', x_3' - x_3'', \xi' - \xi'')$$
(3.40)

can be rewritten as

$$q_{j,k}(\eta', \eta'', x_3' - x_3'', \xi' - \xi'') = q_{j,k}(\eta', \eta'', x_3 - x_3'' - [x_3 - x_3'], \xi - \xi'' - [\xi - \xi']).$$
(3.41)

Thus, defining

$$v'' = \xi - \xi'' \tag{3.42}$$

and

$$\theta'' = x_3 - x_3'', (3.43)$$

it follows that $q_{j,k}$ can be written as

$$q_{j,k}(\eta', \eta'', x_3' - x_3'', \xi' - \xi'') = q_{j,k}''(\eta', \eta'', \theta'' - \theta, v'' - v)$$
(3.44)

The new function $q''_{j,k}$ is defined for convenience to emphasize the new manner of writing the arguments of the functions. It is also useful to define the function

$$t_{i,kl}^{2"}(\eta', \eta'', \theta'' - \theta, \upsilon'' - \upsilon) = t_{i,kl}^{2}(\eta', \eta'', x_3' - x_3'', \xi' - \xi'')$$
(3.45)

Using these definitions and the scales for the similarity solutions defined in equations 3.19, 3.22, and 3.23, the contribution of the flow in the similarity region to the pressure-velocity correlation can be written as

$$\begin{split} \overline{\frac{\rho u'_j}{\rho}} &= +\frac{1}{4\pi} \left[U_s^2(x_1) U_s(x'_1) \frac{d\delta}{dx_1}^{1+a(j)} \right] \left\{ \int \int \int e^{2v''} \left[2 \left(f'' + \eta'' \frac{df''}{d\eta''} \right) \left(\frac{\partial q''_{j,1}}{\partial v''} + \eta'' \frac{\partial q''_{j,1}}{\partial \eta''} + q''_{j,1} \right) \right. \\ & \left. - 2 \frac{df''}{d\eta''} \left(\frac{\partial q''_{j,2}}{\partial v''} + \eta'' \frac{\partial q''_{j,2}}{\partial \eta''} + q''_{j,2} \right) - 2 \left(\eta'' f'' + \eta'' \frac{d^2 f''}{d\eta''^2} \right) \frac{\partial q''_{j,1}}{\partial \eta''} \right. \\ & \left. + 2 \left(\eta'' \frac{df''}{d\eta''} + \frac{F''}{\eta^{2n}} \right) \frac{\partial q''_{j,2}}{\partial \eta''} + 2 \left(- \frac{F''}{\eta''} + \eta'' f'' \right) \frac{q''_{j,2}}{\eta''^2} \right. \\ & \left. - 2 \left(- \frac{F''}{\eta''} + \eta'' f'' \right) \frac{1}{\eta''^2} \frac{\partial q''_{k,3}}{\partial \theta''} \right] \frac{\eta'' d\theta'' d\eta'' dv''}{\left[\eta''^2 + e^{2v''} \eta^2 - 2e^{v''} \eta'' \eta \cos \theta'' + \left(d\delta / dx_1 \right) - 2 \left(1 - e^{v''} \right)^2 \right]^{1/2}} \\ & \left. - \frac{1}{4\pi} \int \int \int e^{2v''} \left[\left(6 + 3 \frac{\partial}{\partial v''} + \frac{\partial^2}{\partial v''} + 4 \eta'' \frac{\partial}{\partial \eta''} + \eta''^2 \frac{\partial^2}{\partial \eta''^2} + 2 \eta'' \frac{\partial^2}{\partial v'' \partial \eta''} \right) t''_{j,11} \right. \\ & \left. + \left(\frac{\partial^2}{\partial \eta''^2} - \frac{2}{\eta''} \frac{\partial}{\partial \eta''} \right) t''_{j,22} - 2 \left(3 \frac{\partial}{\partial \eta''} + \frac{\partial^2}{\partial v'' \partial \eta''} + \eta'' \frac{\partial^2}{\partial \eta''^2} + \frac{2}{\eta''} + \frac{1}{\eta''} \frac{\partial}{\partial v''} + \frac{\partial}{\partial \eta''} \right) t''_{j,12} \right. \\ & \left. + 2 \left(\frac{2}{\eta''} \frac{\partial}{\partial \theta''} + \frac{1}{\eta''} \frac{\partial^2}{\partial v'' \partial \theta''} + \frac{\partial^2}{\partial \eta'' \partial \theta''} \right) t''_{j,13} + \left(\frac{1}{\eta''^2} \frac{\partial}{\partial \theta''^2} - \frac{1}{\eta''} \frac{\partial}{\partial \eta''} \right) t''_{j,33} \right. \\ & \left. - \left(\frac{2}{\eta''} \frac{\partial^2}{\partial \theta''} + \frac{\partial^2}{\partial \eta'' \partial \theta''} + \frac{2}{\eta''^2} \frac{\partial}{\partial \theta''} \right) t''_{k,32} \right] \end{split}$$

$$\frac{\eta'' d\theta'' d\eta'' dv''}{\left[\eta''^2 + e^{2v''}\eta^2 - 2e^{v''}\eta''\eta\cos\theta'' + (d\delta/dx_1)^{-2}(1 - e^{2v''})\right]^{1/2}}\right\},$$
(3.46)

where a(k) is equal to 0 when k is 1 and it has a value of 1 when k is 2 or 3, while F'' is given by

$$F'' = \int_0^{\eta''} \tilde{\eta} f(\tilde{\eta}) d\tilde{\eta} \tag{3.47}$$

In this equation the singularity at the virtual origin is mapped to the line $-\infty$ is the v'' coordinate system.

In this form, equation 3.46 is now a product of a scale, given by

$$U_s(x_1)U_s(x_1')\left(\frac{d\delta}{dx_1}\right)^{1+a(k)},\tag{3.48}$$

that is consistent with that required by the previous similarity analysis and an expression that is only a function of the similarity variables v, η , η' , and θ . Thus, the similarity hypothesis is internally consistent in the sense that if the motion in the jet is consistent with a two point-similarity hypothesis, then the pressure field generated by the motion in the jet yields a pressure-velocity correlation that also satisfies the similarity hypothesis.

The essence of what has been accomplished in this analysis can be seen by looking at the velocity field in the incompressible jet kinematically as the sum of a rotational solenoidal velocity field due to the vorticity distribution in the flow and an irrotational and solenoidal field (or a potential flow) which is included to satisfy the boundary conditions (c.f. pg. 87 Batchelor 1967). (Note, in general it is also necessary to incorporate an irrotational portion due to fluid expansion.) The analysis herein examined the dynamics of the flow caused by the thin vortical region in the jet. It was demonstrated that the equations that govern the evolution of this motion admit

to an internally self-consistent similarity solution. In general, this motion may not satisfy the boundary conditions imposed on the flow, so there is an addition potential velocity field that must be added to the velocity field 'induced' by the vorticity field in order to satisfy the kinematic boundary conditions³ of the flow. In this analysis the contribution of this portion has not been considered. The non-linear terms in the Navier Stokes equations will cause coupling between these two velocity fields (in both the velocity and the pressure terms), so that, in general, the flow in the jet will not evolve self-similarly unless the potential flow necessary to satisfy the boundary conditions also evolves in accordance with a similarity solution.⁴ For the temporally evolving wake, where the similarity coordinate system covers the entire flow domain, it is evident that a fluid of infinite extent is sufficient to satisfy this condition. The same can not be proven here because the similarity coordinate system does not describe the entire flow domain. It is reasonable to argue that in theory some set of boundary conditions (probably free boundary conditions) exist that yields a flow behind the jet, whose contribution to the integral for the pressure-velocity correlation (eqn. 3.39) is consistent with the similarity hypothesis. If this is in fact true, then the equations that govern the evolution of the two-point correlation in the axisymmetric jet flow admit to a similarity solution.

This discussion also illustrates the important role that the boundary conditions of a flow play in the evolution of the flow, a point which must be considered when

³There would also need to be an adjustment of the vorticity field if the boundary condition was a no-slip condition since a potential field cannot satisfy the no-slip condition (Batchelor 1967).

⁴Note, if this coupling does not play a role in the evolution of the flow, then it would be possible to carry out a similarity analysis of the vorticity equations and argue that the evolution of the purely vortical motions in the jet were consistent with the similarity solution. This is, in general, not possible since the velocity field introduced by the boundary conditions convects the vortical motions.

comparing experimental or numerical data to theory or each other (v. Batchelor 1953, George 1990, or Grinstein 1994 for further discussion). In the present context, if the boundary conditions of the flow are not consistent with those required by the similarity theory, then the flow (particularly the large scale motions) would not be expected to evolve in accordance the similarity hypothesis. Of course, the similarity solution may still be a good approximation of the solution for the flow. This is, in fact, evident in the data from the simulations of the temporally developing wake examined in section 2.6. In these simulations of the flow, the boundary conditions are not consistent with the similarity hypothesis, yet the statistical measures of the moderate- and small-scale motions are in fairly good agreement with the prediction of the two-point similarity hypothesis.

3.3 Similarity of the Velocity-Gradient Moments

It is, again, reasonable to anticipate that other moments which are directly related to the two-point correlation tensor, such as the two-point, velocity-gradient moments have a similarity form in this case. The velocity-gradient moments are particularly important because they can be related to the dissipation of kinetic energy.

The dissipation of the kinetic energy per unit mass, ϵ , can be written as

$$\epsilon = \lim_{x_k \to x_k'} 2\nu \overline{e_{ij}} e_{ij} \tag{3.49}$$

where the e_{ij} is the rate-of-strain tensor. For a cylindrical coordinate system, the rate-of-strain tensor is given by (v. Batchelor 1967)

$$e_{ij} = \frac{1}{2} \left(\frac{1}{h^j} \frac{\partial u_i}{\partial x_j} + \frac{1}{h^i} \frac{\partial u_j}{\partial x_i} \right) + \frac{u_2}{x_2} \delta_{j3} \delta_{i3} - \frac{1}{2} \frac{u_3}{x_2} \left[\delta_{i2} \delta_{j3} + \delta_{i3} \delta_{j2} \right]$$
(3.50)

Therefore, the dissipation of kinetic energy can be written as

$$\epsilon = \lim_{x_k \to x_k'} 2\nu \left\{ \frac{1}{2} \frac{1}{h^j} \frac{1}{h^{j'}} \frac{\partial^2 R_{i,i}}{\partial x_j \partial x_j'} + \frac{1}{2} \frac{1}{h^i} \frac{1}{h^{j'}} \frac{\partial^2 R_{i,i}}{\partial x_i \partial x_j'} \right. \\
+ \frac{1}{x_2 x_2'} \left(\frac{\partial (R_{3,2} - R_{2,3}/2)}{\partial x_3} + \frac{\partial (R_{2,3} - R_{3,2}/2)}{\partial x_3'} \right) \\
- \frac{1}{2} \left(\frac{1}{x_2} \frac{\partial R_{3,3}}{\partial x_2'} + \frac{1}{x_2'} \frac{\partial R_{3,3}}{\partial x_2} \right) + \frac{R_{2,2}}{x_2 x_2'} + \frac{1}{2} \frac{R_{3,3}}{x_2 x_2'} \right\},$$
(3.51)

where $R_{i,j}$ is the two-point velocity correlation tensor; i.e.,

$$R_{i,j} = \overline{u_i(x_1, x_2, x_3, t)u'_j(x'_1, x'_2, x'_3, t)}$$
(3.52)

Substituting the similarity solution for the components of the two-point velocity correlation tensor (i.e., equation 3.8) into the terms in equation 3.51 yields

$$\frac{\partial^{2} R_{k,n}}{\partial x_{1} \partial x_{1}'} = \left[\frac{Q^{k,n}}{x_{1} x_{1}'} \right] \left\{ q_{k,n} + \eta \frac{\partial}{\partial \eta} + \eta' \frac{\partial}{\partial \eta'} + \eta \eta' \frac{\partial^{2}}{\partial \eta \partial \eta'} - \eta' \frac{\partial^{2}}{\partial \eta' \partial \upsilon} + \eta \frac{\partial^{2}}{\partial \eta' \partial \upsilon} - \frac{\partial^{2}}{\partial \eta' \partial \upsilon} \right\} q_{k,n}$$
(3.53)

$$\frac{\partial^2 R_{k,n}}{\partial x_2 \partial x_2'} = \left[\frac{Q^{k,n}}{\delta(x_1)\delta(x_1')} \right] \frac{\partial^2 q_{k,n}}{\partial \eta \partial \eta'}$$
(3.54)

$$\frac{1}{x_2 x_2'} \frac{\partial^2 R_{k,n}}{\partial x_3 \partial x_3'} = -\left[\frac{Q^{k,n}}{\delta(x_1) \delta(x_1')} \right] \frac{1}{\eta \eta'} \frac{\partial^2 q_{k,n}}{\partial \theta^2}$$
(3.55)

$$\frac{\partial^2 R_{k,n}}{\partial x_1 \partial x_2'} = -\left[\frac{Q^{k,n}}{x_1 \delta(x_1')}\right] \left\{\frac{\partial}{\partial \eta'} + \eta \frac{\partial^2}{\partial \eta \eta'} - \frac{\partial^2}{\partial \eta' \partial \upsilon}\right\} q_{k,n} \tag{3.56}$$

$$\frac{\partial^2 R_{k,n}}{\partial x_1' \partial x_2} = -\left[\frac{Q^{k,n}}{x_1' \delta(x_1)}\right] \left\{ \frac{\partial}{\partial \eta} + \eta' \frac{\partial^2}{\partial \eta \eta'} + \frac{\partial^2}{\partial \eta \partial \upsilon} \right\} q_{k,n}$$
(3.57)

$$\frac{1}{x_2'} \frac{\partial^2 R_{k,n}}{\partial x_1 \partial x_3'} = \left[\frac{Q^{k,n}}{x_1 \delta(x_1')} \right] \frac{1}{\eta'} \left\{ \frac{\partial}{\partial \theta} + \eta \frac{\partial^2}{\partial \eta \partial \theta} - \frac{\partial^2}{\partial \upsilon \partial \theta} \right\} q_{k,n} \tag{3.58}$$

$$\frac{1}{x_2} \frac{\partial^2 R_{k,n}}{\partial x_1' \partial x_3} = -\left[\frac{Q^{k,n}}{x_1' \delta(x_1)} \right] \frac{1}{\eta} \left\{ \frac{\partial}{\partial \theta} + \eta' \frac{\partial^2}{\partial \theta \partial \eta'} + \frac{\partial^2}{\partial \theta \partial \upsilon} \right\} q_{k,n} \tag{3.59}$$

$$\frac{1}{x_2} \frac{\partial^2 R_{k,n}}{\partial x_3 \partial x_2'} = \left[\frac{Q^{k,n}}{\delta(x_1)\delta(x_1')} \right] \frac{1}{\eta} \frac{\partial^2 q_{k,n}}{\partial \eta' \partial \theta}$$
(3.60)

$$\frac{1}{x_2'} \frac{\partial^2 R_{k,n}}{\partial x_3' \partial x_2} = -\left[\frac{Q^{k,n}}{\delta(x_1)\delta(x_1')} \right] \frac{1}{\eta'} \frac{\partial^2 q_{k,n}}{\partial \eta \partial \theta}$$
(3.61)

$$\frac{1}{x_2 x_2'} \frac{\partial R_{k,n}}{\partial x_3} = \left[\frac{Q^{k,n}}{\delta(x_1)\delta(x_1')} \right] \frac{1}{\eta \eta'} \frac{\partial q_{k,n}}{\partial \theta}$$
(3.62)

$$\frac{1}{x_2 x_2'} \frac{\partial R_{k,n}}{\partial x_3'} - \left[\frac{Q^{k,n}}{\delta(x_1) \delta(x_1')} \right] \frac{1}{\eta \eta'} \frac{\partial q_{k,n}}{\partial \theta}, \tag{3.63}$$

$$\frac{1}{x_2} \frac{\partial R_{k,n}}{\partial x_2'} = \left[\frac{Q^{k,n}}{\delta(x_1)\delta(x_1')} \right] \frac{1}{\eta} \frac{\partial q_{k,n}}{\partial \eta'},\tag{3.64}$$

$$\frac{1}{x_2'} \frac{\partial R_{k,n}}{\partial x_2} = \left[\frac{Q^{k,n}}{\delta(x_1)\delta(x_1')} \right] \frac{1}{\eta'} \frac{\partial q_{k,n}}{\partial \eta'}, \tag{3.65}$$

and

$$\frac{R_{k,n}}{x_2 x_2'} = \left[\frac{Q^{k,n}}{\delta(x_1)\delta(x_1')}\right] \frac{q_{k,n}}{\eta \eta'}.$$
(3.66)

Thus, when the two-point velocity correlation tensor can be written as a similarity solution, all of the two-point velocity-gradient correlations in the equation 3.51 can be written as the product of a scale (which is proportional for all of the moments) and a function that is dependent on the similarity variables. Thus, it follows that the dissipation of kinetic energy per unit mass can be written as

$$\epsilon = \lim_{x_k \to x_k'} \left[\frac{U_s(x_1)U_s(x_1')}{\delta(x_1)\delta(x_1')} \right] D(\eta, \eta', \theta, \upsilon) = \left[2\nu \frac{U_s^2(x_1)}{\delta^2(x_1)} \right] D(\eta), \tag{3.67}$$

which is consistent with the similarity solution for the dissipation required in the similarity analysis of the equations for single-point moments (v. App. A).

It is also straightforward to demonstrate that the two-point vorticity correlation tensor can be written in a similarity form when the two-point velocity correlation tensor has a similarity form. In a cylindrical coordinate system the components of the fluctuating vorticity are given by (v. Batchelor 1967)

$$\omega_i = \frac{1}{2} \epsilon_{ijk} \left(\frac{1}{h^j} \frac{\partial u_k}{\partial x_j} + \frac{u_3}{x_2} \delta_{j2} \delta_{k3} \right)$$
 (3.68)

where ϵ_{ijk} is the alternating tensor. Thus, the two-point vorticity correlation tensor can be written as

$$\overline{\omega_{i}\omega_{l}'} = \frac{1}{4}\epsilon_{ijk}\epsilon_{lmn} \left\{ \frac{1}{h^{j}h^{ml}} \frac{\partial^{2}R_{k,n}}{\partial x_{j}\partial x_{m}'} + \frac{1}{x_{2}} \frac{1}{h^{ml}} \frac{\partial R_{3,n}}{\partial x_{m}'} \delta_{k3}\delta_{j2} + \right. \\
\left. + \frac{1}{x_{2}'} \frac{1}{h^{j}} \frac{\partial R_{k,3}}{\partial x_{j}} \delta_{n3}\delta_{m2} + \frac{R_{3,3}}{x_{2}x_{2}'} \delta_{k3}\delta_{j2}\delta_{n3}\delta_{m2} \right\}$$
(3.69)

Utilizing the similarity solution for the velocity-gradient moments outlined previously and the following additional moments

$$\frac{1}{x_2} \frac{\partial R_{k,m}}{\partial x_1'} = -\left[\frac{Q^{k,m}}{\delta(x_1)x_1'}\right] \frac{1}{\eta} \left\{1 + \eta' \frac{\partial}{\partial \eta'} + \frac{\partial}{\partial \upsilon}\right\} q_{k,m}$$
(3.70)

$$\frac{1}{x_2'} \frac{\partial R_{k,m}}{\partial x_1} = -\left[\frac{Q^{k,m}}{\delta(x_1')x_1}\right] \frac{1}{\eta'} \left\{1 + \eta \frac{\partial}{\partial \eta} - \frac{\partial}{\partial \upsilon}\right\} q_{k,m} \tag{3.71}$$

$$\frac{1}{x_2} \frac{\partial R_{k,m}}{\partial x_2'} = \left[\frac{Q^{k,m}}{\delta(x_1)\delta(x_1')} \right] \frac{1}{\eta} \frac{\partial q_{k,m}}{\partial \eta'}$$
(3.72)

$$\frac{1}{x_2'} \frac{\partial R_{k,m}}{\partial x_2} = \left[\frac{Q^{k,m}}{\delta(x_1)\delta(x_1')} \right] \frac{1}{\eta'} \frac{\partial q_{k,m}}{\partial \eta}$$
(3.73)

it is straightforward to demonstrate that the two-point vorticity correlation tensor can be written as

$$\overline{\omega_i \omega_l'} = \left[\frac{U_s(x_1) U_s(x_1')}{\delta(x_1) \delta(x_1')} \left(\frac{d\delta}{dx_1} \right)^{e(i,j)} \right] h_{i,l} \left(\eta, \eta', \theta, \upsilon, \frac{d\delta}{dx_1} \right)$$
(3.74)

The power e(i, j) is included to account for any differences in the scaling of the members of the vorticity correlation tensor. It also follows that the single-point vorticity moments can be written as

$$\overline{\omega_i \omega_l} = \left[\frac{U_s^2(x_1)}{\delta(x_1)^2} \left(\frac{d\delta}{dx_1} \right)^{e(i,j)} \right] \tilde{h}(\eta)$$
(3.75)

when the two-point velocity correlation tensor has a similarity form.

Figure 3.1: Geometry of the spatially developing axisymmetric wake.

Chapter 4

A Varying-Reynolds-Number,
Spatially Developing Flow With a
Constant Growth Rate: The Plane
Jet

The analysis in the previous chapter illustrated that the governing equations for the two-point velocity correlations in far field of the spatially-developing axisymmetric jet admit similarity solutions, since the Reynolds number of the flow based on the similarity variable is a constant. In the plane jet (illustrated in figure 4.1), the Reynolds number based on the similarity variables increases as the flow evolves downstream (v. George, 1994) and approaches infinity. In this case, the traditional theory put forth by Kolmogorov (v. Monin and Yaglom, 1975) argues that the smallest scales of the turbulence reach an universal equilibrium state whose two-point statistical description is a function of only the dissipation of kinetic energy per unit mass

 ϵ (which occurs at the smallest scales but is determined by the large scales) and the kinematic viscosity of the fluid.

It will be shown later, that it is not possible to find a similarity solution for the two-point velocity correlations tensor that is valid for all separation distances in this flow because the Reynolds number of the flow based on the similarity variables is not a constant. Instead, the equations that govern the correlation tensor for large separation distances (which emphasize the large-scale motions) and the governing equations for the second-order structure functions (which emphasize the small-scale motions) are examined separately to determine whether they admit similarity solutions. It is shown that these equations admit similarity solutions in the limit of an infinite Reynolds number, when terms in each set of equations are negligible. The similarity solutions for the small-scale motions are also compared to the similarity solution proposed by Kolmogorov to determine if the solutions are consistent.

4.1 Review of the Results of the Single-Point Similarity Analysis

The similarity analysis of the equations governing the single-point moments, including the equations for the individual Reynolds stresses, was reported by George (1994). George (1994) found that a similarity solution was only possible for these equations when

$$\frac{d\delta}{dx_1} \propto const \tag{4.1}$$

and

$$U_s^2 \delta \propto M_0 \tag{4.2}$$

where, δ and U_s are the similarity length and velocity scales for the mean-velocity profile and M_0 is the initial moment added at the source of the jet.

Thus, choosing the origin of the coordinate system at the virtual origin of the asymptotic jet, it follows that

$$\delta \propto x_1 \tag{4.3}$$

and

$$U_s \propto x_1^{-1/2}$$
. (4.4)

Therefore, the Reynolds number of the jet based on the similarity variables,

$$Re_{\delta} = \frac{U_s \delta}{\nu} \propto x^{1/2},$$
 (4.5)

increases to infinity as the flow evolves downstream.

4.2 Similarity Analysis of the Two-Point Velocity Correlation Tensor

The equations that govern the two-point (single-time) velocity correlation tensor in this flow are given by (Hinze, 1975)

$$U_{k} \frac{\partial \overline{u_{i}u_{j}'}}{\partial x_{k}} + U_{k}' \frac{\partial \overline{u_{i}u_{j}'}}{\partial x_{k}'} = -\frac{1}{\rho} \frac{\partial \overline{\rho u_{j}'}}{\partial x_{i}} - \frac{1}{\rho} \frac{\partial \overline{\rho' u_{i}}}{\partial x_{j}'}$$

$$-\frac{\partial \overline{u_{k}u_{i}u_{j}'}}{\partial x_{k}} - \frac{\partial \overline{u_{k}'u_{i}u_{j}'}}{\partial x_{k}'} - \overline{u_{j}'u_{k}} \frac{\partial U_{i}}{\partial x_{k}} - \overline{u_{i}u_{k}'} \frac{\partial U_{j}'}{\partial x_{k}'}$$

$$+\nu \left\{ \frac{\partial^{2}}{\partial x_{k} \partial x_{k}} + \frac{\partial^{2}}{\partial x_{k}' \partial x_{k}'} \right\} \overline{u_{i}u_{j}'}, \tag{4.6}$$

where the prime and unprimed variables are evaluated at the two arbitrary points in the flow.

It is straightforward to demonstrate that these equations do not admit similarity solutions of the type outlined previously when the Reynolds number, Re_{δ} is not a constant. For instance, if the hypothesized similarity solution for the two point correlation tensor is given by

$$\overline{u_i u'_j} = Q^{i,j}(x_1, x'_1) q_{i,j}(v, \eta, \eta', \zeta)$$
(4.7)

(where ζ and v are as yet undefined similarity variables in the x_1 - and x_3 -directions), then it follows that the ratio of the convective and viscous terms at one of the points in space is given by

$$U_2 \frac{\partial \overline{u_i u_j'}}{\partial x_2} \left(\nu \frac{\partial^2 \overline{u_i u_j'}}{\partial x_2^2} \right)^{-1} \propto \frac{U_s \delta}{\nu}. \tag{4.8}$$

This ratio is a function of the position of only one of the points downstream of the virtual origin, so it can not be written as a function of the separation distance between the points in a transformed streamwise coordinate. Thus, the full governing equations do not admit similarity solutions.

In the infinite-Reynolds-numbers limit, however, it is generally argued that the viscous transport terms have a negligible effect on the large-scale motions. It is also argued that the convective terms play a negligible role in the equations for the small-scale motions. Thus, the obvious question to ask is whether the governing equations for the correlations that characterize the large- and small-scale motions individually admit similarity solutions in the infinite-Reynolds-number limit. This is really a formal statement of the usually assumed 'local' similarity for the small-scales, and

analogous to the inner/outer similarity solution George et al. (1995) applied to the turbulent boundary layer.

4.2.1 The Large-Scale Motions

The large-scale motions of the turbulence are correlated over much larger separation distances than the small-scale motions in the flow. In non-homogeneous shear flows, such as the plane jet, the sizes of the large-scale motions are typically on the same order as the half-width of the jet. For these large-separation distances the ratios of the convective terms and the viscous terms in equation 4.6 are on the order of

$$U_k \frac{\partial \overline{u_i u_j'}}{\partial x_k} \left(\nu \frac{\partial^2}{\partial x_k \partial x_k} \overline{u_i u_j'} \right)^{-1} \sim \frac{U_s C_s}{x_1} \frac{\delta^2}{C_s \nu} \sim O(Re_\delta), \tag{4.9}$$

where C_s is an appropriate scale for the two-point correlation tensor. Similarly, the ratio of the turbulent transfer and the viscous terms is given by

$$\frac{\partial \overline{u_k u_i u'_j}}{\partial x_k} \left(\nu \frac{\partial^2}{\partial x_k \partial x_k} \overline{u_i u'_j} \right)^{-1} \sim \frac{T_s}{\delta(x_1)} \frac{\delta^2}{C_s \nu} \sim O\left(Re_{\delta} \frac{T_s}{C_s U_s} \right). \tag{4.10}$$

Thus, if the convective terms and the turbulent transfer terms are of the same order; i.e.,

$$\lim_{Re_{\delta} \to \infty} \frac{T_s}{C_s U_s} \sim O(1), \tag{4.11}$$

as is generally argued (v. Hinze 1975), it follows that in the infinite-Reynolds-number limit the viscous diffusion terms play are negligible in the equation for the correlation at large separation distances.

In this case, the equations that govern the evolution of the correlation tensor for

large-separation distances are given by

$$U_{k} \frac{\partial \overline{u_{i}u'_{j}}}{\partial x_{k}} + U'_{k} \frac{\partial \overline{u_{i}u'_{j}}}{\partial x'_{k}} = -\frac{1}{\rho} \frac{\partial \overline{pu'_{j}}}{\partial x_{i}} - \frac{1}{\rho} \frac{\partial \overline{p'u_{i}}}{\partial x'_{j}}$$
$$-\frac{\partial \overline{u_{k}u_{i}u'_{j}}}{\partial x_{k}} - \frac{\partial \overline{u'_{k}u_{i}u'_{j}}}{\partial x'_{k}} - \overline{u'_{j}u_{k}} \frac{\partial U_{i}}{\partial x_{k}} - \overline{u_{i}u'_{k}} \frac{\partial U'_{j}}{\partial x'_{k}}. \tag{4.12}$$

It follows from the previous analysis of the axisymmetric jet that the similarity coordinate in the non-homogeneous x_1 -direction must be a transformed coordinate. It is straightforward to demonstrate that a transformed coordinate that is compatible with the equations is the same one used in the analysis of the axisymmetric jet; *i.e.*,

$$v = \ln(x_1/x_1'). (4.13)$$

The large-scale, energy-containing motions make a significant contribution to the single-point Reynolds stresses, so the similarity solution for the large-scale motions must be consistent with the similarity solution for these moments. Consequently, the similarity coordinate in the x_2 direction is chosen to be

$$\eta = \frac{x_2}{\delta}.\tag{4.14}$$

The similarity variable in the homogeneous x_3 direction is defined as for the homogeneous directions in the two-point, two-time similarity solution for the temporally evolving wake. The similarity variable in the x_3 -direction is given by

$$\zeta = \frac{x_3 - x_3'}{\delta_3(x_1)}. (4.15)$$

where the length scale δ_3 is not yet defined. The variable ζ' given by

$$\zeta' = \frac{x_3 - x_3'}{\delta_3(x_1')}. (4.16)$$

could also be used in the similarity solution (similar to what was done for the temporally evolving wake), but it is not included here because it is not independent of zeta and v.

It is hypothesized that the equations for the two-point velocity correlations admit similarity solutions where

$$\overline{u_i u'_j} = Q^{i,j}(x_1, x'_1) q_{i,j}(v, \eta, \eta', \zeta), \tag{4.17}$$

$$\overline{u_k u_i u_j'} = T_1^{ki,j}(x_1, x_1') t_{ki,j}^1(v, \eta, \eta', \zeta), \tag{4.18}$$

$$\overline{u_k'u_iu_j'} = T_2^{i,kj}(x_1, x_1')t_{i,kj}^2(v, \eta, \eta', \zeta), \tag{4.19}$$

$$\overline{pu'_{j}} = \Pi_{1}^{j}(x_{1}, x'_{1})\pi_{j}^{1}(v, \eta, \eta', \zeta), \tag{4.20}$$

$$\overline{p'u_i} = \Pi_2^i(x_1, x_1') \pi_i^2(v, \eta, \eta', \zeta). \tag{4.21}$$

Note, the scales for these functions must be compatible with the relevant scales for the single-point moments.

Substituting the hypothesized similarity solution into equation 4.12 yields

$$\begin{bmatrix} U_{s}(x_{1}) \frac{\partial Q^{i,j}}{\partial x_{1}} \end{bmatrix} f(\eta) q_{i,j} + \begin{bmatrix} Q^{i,j}U_{s}(x_{1}) \\ x_{1} \end{bmatrix} f(\eta) \frac{\partial q_{i,j}}{\partial v} - \begin{bmatrix} Q^{i,j}U_{s}(x_{1}) \\ \delta_{3}(x_{1}) \end{bmatrix} f(\eta) \zeta \frac{\partial q_{i,j}}{\partial \zeta} \\
- \left\{ \begin{bmatrix} Q^{i,j} \frac{\partial U_{s}}{\partial x_{1}} \end{bmatrix} + \begin{bmatrix} Q^{i,j}U_{s}(x_{1}) \\ x_{1} \end{bmatrix} \right\} \frac{\partial q_{i,j}}{\partial \eta} \int_{0}^{\eta} f(\tilde{\eta}) d\tilde{\eta} + \begin{bmatrix} U_{s}(x'_{1}) \frac{\partial Q^{i,j}}{\partial x'_{1}} \end{bmatrix} f(\eta') q_{i,j} \\
- \begin{bmatrix} Q^{i,j}U_{s}(x'_{1}) \\ x'_{1} \end{bmatrix} f(\eta') \frac{\partial q_{i,j}}{\partial v} - \left\{ \begin{bmatrix} Q^{i,j} \frac{\partial U_{s}}{\partial x'_{1}} \end{bmatrix} + \begin{bmatrix} Q^{i,j}U_{s}(x'_{1}) \\ x'_{1} \end{bmatrix} \right\} \frac{\partial q_{i,j}}{\partial \eta'} \int_{0}^{\eta'} f(\tilde{\eta}) d\tilde{\eta}$$

$$= -\frac{1}{\rho} \left\{ \left[\frac{\partial \Pi_{1}^{j}}{\partial x_{1}} \right] \pi_{j}^{1} + \left[\frac{\Pi_{1}^{j}}{x_{1}} \right] \left(-\eta \frac{\partial \pi_{j}^{j}}{\partial \eta} + \frac{\partial \pi_{j}^{j}}{\partial v} \right) - \left[\frac{\Pi_{1}^{j}}{\delta_{3}(x_{1})} \frac{\partial \delta_{3}}{\partial x_{1}} \right] \zeta \frac{\partial \pi_{j}^{j}}{\partial \zeta} \right\} \delta_{i1}$$

$$- \frac{1}{\rho} \left[\frac{\Pi_{1}^{j}}{\delta(x_{1})} \right] \frac{\partial \pi_{j}^{j}}{\partial \eta} \delta_{i2} - \frac{1}{\rho} \left[\frac{\Pi_{1}^{j}}{\delta_{3}(x_{1})} \right] \frac{\partial \pi_{j}^{j}}{\partial \zeta} \delta_{i3}$$

$$- \frac{1}{\rho} \left\{ \left[\frac{\partial \Pi_{2}^{j}}{\partial x_{1}'} \right] \pi_{i}^{2} + \left[\frac{\Pi_{1}^{i}}{x_{1}'} \right] \left(-\eta' \frac{\partial \pi_{i}^{2}}{\partial \eta'} - \frac{\partial \pi_{i}^{2}}{\partial v} \right) \right\} \delta_{j1} - \frac{1}{\rho} \left[\frac{\Pi_{2}^{i}}{\delta(x_{1}')} \right] \frac{\partial \pi_{i}^{2}}{\partial \eta'} \delta_{j2} + \frac{1}{\rho} \left[\frac{\Pi_{2}^{i}}{\delta_{3}(x_{1})} \right] \frac{\partial \pi_{i}^{2}}{\partial \zeta} \delta_{j3}$$

$$- \left[\frac{\partial T_{1}^{1i,j}}{\partial x_{1}} \right] t_{1,i,j}^{1} - \left[\frac{T_{1}^{1i,j}}{x_{1}} \right] \left(-\eta \frac{\partial t_{1i,j}}{\partial \eta} + \frac{\partial t_{1i,j}}{\partial v} \right) + \left[\frac{T_{1}^{1i,j}}{\delta_{3}(x_{1})} \frac{\partial \delta_{3}}{\partial x_{1}} \right] \zeta \frac{\partial t_{1i,j}^{1}}{\partial \zeta} - \left[\frac{T_{1}^{2i,j}}{\delta(x_{1})} \right] \frac{\partial t_{2i,j}^{2}}{\partial \eta}$$

$$- \left[\frac{T_{1}^{2i,j}}{\delta(x_{1})} \right] \frac{\partial t_{3i,j}^{2}}{\partial \zeta} - \left[\frac{\partial T_{2}^{i,1j}}{\partial x_{1}'} \right] t_{i,1,j}^{2} + \left[\frac{T_{2}^{i,1j}}{x_{1}'} \right] \left(\eta' \frac{\partial t_{i,1j}^{2}}{\partial \eta'} + \frac{\partial t_{i,1j}^{2}}{\partial v} \right) - \left[\frac{T_{2}^{2i,j}}{\delta(x_{1})} \right] \frac{\partial t_{i,2j}^{2}}{\partial \eta'}$$

$$+ \left\{ \left[\frac{T_{2}^{i,3j}}{\delta_{3}(x_{1})} \right] \frac{\partial t_{i,3j}^{2}}{\partial \zeta} + \left\{ \left[\frac{Q^{1,j}U_{s}(x_{1})}{x_{1}} \right] q_{1,j} \left(\eta^{2} \frac{df}{d\eta} + \eta f(\eta) - \frac{1}{4} \int_{0}^{\eta} f(\tilde{\eta}) d\tilde{\eta} \right)$$

$$- \left[\frac{U_{s}(x_{1})Q^{i,j}}{x_{1}} \right] q_{i,1} \left(\frac{1}{2} f(\eta') + \eta' \frac{df}{d\eta'} \right) - \left[\frac{Q^{i,2}U_{s}(x_{1}')}{\delta(x_{1}')} \right] q_{i,2} \frac{df}{d\eta'} \right\} \delta_{j1}$$

$$+ \left\{ \left[\frac{U_{s}(x_{1}')Q^{i,1}}{x_{1}'} \right] q_{i,1} \left(\frac{1}{2} f(\eta') + \eta' \frac{df}{d\eta'} \right) - \left[\frac{Q^{i,2}U_{s}(x_{1}')}{\delta(x_{1}')} \right] q_{i,2} \frac{df}{d\eta'} \right\} \delta_{j1}$$

$$- \left[\frac{U_{s}(x_{1}')Q^{i,1}}{x_{1}'} \right] q_{i,1} \left(\frac{1}{2} f(\eta') + \eta' \frac{df}{d\eta'} + \eta' f(\eta') - \frac{1}{4} \int_{0}^{\eta'} f(\tilde{\eta}) d\tilde{\eta} \right)$$

$$- \left[\frac{U_{s}(x_{1}')Q^{i,1}}{x_{1}'} \right] q_{i,1} \left(\frac{1}{2} f(\eta') + \eta' \frac{df}{d\eta'} + \eta' f(\eta') - \frac{1}{4} \int_{0}^{\eta'} f(\tilde{\eta}) d\tilde{\eta} \right)$$

This expression has been simplified by defining the origin of the coordinate to be at the virtual origin of the jet and using the relationships

$$\frac{1}{\delta} \frac{d\delta}{dx_1} = \frac{1}{x_1} \tag{4.23}$$

and

$$\frac{1}{U_s} \frac{dU_s}{dx_1} = \frac{-1}{2x_1},\tag{4.24}$$

which are valid for this flow.

The portion of each term that is dependent on the position of the two points relative to the virtual origin in equation 4.22 is included in square brackets. As in the analysis of the axisymmetric jet flow, there is not a choice of the similarity scales that makes the terms in square brackets proportional. Hence, it is necessary to choose the similarity scales so that the ratios of the terms are only a function of v.

The allowable choices for the length scale in the homogeneous x_3 -direction can be determined by examining the terms in the transport equation for the $\overline{u_2u_3'}$ correlation given by

$$-\frac{1}{\rho} \left[\frac{\Pi_1^3}{\delta(x_1)} \right] \frac{\partial \pi_1^3}{\partial \eta} - \left[\frac{T_1^{32,3}}{\delta_3(x_1)} \right] \frac{\partial t_{32,3}^1}{\partial \zeta}$$
(4.25)

and the terms in the $\overline{u_3u_3'}$ transport equation given by

$$-\frac{1}{\rho} \left[\frac{\Pi_1^3}{\delta_3(x_1)} \right] \frac{\partial \pi_1^3}{\partial \zeta} - \left[\frac{T_1^{23,3}}{\delta_{\ell}(x_1)} \right] \frac{\partial t_{23,3}^1}{\partial \eta}. \tag{4.26}$$

The governing equations for $\overline{u_2u_3'}$ and $\overline{u_3u_3'}$ only admit similarity solutions if the ratios of the terms in square brackets in equations 4.25 and 4.26 are a function of v only, so that

$$\left[\frac{\Pi_1^3 \delta_3(x_1)}{T_1^{32,3} \delta(x_1)}\right] = h_1(v) \tag{4.27}$$

and

$$\left[\frac{\Pi_1^3 \delta(x_1)}{T_1^{23,3} \delta_3(x_1)}\right] = h_2(v). \tag{4.28}$$

Noting that $T_1^{32,3} = T_1^{23,3}$ (since $\overline{u_i u_k u_j'} = \overline{u_k u_i u_j'}$), it follows that both of these ratios can be a function of v only if

$$\delta_3(x_1) \propto \delta(x_1). \tag{4.29}$$

The scale for the two-point correlation tensor can also be determined from equation 4.22. One choice for the scales is to require the convective terms at each point to be proportional; *i.e.*,

$$\frac{\partial Q^{i,j}}{\partial x_1} \propto \frac{Q^{i,j}}{x_1} \tag{4.30}$$

and

$$\frac{\partial Q^{i,j}}{\partial x_1'} \propto \frac{Q^{i,j}}{x_1'},\tag{4.31}$$

in which case it follows that

$$Q^{i,j} \propto x_1^m x_1'^n. \tag{4.32}$$

In order to ensure that the similarity solution for the two-point velocity correlation tensor is consistent with the hypothesized similarity solution for the single-point Reynolds stresses, the scale for the two-point correlation tensor is chosen such that¹

$$Q^{i,j} \propto U_s^n(x_1) U_s^{2-n}(x_1') \frac{d\delta}{dx_1}^{e(i,j)}.$$
 (4.33)

The reasonable choice is n = 1, so the scale for the correlation is equally weighted by the velocity scale at each point; *i.e.*,

$$Q^{i,j} \propto U_s(x_1)U_s(x_1') \frac{d\delta}{dx_1}^{e(i,j)}$$
 (4.34)

¹In general, this could be multiplied by an arbitrary function of v such as $U_s(x_1)/U_s(x_1') = e^{-v/2}$ or $\delta(x_1)/\delta(x_1') = e^v$ and the equations of motion would still admit similarity solutions. Of course, in this case these factors would appear in the governing equation for the similarity solution. The choices outlined here were made because they appeared to be the most appropriate.

It is straightforward to demonstrate that the ratio of all of the terms in square brackets will be only a function of v if the scales for the other moments are chosen such that

$$\Pi_1^j \propto Q^{i,j} U_s(x_1), \tag{4.35}$$

$$\Pi_2^i \propto Q^{i,j} U_s(x_1'), \tag{4.36}$$

$$T_1^{i1,j} \propto Q^{i,j} U_s(x_1),$$
 (4.37)

$$T_2^{i,1j} \propto Q^{i,j} U_s(x_1'),$$
 (4.38)

$$T_1^{i2,j} \propto T_1^{i3,j} \propto Q^{i,j} U_s(x_1) \frac{d\delta}{dx_1},$$
 (4.39)

and

$$T_2^{i,2j} \propto T_2^{i,3,j} \propto Q^{i,j} U_s(x_1') \frac{d\delta}{dx_1'},$$
 (4.40)

which are consistent with the scales for the hypothesized similarity solutions.

Thus, the equations that govern the two-point velocity correlation function for large-separation distances (which emphasize the large-scale motions) admit similarity solutions in the infinite-Reynolds-number limit. Note, the discussion regarding boundary conditions in the previous chapter is equally applicable here and may in many ways be important since this is a planar flow. For example, even the mean velocity U_2 must be finite in a theoretical plane flow as $x_2 \to \infty$ in order to satisfy mass conservation as a result of entrainment.

4.2.2 The Small-Scale Motions

In the infinite-Reynolds-number limit, Kolmogorov (1941) hypothesized that the probability density function of the small-scale motions achieved an universal form

that is characterized by only the dissipation of the kinetic energy and the viscosity of the fluid. The objective of this section is to derive a similarity solution for statistical measures characteristic of the small-scale motions using the techniques outlined previously. This similarity solution can then be compared to the similarity solution proposed by Kolmogorov to determine if the solutions are consistent.

It is not possible to directly examine the evolution of the small-scale motions using the velocity correlation function because the correlation function at all separation distances is biased by information from the large-scale motions. Instead, it is conventional (e.g. Kolmogorov 1941 or Batchelor 1947) to examine the statistics of the velocity difference between points separated by a small distance (or the structure function), such as

$$\overline{\left(u_{\alpha} - u_{\beta}'\right)^2},\tag{4.41}$$

which is a measure of motions on the order of the separation distance between the points, particularly when α equal β . Following the approach outline by Batchelor (1947) for isotropic turbulence, the equation for the evolution of the second-order structure function can be written as (v) appendix B

$$U_{k} \frac{\partial}{\partial x_{k}} \overline{\left(u_{\alpha} - u_{\beta}'\right)^{2}} + U_{k}' \frac{\partial}{\partial x_{k}'} \overline{\left(u_{\alpha} - u_{\beta}'\right)^{2}} = 2 \frac{\overline{p} \frac{\partial u_{\alpha}}{\partial x_{\alpha}}}{\overline{p} \frac{\partial u_{\alpha}}{\partial x_{\alpha}}} + 2 \frac{\overline{p'} \frac{\partial u_{\beta}'}{\partial x_{\beta}'}}{\overline{p'} \frac{\partial u_{\beta}'}{\partial x_{\beta}'}}$$

$$-\frac{2}{\rho} \frac{\partial}{\partial x_{\alpha}} \overline{p} \overline{\left(u_{\alpha} - u_{\beta}'\right)} - \frac{2}{\rho} \frac{\partial}{\partial x_{\beta}'} \overline{p'} \overline{\left(u_{\beta}' - u_{\alpha}\right)} - \frac{\partial}{\partial x_{k}} \overline{u_{k}} \overline{\left(u_{\alpha} - u_{\beta}'\right)^{2}} - \frac{\partial}{\partial x_{k}'} \overline{u_{k}'} \overline{\left(u_{\alpha} - u_{\beta}'\right)^{2}}$$

$$-2\overline{\left(u_{\alpha} - u_{\alpha}'\right)} u_{k}' \frac{\partial U_{\beta}'}{\partial x_{k}'} - 2\overline{\left(u_{\beta} - u_{\beta}'\right)} u_{k}' \frac{\partial U_{\alpha}}{\partial x_{k}} - 2\overline{\left(u_{\beta}' - u_{\alpha}'\right)} u_{k}' \frac{U_{\beta}'}{\partial x_{k}'} - 2\overline{\left(u_{\beta} - u_{\alpha}\right)} u_{k}' \frac{\partial U_{\alpha}}{\partial x_{k}}$$

$$\nu \left\{ \frac{\partial^{2}}{\partial x_{k} \partial x_{k}} + \frac{\partial^{2}}{\partial x_{k} \partial x_{k}} \right\} \overline{\left(u_{\alpha} - u_{\beta}'\right)^{2}} - \epsilon_{\alpha\alpha} - \epsilon_{\beta\beta}$$

$$(4.42)$$

where the index convention is only used for the variable k (i.e., no summation over α and β).

This equation can be simplified by noting that the functional dependence of the structure functions can be written in terms of a variable that is related to the separation distance between the points, given by

$$\tilde{x}_k = \frac{x_k - x_k'}{2},\tag{4.43}$$

and a variable dependent on the average location of the two points, given by

$$\hat{x}_k = \frac{x_k + x_k'}{2}. (4.44)$$

Therefore,

$$x_k = \tilde{x}_k + \hat{x}_k \tag{4.45}$$

and

$$x_k' = \hat{x}_k - \tilde{x}_k. \tag{4.46}$$

In the limit of infinite Reynolds number, it is generally argued (v. Tennekes and Lumley 1972) that the dissipation of kinetic energy occurs in motions with a characteristic length scale, l_s , which is negligible relative to the characteristic length scale of the large scale motions in the jet. Further, it is argued that the structure function are measures of the small-scale motions and thus, vary significantly for changes in the separation distance on the order of the length scale l_s . However, the structure functions only varies significantly when the average location of the two points, \hat{x}_k , changes by a distance on the order of the characteristic length scale of the large-scale motions, δ . In other words,

$$\frac{\partial \overline{\left(u_{\alpha} - u_{\beta}'\right)^{2}}}{\partial \hat{x}_{k}} \left[\frac{\partial \overline{\left(u_{\alpha} - u_{\beta}'\right)^{2}}}{\partial \tilde{x}_{k}} \right]^{-1} \sim O\left(\frac{l_{s}}{\delta}\right), \tag{4.47}$$

so the motions on the order of the length scale l_s are locally homogeneous in the infinite-Reynolds-number limit, since

$$\lim_{Re_{\delta} \to \infty} \frac{l_s}{\delta} = 0. \tag{4.48}$$

In this case, the governing equations for the second-order structure functions can be written as

$$(U_{k} + U_{k}') \frac{\partial}{\partial \hat{x}_{k}} \overline{\left(u_{\alpha} - u_{\beta}'\right)^{2}} + (U_{k} - U_{k}') \frac{\partial}{\partial \tilde{x}_{k}} \overline{\left(u_{\alpha} - u_{\beta}'\right)^{2}} + 2 \frac{\overline{p} \frac{\partial u_{\alpha}}{\partial x_{\alpha}}}{\rho \frac{\partial u_{\alpha}}{\partial x_{\alpha}}} + 2 \frac{\overline{p} \frac{\partial u_{\beta}}{\partial x_{\beta}}}{\rho \frac{\partial u_{\beta}}{\partial x_{\beta}}}$$

$$- \frac{2}{\rho} \frac{\partial}{\partial \tilde{x}_{\alpha}} \overline{p} \left(u_{\alpha} - u_{\beta}'\right) - \frac{2}{\rho} \frac{\partial}{\partial \tilde{x}_{\beta}'} \overline{p}' \left(u_{\beta}' - u_{\alpha}\right) - \frac{\partial}{\partial \tilde{x}_{k}} \overline{\left(u_{k} - u_{k}'\right) \left(u_{\alpha} - u_{\beta}'\right)^{2}}$$

$$- 2 \overline{\left(u_{\alpha} - u_{\alpha}'\right) u_{k}'} \frac{\partial U_{\beta}'}{\partial x_{k}'} - 2 \overline{\left(u_{\beta} - u_{\beta}'\right) u_{k}} \frac{\partial U_{\alpha}}{\partial x_{k}} - 2 \overline{\left(u_{\beta}' - u_{\alpha}'\right) u_{k}'} \frac{U_{\beta}'}{\partial x_{k}'} - 2 \overline{\left(u_{\beta} - u_{\alpha}\right) u_{k}} \frac{\partial U_{\alpha}}{\partial x_{k}}$$

$$+ 2 \nu \frac{\partial^{2}}{\partial \tilde{x}_{k}^{2}} \overline{\left(u_{\alpha} - u_{\beta}'\right)^{2}} - \epsilon_{\alpha\alpha} - \epsilon_{\beta\beta}$$

$$(4.49)$$

Note, at this point the non-homogeneous convective terms have not been neglected because, as it is shown later, these terms are approximately the same order as the homogeneous convection terms. (It is also shown later that both are negligible in the infinite-Reynolds-number limit.)

This equation can be further simplified by neglecting terms in this equation that are negligible in the infinite-Reynolds-number limit. In particular, the convective terms and the production terms are examined. In order to neglect these terms it is necessary to demonstrate that these terms are higher-order terms compared to at least two terms that are being retained in the equation.

For the small-scale motions, it is assumed that the viscous terms and the turbulent transfer terms are of the same order since it is assumed that the turbulent transfer terms move the energy to the small scales where it is dissipated (Monin and Yaglom 1975); *i.e.*,

$$\frac{\partial}{\partial \tilde{x}_k} \overline{\left(u_k - u_k'\right) \left(u_\alpha - u_\beta'\right)^2} \left(2\nu \frac{\partial^2}{\partial \tilde{x}_k^2} \overline{\left(u_\alpha - u_\beta'\right)^2}\right)^{-1} \sim O\left(\frac{T_s^d l_s}{B_s^d \nu}\right) \sim O(1), \tag{4.50}$$

where T_s^d is the scale for the turbulent transfer term and B_s^d is the scale for the two point velocity correlation tensor. (Note, no assumptions have been made about the value of the scales B_s^d and T_s^d ; it has only been assumed that the ratio of the two terms is of order 1).

The ratio of the convective terms and the viscous terms can be approximated as

$$(U_k - U_k') \frac{\partial}{\partial \tilde{x}_k} \overline{\left(u_\alpha - u_\beta'\right)^2} \left\{ 2\nu \frac{\partial^2}{\partial \tilde{x}_k^2} \overline{\left(u_\alpha - u_\beta'\right)^2} \right\}^{-1} \sim O\left(\frac{U_s^d l_s}{\nu}\right) \tag{4.51}$$

and

$$(U_k + U_k') \frac{\partial}{\partial \hat{x}_k} \overline{\left(u_\alpha - u_\beta'\right)^2} \left\{ 2\nu \frac{\partial^2}{\partial \tilde{x}_k^2} \overline{\left(u_\alpha - u_\beta'\right)^2} \right\}^{-1} \sim O\left(\frac{U_s l_s^2}{x_1 \nu}\right), \tag{4.52}$$

where U_s^d is the scale for the velocity difference.

If the origin of the coordinate system is placed at the virtual origin of the jet, the scale for the difference between the mean velocities at the two points can be deduced by examining the velocity difference in the x_1 direction for a length on the order of l_s given by

$$U_s(x_1) - U_s(x_1 + l_s) = \frac{k_2}{x_1^{1/2}} - \frac{k_2}{(x_1 + l_s)^{1/2}}.$$
 (4.53)

This expression can be binomially expanded to yield

$$U_s(x_1) - U_s(x_1 + l_s) \approx \frac{k_2}{2x_1^{1/2}} \frac{l_s}{x_1} \left(1 - \frac{3}{4} \frac{l_s}{x_1} \right) \approx \frac{U_s l_s}{2x_1} \propto \frac{U_s}{2} \frac{l_s}{\delta}$$
 (4.54)

if $l_s \ll x_1$, which is valid in the infinite-Reynolds-number limit.

Hence, the two sets of convective terms are of the same order² in the infinite-Reynolds-number limit and the ratio of the convective and viscous terms can be approximated by

$$O\left(\frac{U_s\delta}{\nu}\frac{l_s^2}{\delta^2}\right) \tag{4.55}$$

Consequently, the convective terms are negligible relative to the viscous terms if this ratio is negligible, or if

$$l_s \ll x^{3/4}. (4.56)$$

as $x_1 \to \infty$.

The ratios of the velocity-difference production terms and the viscous are given by

$$2\overline{(u_{\alpha} - u_{\alpha}')u_{k}'}\frac{\partial U_{\beta}'}{\partial x_{k}'}\left[\nu\frac{\partial}{\partial \tilde{x}_{k}\partial \tilde{x}_{k}}\overline{(u_{\alpha} - u_{\beta}')^{2}}\right]^{-1} \sim O\left(\frac{U_{s}C_{s}^{d}l_{s}^{2}}{\delta\nu B_{s}^{d}}\right),\tag{4.57}$$

where C_s^d is the scale for the difference of the correlation function in the production terms; *i.e.*,

$$\overline{(u_{\alpha} - u_{\alpha}')u_{k}'} = \overline{u_{\alpha}u_{k}'} - \overline{u_{\alpha}'u_{k}'}$$

$$\tag{4.58}$$

(which is zero in the limit of zero separation). The order of this term can be approximated by expanding the correlation function into a Taylor series; *i.e.*,

$$\overline{u_{\alpha}u_{k}'} - \overline{u_{\alpha}'u_{k}'} \approx \left. \frac{\partial \overline{u_{\alpha}u_{k}'}}{\partial r} \right|_{x_{m} = x_{m}'} l_{s} + \left. \frac{1}{2} \frac{\partial^{2} \overline{u_{\alpha}u_{k}'}}{\partial r^{2}} \right|_{x_{m} = x_{m}'} l_{s}^{2}, \tag{4.59}$$

where r is the arbitrary separation distance and l_s is the magnitude of the separation. The scale for these terms can be approximated using the second term in this expansion

²The two scales do differ by the growth rate of the jet

by noting that (Tennekes and Lumley 1972)

$$\left. \frac{\partial^2 \overline{u_\alpha u'_\alpha}}{\partial r^2} \right|_{x_m = x'_m} = -2 \frac{\overline{u_\alpha u_\alpha}}{\lambda^2},\tag{4.60}$$

where λ is a Taylor microscale. For isotropic turbulence, this ratio can be related to the dissipation of kinetic energy by (v. Tennekes and Lumley 1972)

$$\epsilon = 15\nu \frac{\overline{u_1^2}}{\lambda^2} \tag{4.61}$$

In the current analysis where it has been assumed that the turbulence is 'locally' homogeneous, it is reasonable to approximate the scale C_s^d by

$$\frac{C_s^d}{\epsilon l_s^2} \sim O(1),\tag{4.62}$$

in which case the production terms are small relative to the turbulent transport terms if

$$\frac{l_s^4}{B_s^d} \frac{U_s}{\delta} \epsilon \ll 1 \tag{4.63}$$

It is instructive to check whether these criteria are satisfied for the similarity hypothesis proposed by Kolmogorov's for the small-scale motions. In this case, the moments of the small-scale motions are described by a single length and velocity scale given by

$$\eta_k = \left(\nu^3/\epsilon\right)^{1/4} \tag{4.64}$$

and

$$u_k = (\nu \epsilon)^{1/4} \,. \tag{4.65}$$

The similarity analysis of the single-point equations (George 1994) demonstrated that the these equations admit similarity solutions only when the scale for the rate

of dissipation per unit mass is given by

$$\epsilon \propto \frac{U_s^3}{\delta} \propto x^{-5/2},$$
(4.66)

which is in agreement with Kolmogorov's hypothesis (Monin and Yaglom, 1975). Thus,

$$\eta_k \propto x^{5/8} \tag{4.67}$$

and

$$u_k \propto x^{-5/8},$$
 (4.68)

which satisfy the criterion in equations 4.56 and 4.63. Therefore, it is reasonable to assume that the convective and production terms for the velocity difference are negligible, since the criteria outlined in equations 4.56 and 4.63 are satisfied for at least this case.

Neglecting the convective and production terms, the equation for the second order structure function is given by

$$0 = +2\frac{\overline{\rho}\frac{\partial u_{\alpha}}{\partial x_{\alpha}}}{\rho} + 2\frac{\overline{\rho}\frac{\partial u_{\beta}}{\partial x_{\beta}}}{\rho} - \epsilon_{ii} - \epsilon_{jj} - 2\overline{(u'_{\beta} - u'_{\alpha})u'_{k}}\frac{\partial U'_{\beta}}{\partial x'_{k}} - 2\overline{(u_{\beta} - u_{\alpha})u_{k}}\frac{\partial U_{\alpha}}{\partial x_{k}}$$
$$-\frac{2}{\rho}\frac{\partial}{\partial \tilde{x}_{\alpha}}\left[\overline{p\left(u_{\alpha} - u'_{\beta}\right)} + \frac{2}{\rho}\frac{\partial}{\partial \tilde{x}'_{\beta}}\overline{p'\left(u_{\alpha} - u'_{\beta}\right)}\right] - \frac{\partial}{\partial \tilde{x}_{k}}\overline{(u_{k} - u'_{k})\left(u_{\alpha} - u'_{\beta}\right)^{2}}$$
$$+2\nu\frac{\partial^{2}}{\partial \tilde{x}_{k}^{2}}\overline{\left(u_{\alpha} - u'_{\beta}\right)^{2}}.$$
 (4.69)

In order to find a similarity solution for this equation it is necessary to make assumptions in the similarity analysis that are consistent with the assumption that the turbulence is 'locally' homogeneous.

First, it is necessary to examine the length scale that is used to normalize the separation distance in the three coordinate directions. It is straightforward to demonstrate that it is not possible to find a similarity solution for equation 4.69 using individual length scales for both points. Instead, it is necessary to assume that the length scale does not vary significantly over distances on the order of l_s . The variation of this length scale in the x_1 -direction can be approximated by

$$l_s(x_1') \approx l_s(x_1) + \frac{dl_s}{dx_1}(x_1 - x_1') + \dots$$
 (4.70)

If the length scale evolves as a power law, it follows that for separation distances on order of l_s , l'_s is given by

$$l_s(x_1') \approx l_s(x_1) \left(1 + c_4 \frac{l_s}{x_1} + O\left(\frac{l_s^2}{x_1^2}\right) \right).$$
 (4.71)

Hence, to first approximation, the length scale at the two points is equal in the infinite-Reynolds-number limit. A similar argument can be made for the velocity scale for the small scale motions, so to first approximation the similarity scale for velocity moments can be evaluated at a single point in the large-scale coordinate system.

Using these approximations, the hypothesized similarity solutions for the moments in equation 4.69 are given by

$$\overline{\left(u_{\alpha} - u_{\beta}'\right)^{2}} = B^{\alpha\beta}(x_{1})b_{\alpha\beta}(\xi, \gamma, \zeta, \eta), \tag{4.72}$$

$$\overline{(u_k - u_k') \left(u_\alpha - u_\beta'\right)^2} = T^{\alpha\beta k}(x_1) t_{\alpha\beta k}(\xi, \gamma, \zeta, \eta), \tag{4.73}$$

$$\overline{p(u_{\alpha} - u_{\beta})} = P_1^{\alpha}(x_1)p_{\alpha}^1(\xi, \gamma, \zeta, \eta), \tag{4.74}$$

and

$$\overline{p'(u_{\alpha} - u_{\beta})} = P_2^{\beta}(x_1)p_{\beta}^2(\xi, \gamma, \zeta, \eta), \tag{4.75}$$

where

$$\xi = \frac{\tilde{x}_1}{l_s},\tag{4.76}$$

$$\gamma = \frac{\tilde{x}_2}{l_s},\tag{4.77}$$

$$\zeta = \frac{\tilde{x}_3}{l_s},\tag{4.78}$$

and η is the similarity coordinate from the single-point similarity analysis; i.e.,

$$\eta = \frac{x_2}{\delta}.\tag{4.79}$$

The functional form of the velocity difference correlations includes the variable η because the similarity solution for the structure function may differ for different locations in the jet. Of course, the variation occurs over distances much larger than the characteristic length scale of the motions where the dissipation occurs.

A similar approximation can be utilized to evaluate the single-point moments in equation 4.69. Since points that are separated by distance of order l_s are, to first approximation, at the same point in the large-scale coordinate system in the infinte-Reynolds-number limit, the single-point moments in equation 4.69 can be evaluated at the same point. The similarity analysis of the single-point moments reported by (George 1994) illustrated that all of the terms in equation 4.69 are all proportional, so they can combined into a single term given by

$$+2\frac{\overline{\rho}\frac{\partial u_{\alpha}}{\partial x_{\alpha}}}{\rho} + 2\frac{\overline{\rho}\frac{\partial u_{\beta}}{\partial x_{\beta}}}{\rho} - \epsilon_{\alpha\alpha} - \epsilon_{\beta\beta} - 2\overline{(u'_{\beta} - u'_{\alpha})u'_{k}}\frac{\partial U'_{\beta}}{\partial x'_{k}} - 2\overline{(u_{\beta} - u_{\alpha})u_{k}}\frac{\partial U_{\alpha}}{\partial x_{k}}$$
$$= Z^{\alpha\beta}(x_{1})z_{\alpha\beta}(\eta), \tag{4.80}$$

where $Z^{\alpha\beta}(x_1)$ satisfies (George 1994)

$$Z^{\alpha\beta}(x_1) \propto \frac{U_s^3}{\delta},$$
 (4.81)

which is, of course, the scale for the dissipation of kinetic energy per unit mass.

Substituting these similarity solutions into equation 4.69 yields

$$O = \left[Z^{\alpha\beta}(x_1) \right] z_{\alpha\beta}(\eta) - \frac{1}{\rho} \left\{ \left[\frac{P_1^{\beta}}{l_s} \right] \frac{\partial p_{\beta}^1}{\partial \xi} \delta_{\alpha 1} + \left[\frac{P_1^{\beta}}{l_s} \right] \frac{\partial p_{\beta}^1}{\partial \gamma} \delta_{\alpha 2} + \left[\frac{P_1^{\beta}}{l_s} \right] \frac{\partial p_{\beta}^1}{\partial \zeta} \delta_{\alpha 3} - \left[\frac{P_2^{\alpha}}{l_s} \right] \frac{\partial p_{\alpha}^2}{\partial \zeta} \delta_{j 1} - \left[\frac{P_2^{\alpha}}{l_s} \right] \frac{\partial p_{\alpha}^2}{\partial \gamma} \delta_{j 2} - \left[\frac{P_2^{\alpha}}{l_s} \right] \frac{\partial p_{\alpha}^2}{\partial \zeta} \delta_{j 3} \right\} - \left[\frac{T^{\alpha\beta 1}}{l_s} \right] \frac{\partial t_{\alpha\beta 1}}{\partial \xi} - \left[\frac{T^{\alpha\beta 2}}{l_s} \right] \frac{\partial t_{\alpha\beta 2}}{\partial \gamma} - \left[\frac{T^{\alpha\beta 3}}{l_s} \right] \frac{\partial t_{\alpha\beta 3}}{\partial \zeta} + 2 \left[\frac{\nu B^{\alpha\beta}}{l_s^2} \right] \left\{ \frac{\partial^2}{\partial \xi^2} + \frac{\partial^2}{\partial \gamma^2} + \frac{\partial^2}{\partial \zeta^2} \right\} b_{\alpha\beta}.$$

$$(4.82)$$

This equation admits to a similarity solution when

$$\left[Z^{\alpha\beta}(x_1)\right] \propto \left[\frac{P_1^{\beta}}{l_s}\right] \propto \left[\frac{P_2^{\alpha}}{l_s}\right] \propto \left[\frac{T^{\alpha\beta k}}{l_s}\right] \propto \left[\frac{\nu B^{\alpha\beta}}{l_2^s}\right]. \tag{4.83}$$

Therefore, the similarity scales for the measures of the small-scale motions are imposed by the single point-moments or the large-scale motions (analogous to the result reported by Batchelor 1947).

In this case, the scale for the structure function is given by

$$B^{\alpha\beta} \propto \frac{Z^{\alpha\beta} l_s^2}{\nu} \propto \frac{U_s^3 l_s^2}{\delta \nu} \tag{4.84}$$

and the scales for the other moments are given by

$$P_1^{\beta} \propto P_2^{\alpha} \propto T^{\alpha\beta k} \propto B^{\alpha\beta} u_s \frac{\nu}{u_s l_s} \propto U_s^3 \frac{l_s}{\delta}$$
 (4.85)

Thus, the equations that govern the second-order structure functions admit similarity solutions in the infinite-Reynolds-number limit. The similarity scales are not uniquely determined by equation 4.84, but the scales must approach a finite value

that is independent of Reynolds number in this limit. Further, Kolmogorov's hypothesis, in which the scale for the second- and third-order structure functions are given by

$$B^{\alpha\beta} \propto u_k^2 \propto x^{-5/4} \tag{4.86}$$

and

$$T^{\alpha\beta k} \propto u_k^3 \propto x^{-15/8},\tag{4.87}$$

is consistent with the similarity solution outlined here.

Figure 4.1: Geometry for the spatially developing plane jet.

Chapter 5

Implications of the Two-Point Similarity Hypothesis

The analysis in the previous sections illustrated that the equations that govern the two-point correlation in a number of free-shear flows admit similarity solutions. These solutions have a number of implications for the evolution of free shear flows, some of which (the similarity of the derivative moments, the evolution of the lengths scales in the flow, and the evolution of the pressure-velocity correlation), were outlined in the previous section. This section will discuss two other important implications of the similarity solution. The similarity of the single-point moments at a finite Reynolds number. The representation of a velocity field whose evolution is in agreement with the predictions of the similarity theory.

5.1 Single-Point Similarity Solution For Finite-Reynolds-Number Flows

Traditionally, the single-point similarity analyses have been carried out only for equations that have been simplified using the standard high-Reynolds-number, thin shear-layer approximations. The analysis of the equations that govern the two-point velocity correlation tensor in a finite-Reynolds-number temporally evolving wake and spatially evolving axisymmetric jet illustrated that these equations admit similarity solutions without any simplifying assumptions. This also implies that similarity solutions exist for the single-point moments in these flows that are valid at finite Reynolds number (since the single-point moments are a particular solutions of the two-point correlations).¹

The mean velocity profile cannot be determined from the two-point velocity correlation, so it is necessary to illustrate that the finite-Reynolds-number, mean momentum equation admits a similarity solution. For example, in the temporally evolving wake, substituting the hypothesized similarity solutions into the full differential mean momentum equation yields

$$\left\{ \left[\frac{dU_s}{dt} \right] f - \left[\frac{U_s}{\delta} \frac{d\delta}{dt} \right] \right\} \eta \frac{df}{d\eta} = \left[\frac{R_s}{\delta} \right] \frac{dg}{d\eta} + \left[\nu \frac{U_s}{\delta^2} \right] \frac{d^2 f}{d\eta^2}. \tag{5.1}$$

The viscous terms are proportional to the unsteady terms if

$$\frac{U_s}{\delta} \frac{d\delta}{dt} \propto \nu \frac{U_s}{\delta^2} \tag{5.2}$$

¹The similarity solution for the two-point velocity correlations also yields sufficient information to evaluate the viscous redistribution terms that could not be formally evaluated without the two-point information and were neglect in the approximated single-point equations.

or,

$$\frac{d\delta^2}{dt} \propto const. \tag{5.3}$$

Equation 5.2 can also be manipulated to yield

$$Re_{\delta} = \frac{U_s \delta}{\nu} = const.$$
 (5.4)

Thus, the differential mean momentum equation admits a similarity solution in this flow at a *finite* Reynolds number, since the Reynolds number of the flow based on the similarity variables is a constant. A similar result can be derived for the mean momentum equation in the axisymmetric jet.

In the case of the plane jet, where the Reynolds number based on the similarity variables is not a constant, it follows the equations for the single-point moments do not admit similarity solutions at finite Reynolds number, even for an idealized line source jet, so the similarity solutions must be viewed as an asymptotic state of the jet.

5.2 The Representation of the Velocity Field

.

Although it is not possible to uniquely determine the structure of a turbulent flow using the two-point velocity correlation tensor, a number of attempts have been made to deduce the possible structures in the flow using this measure (eg., Grant, 1958 or Towsend, 1970,1979). The difficulty with many of these approaches is that they do not incorporate an objective manner for finding the coherent structures. Instead, the experimentalist proposes arbitrary structures whose correlation function is then compared those measured in the flow. A more objective technique introduced by

Lumley (1970), determines an orthogonal basis which is optimally representative of the flow in a mean square sense. ²

The objective of the orthogonal decomposition technique is to find functions that yield the largest mean-square coefficient when the velocity field is projected onto them, where the coefficients a^n are given by

$$a^{n}(t) = \frac{\int_{-\infty}^{\infty} u_{i}(x_{l}, t) \Psi_{i}^{n*}(x_{l}; t) dx_{l}}{(\int_{-\infty}^{\infty} \Psi_{k}^{n}(x_{l}''; t) \Psi_{k}^{n*}(x_{l}''; t) dx_{l}'')^{1/2}}.$$
(5.5)

Hence, the objective is to maximize the value of $\lambda^n = \langle a^n(t)a^{n*}(t) \rangle$, or

$$\lambda^{n}(t) = \frac{\int_{-\infty}^{\infty} \int_{-\infty}^{\infty} \overline{u_{i}(x_{l}, t) u_{j}^{\prime *}(x_{m}^{\prime}, t)} \Psi_{i}^{n *}(x_{l}; t) \Psi_{j}^{n}(x_{m}^{\prime}; t) dx_{l} dx_{m}^{\prime}}{\int_{-\infty}^{\infty} \Psi_{k}^{n}(x_{l}^{\prime \prime}; t) \Psi_{k}^{n *}(x_{l}^{\prime \prime}; t) dx_{l}^{\prime \prime}}$$
(5.6)

The time dependence is maintained in the functional form of the orthogonal functions because in non-stationary flows, such as the temporally evolving wake, the functional form of the two point velocity correlation tensor varies as a function of time. Consequently, the orthogonal functions determined from the two-point velocity are, in general, a function of time. Following Lumley (1970), the orthogonal functions which maximize $\lambda^n(t)$ can be determined using variational calculus.

It is evident from equation 5.6 that it is the information in the two-point velocity correlation tensor that is used to characterize the flow in this orthogonal decomposition. Thus, when the equations for the two-point velocity correlation tensor admit similarity solutions, it is reasonable to expect that the functions determined from this orthogonal decomposition can be written in a similarity form. In the following sections this hypothesis is examined for the temporally evolving plane wake and the spatially evolving axisymmetric jet.

²Note, other techniques of finding structure in the flow are available (v. Hussain, 1989 or Zhou and Antonia, 1993), but they are not discussed here.

5.2.1 The Temporally Evolving, Plane Wake

The optimal representation of the flow in physical variables can be determined by applying variation calculus to equation 5.6. Fourier transforming the information in the homogeneous x_1 - and x_3 -directions (v. Lumley 1970) this yields

$$\int_{-\infty}^{\infty} y_{i,j}(k_1, x_2, x_2', k_3) \hat{\Psi}_j^n(x_2', k_1, k_3, t) dx_2' = \hat{\lambda}^n(k_1, k_3) \hat{\Psi}_i^n(x_2, k_1, k_3, t),$$
 (5.7)

where

$$y_{i,j}(k_1, x_2, x_2', k_3) = \frac{1}{4\pi^2} \int_{-\infty}^{\infty} \int_{-\infty}^{\infty} R_{i,j}(\varsigma, x_2, x_2', \gamma) e^{-i(k_1\varsigma + k_3\gamma)} d\varsigma d\gamma$$
 (5.8)

and

$$\hat{\Psi}_i^n(x_2, k_1, k_3, t) = \frac{1}{4\pi^2} \int_{-\infty}^{\infty} \int_{-\infty}^{\infty} \Psi_i^n(x_l; t) e^{-i(k_1 x_1 + k_3 x_1)} dx_1 dx_3.$$
 (5.9)

It is straightforward to demonstrate that the functions determined from equation 5.7 are unique and orthogonal (v. Lumley, 1970 or Berkooz et al., 1993), so they can be normalized to form an orthonormal basis; i.e.,

$$\int_{-\infty}^{\infty} \hat{\Psi}_{j}^{n}(x_{2}', k_{1}, k_{3}, t) \hat{\Psi}_{j}^{m*}(x_{2}', k_{1}, k_{3}, t) dx_{2}' = \delta_{nm}, \tag{5.10}$$

where δ_{nm} is a Kronecker delta.

It is evident that the orthogonal functions determined using this technique are time-dependent since the physical dimension of the wake is increasing as the flow evolves. When the flow is evolving such that the two-point velocity correlation tensor admits a similarity solution, it is hypothesized that the orthogonal function can be written as

$$\hat{\Psi}_i(k_1, x_2, k_3; t) = \Upsilon(t)\hat{\chi}_i(\tilde{k}_1, \eta, \tilde{k}_3), \tag{5.11}$$

where

$$\tilde{k}_3 = k_3 \delta \tag{5.12}$$

and

$$\tilde{k}_1 = k_1 \delta. \tag{5.13}$$

Note, the orthogonal functions at a given value of k_1 and k_3 in the physical wavenumber space are equated to orthogonal functions at continuously changing wavenumbers \tilde{k}_1 and \tilde{k}_3 in the similarity wavenumber space as the flow evolves. This occurs because the spectrum of the turbulence is continuously being shifted to the smaller wavenumbers as the flow evolves.

Substituting the similarity solution for the orthogonal function (eq. 5.11) and the similarity solution for the Fourier transform of the two-point velocity correlation given by

$$y_{i,j}(k_{1}, x_{2}, x_{2}', k_{3}, t) = \frac{1}{4\pi^{2}} \int_{-\infty}^{\infty} \int_{-\infty}^{\infty} R_{i,j}(\varsigma, x_{2}, x_{2}', \beta, t) e^{-i(k_{1}\varsigma + k_{3}\beta)} d\varsigma d\beta$$

$$= \left[Q^{i,j} \delta^{2} \right] \frac{1}{4\pi^{2}} \int_{-\infty}^{\infty} \int_{-\infty}^{\infty} q_{i,j}(\gamma, \eta, \eta', \zeta) e^{-i(\tilde{k}_{1}\gamma + \tilde{k}_{3}\zeta)} d\gamma d\zeta$$

$$= \left[Q^{i,j} \delta^{2} \right] \hat{q}_{i,j}(\tilde{k}_{1}, \eta, \eta', \tilde{k}_{3})$$
(5.14)

into equation 5.7 yields

$$V^{i,j} \int_{-\infty}^{\infty} \hat{q}_{i,j}(\tilde{k}_1, \eta, \eta', \tilde{k}_3) \hat{\chi}_j^n(\tilde{k}_1, \eta, \tilde{k}_3) d\eta' = \Lambda^n(\tilde{k}_1, \tilde{k}_3) \hat{\chi}_i^n(\tilde{k}_1, \eta, \tilde{k}_3), \tag{5.15}$$

where

$$V^{i,j} = \frac{Q^{i,j}}{U_s^2} \tag{5.16}$$

and

$$\Lambda^{n}(\tilde{k}_{1}, \tilde{k}_{3}) = \frac{\hat{\lambda}^{n}(k_{1}, k_{3}, t)}{U_{s}^{2} \delta^{3}}$$
(5.17)

are both independent of time.

Following the methodology outlined by Lumley (1970), it is straightforward to demonstrate that the functions determined from this equation are orthogonal so they can be normalized to form an orthonormal set of functions; *i.e.*,

$$\int_{-\infty}^{\infty} \hat{\chi}_i^n(\tilde{k}_1, \eta, \tilde{k}_3) \hat{\chi}_i^{m*}(\tilde{k}_1, \eta, \tilde{k}_3) d\eta = \delta_{nm}$$

$$(5.18)$$

The similarity scale for the orthogonal functions can be deduced by examining the orthogonality condition for the two sets of orthogonal functions. Substituting equation 5.11 into the orthogonality condition for the functions in physical variables and transforming yields

$$\left[\Upsilon^2 \delta\right] \int_{-\infty}^{\infty} \hat{\chi}_i^n(\tilde{k}_1, \eta, \tilde{k}_3) \hat{\chi}_i^m(\tilde{k}_1, \eta, \tilde{k}_3) d\eta = \delta_{nm}. \tag{5.19}$$

Thus, the functions in the similarity variables form an orthonormal set when

$$\Upsilon = \delta^{-1/2}. (5.20)$$

The relationship between the coefficients of the orthogonal functions in similarity variables and the coefficients of the functions in physical variables is given by

$$a^{n}(k_{1}, k_{3}, t) = \int_{-\infty}^{\infty} \hat{u}_{i}(k_{1}, x_{2}, k_{3}, t) \hat{\Psi}_{i}^{n*}(k_{1}, x_{2}, k_{3}, t) dx_{2}$$

$$= \left[U_{s} \delta^{3} \Upsilon\right] \int_{-\infty}^{\infty} \hat{u}_{i}(\tilde{k}_{1}, \eta, \tilde{k}_{3}, t) \hat{\chi}_{i}^{n*}(\tilde{k}_{1}, \eta, \tilde{k}_{3}) d\eta$$

$$= \left[U_{s} \delta^{5/2}\right] \hat{b}^{n}(\tilde{k}_{1}, \tilde{k}_{3}, t), \qquad (5.21)$$

where \hat{b}^n is the coefficient of the orthogonal functions in similarity variables,

$$\hat{u}_{i}(\tilde{k}_{1}, \eta, \tilde{k}_{3}, t) = \frac{1}{4\pi^{2}} \int_{-\infty}^{\infty} \int_{-\infty}^{\infty} \frac{u_{i}(\tilde{x}_{1}, \eta, \tilde{x}_{3}, t)}{U_{s}} e^{-i(\tilde{k}_{1}\tilde{x}_{1} + \tilde{k}_{3}\tilde{x}_{3})} d\tilde{x}_{1} d\tilde{x}_{3}$$

$$= \frac{1}{4\pi^{2}} \left[\frac{1}{U_{s}\delta^{2}} \right] \int_{-\infty}^{\infty} \int_{-\infty}^{\infty} u_{i}(x_{1}, x_{2}, x_{3}, t) e^{-i(k_{1}x_{1} + k_{3}x_{3})} dx_{1} dx_{3}$$

$$= \left[\frac{1}{U_{s}\delta^{2}} \right] \hat{u}_{i}(k_{1}, x_{2}, k_{3}, t), \qquad (5.22)$$

$$\tilde{x}_1 = \frac{x_1}{\delta},\tag{5.23}$$

and

$$\tilde{x}_3 = \frac{x_3}{\delta}. (5.24)$$

It is evident from equation 5.21 that the coefficients of the orthogonal functions at a fixed wavenumber in physical space are related to the coefficients of the orthogonal functions at different wavenumbers in similarity space (which is again a consequence of the fact that the information is shifting to lower wavenumbers as the flow evolves). Thus, Fourier coefficients of the velocity field at a fixed wavenumber in physical variables are measures of different regimes of the flow as the wake evolves, since the characteristic length scales of the motions grow as the flow evolves.

It is useful to verify that the relationship between the coefficients in equation 5.21 can be used to derive the relationship between the eigenvalues given in equation 5.17, since

$$\overline{\hat{a}^n(k_1, k_3, t)\hat{a}^{m*}(k_1', k_3', t)} = \hat{\lambda}^n(k_1, k_3, t)\delta_{nm}\delta(k_1 - k_1')\delta(k_3 - k_3')$$
(5.25)

and

$$\overline{\hat{b}^n(\tilde{k}_1, \tilde{k}_3, t)\hat{b}^{m*}(\tilde{k}'_1, \tilde{k}'_3, y)} = \Lambda^n(\tilde{k}_1, \tilde{k}_3)\delta_{nm}\delta(\tilde{k}_1 - \tilde{k}'_1)\delta(\tilde{k}_3 - \tilde{k}'_3), \tag{5.26}$$

where δ_{nm} is the Kronecker delta and $\delta(k_1 - k_1')$, etc., are delta functions in the sense of generalized functions.

Using equation 5.11 it follows

$$\hat{\lambda}^{n}(k_{1}, k_{3}, t)\delta_{nm}\delta(k_{1} - k_{1}')\delta(k_{3} - k_{3}') = \left[U_{s}^{2}\delta^{5}\right]\Lambda^{n}(\tilde{k}_{1}, \tilde{k}_{3})\delta_{nm}\delta(\tilde{k}_{1} - \tilde{k}_{1}')\delta(\tilde{k}_{3} - \tilde{k}_{3}').$$
(5.27)

Integrating this expression yields

$$\hat{\lambda}^{n}(k_{1},k_{3},t) = \int \int_{-\infty}^{\infty} \hat{\lambda}^{n}(k_{1},k_{3},t) \delta_{nm} \delta(k_{1}-k_{1}') \delta(k_{3}-k_{3}') dk_{3}' dk_{1}',$$

which can be transformed to yield

$$\hat{\lambda}^{n}(k_{1}, k_{3}, t) = \int \int_{-\infty}^{\infty} \left[U_{s}^{2} \delta^{5} \right] \Lambda^{n}(\tilde{k}_{1}, \tilde{k}_{3}) \delta_{nm} \delta(\tilde{k}_{1} - \tilde{k}_{1}') \delta(\tilde{k}_{3} - \tilde{k}_{3}') \frac{1}{\delta^{2}} d\tilde{k}_{1} d\tilde{k}_{3}
= \left[U_{s}^{2} \delta^{3} \right] \Lambda^{n}(\tilde{k}_{1}, \tilde{k}_{3})$$
(5.28)

as required.

Thus, when the two-point velocity correlation tensor has a similarity solution, the orthogonal functions that are optimally representative of the velocity field at different times in wake evolution (in a mean square sense) can be related by a similarity transform. In which case, it is possible to find a single set of orthogonal functions that can be used to optimally represent the spatial information in the flow.

5.2.2 The Spatially Developing Axisymmetric Jet

In the axisymmetric jet flow, it is not possible to directly transform the equations for the orthogonal functions that are representative of the flow in the three spatial directions in the physical variables into an equation for the orthogonal functions in similarity space. It is possible, though, to find a set of orthogonal functions that are representative of the flow in similarity variables.

The objective is then to find a set of orthogonal functions that are optimally representative of the scaled velocity field in a mean square sense. That is, the functions that maximize the mean-square value of the coefficient given by

$$b_n(t) = \int \frac{\tilde{u}_i(\xi, \eta, x_3, t)}{\tilde{U}_s(\xi)} \Xi_i^{n*} \eta d\xi d\eta dx_3, \tag{5.29}$$

where $\tilde{u}_i(\xi, \eta, x_3, t)$ is the instantaneous velocity in similarity variables and $\tilde{U}_s(\xi)$ is the velocity scale $U_s(x_1)$ written in similarity variables. Thus, the mean square value of the coefficients, Γ , is given by

$$\Gamma^{n} = \frac{\overline{\left[\int \frac{\tilde{u}_{i}(\xi,\eta,x_{3},t)}{\tilde{U}_{s}(\xi)} \Xi_{i}^{n*} \eta d\xi d\eta dx_{3}\right] \left[\int \frac{\tilde{u}_{j}(\xi',\eta',x_{3}',t)}{\tilde{U}_{s}(\xi')} \Xi_{j}^{n*} \eta' d\xi' d\eta' dx_{3}'\right]^{*}}}{\int \Xi_{k}^{n} \Xi_{k}^{n*} \eta'' d\xi'' d\eta'' dx_{3}''}}$$
(5.30)

Following Lumley (1970), Γ^n can be maximized using variation calculus to yield

$$\left(\frac{d\delta}{dx_1}\right)^{b(i,j)} \int \int q_{i,j}(\eta, \eta', \theta, \upsilon) \Xi_j^n \Omega_i^{n*} \eta d\eta dx_3 d\xi \eta' d\eta' dx_3' d\xi'$$

$$= \Gamma^n \int \Xi_k^n \Omega_k^{n*} \eta'' d\eta'' dx_3'' d\xi'', \tag{5.31}$$

where the exponent b(i, j) includes the possibility that all of the components in the Reynolds stress tensor are not equal to U_s^2 .

Note, the transformed streamwise coordinate ξ is infinite in extent and the twopoint correlation is a function of the separation distance between the points in this direction. Therefore, this coordinate direction can be Fourier transformed out of equation 5.31 along with the x_3 direction to yield (Lumley 1970)

$$\left(\frac{d\delta}{dx_1}\right)^{b(i,j)} \int_0^\infty p_{i,j}(\eta, \eta'; m, k_1) \varphi_j^n(\eta'; m, k_1) = \tilde{\Gamma}(m, k_1) \varphi_i^n(\eta; m, k_1), \tag{5.32}$$

where m is the mode number for the azimuthal direction and k_1 is the wavenumber in the transformed streamwise direction. Following the approach outlined by Lumley (1970), it is straightforward to demonstrate that the functions determined from equation 5.32 are orthogonal.

Note, the orthogonal functions determined from equation 5.32 are dependent on the growth rate of the jet when either the value of b(i,j) is not independent of i and j or the functional form of the similarity solutions are implicitly a function of the growth rate. The explicit dependence on the growth rate to the power b(i,j) in equation 5.32 occurs because the velocity has been scaled as a vector in this analysis. Hence, this growth rate factor incorporates two effects: First, it includes the possibility that the scales for the normal stresses may not be proportional, which would indicate that on average the orientation of the velocity vector changes as the growth rate changes. Second, the scale for the shear stresses may differ from those of the normal stresses, which would indicate that the turbulence has been modified causing the (normalized) motion of two of the components to become more or less correlated.

The coefficients for this orthogonal basis are given by

$$d^{n}(t; m, k_{1}) = \int_{0}^{\infty} \left[\frac{1}{2\pi} \int_{-\infty}^{\infty} \frac{1}{2\pi} \int_{0}^{2\pi} \frac{\tilde{u}_{i}(\xi, \eta, x_{3}, t)}{\tilde{U}_{s}(\xi)} e^{-i(mx_{3} + k_{1}\xi)} dx_{3} d\xi \right] \varphi^{n*}(\eta; m, k_{1}) \eta d\eta,$$
(5.33)

where the integration over ξ is defined in the sense of generalized functions (Lighthill, 1956 or Lumley, 1970). Using these coefficients, the instantaneous velocity field in

the far field of the axisymmetric jet can be written as

$$\frac{\tilde{u}_i(\xi, \eta, x_3, t)}{\tilde{U}_s(\xi)} = \int_{-\infty}^{\infty} \left(\sum_{m = -\infty}^{\infty} \sum_{n = 0}^{\infty} d^n(t; m, k_1) e^{i(mx_3 + k_1 \xi)} \varphi_i^n(\eta; m, k_1) \right) dk_1$$
 (5.34)

where the integration over k_1 is also carried out in the sense of generalized functions.

Note, this representation of the flow differs from that outlined for the temporally evolving wake in that the spatially developing, axisymmetric jet is stationary. Hence, neither the orthogonal functions in similarity space nor a set of orthogonal functions deduced in physical variables are functions of time.

In many applications it is difficult to sample the correlation sufficiently in the semiinfinite streamwise direction to resolve the modes in this direction without introducing
a significant error due to undersampling. Therefore, it may be desirable to decompose
the field in fewer coordinate directions, such as a decomposition of the field on a single
plane normal to the streamwise direction (analogous to the decomposition carried out
by Glauser et al. 1995 in the axisymmetric shear layer). For this type of decomposition in the far field of the axisymmetric jet, Ewing and George (1994) demonstrated
that the orthogonal basis in similarity coordinates can be related to the orthogonal
basis in the physical coordinate system (analogous to the temporally evolving wake)
when the two-point velocity correlation tensor has a similarity solution. Thus, in this
case a single orthogonal basis could be used to optimally decompose the flow on any
plane (orthogonal to the streamwise direction) in the far field of the axisymmetric jet.

Chapter 6

Summary and Concluding Remarks

The analyses outlined in the previous chapters illustrate that the equations that govern the evolution of the two-point velocity correlation tensor admit similarity solutions for three different free-shear flows: the temporally evolving plane wake, the spatially evolving axisymmetric jet, and the spatially evolving plane jet. The similarity solutions for each of these flows have different characteristics that shed insight into the nature of their evolution. The analyses of these flows also outlines many of the techniques that are necessary for extensions to other shear flows. These solutions are consistent with those derived for the single-point moments. In fact, the solutions for the single-point moments can be viewed as a special case of a more general similarity solution for the two-point correlations.

For the temporally evolving wake, the similarity analysis was extended to the more general two-point, two-time correlation tensor in a reference frame which is translating with a velocity equal to the freestream velocity. This was accomplished by defining a new time scale where each differential change in time is normalized by a time scale that was proportional to the local time scales of the flow, yielding a new time coordinate that varies in synchronicity with the flow.

It was also demonstrated that the governing equation for the two-point scalar correlation in the wake admits a similarity solution for two different scalar fields. The first was a field where the mean value of the scalar differs on the two sides of the flow, which physically corresponds to a flow behind a splitter plate with different mean values of the scalar on either side of the wake. The second was a scalar field with a mean deficit (or surplus) in the wake which physically corresponds to the flow over a hot/cold body.

The two-point velocity correlation tensor and the two-point scalar correlation contain a great deal of information about the flow. Thus, a number of observations can be made when a similarity solution exists for the two-point velocity correlation tensor and the two-point scalar correlation. Firstly, it can be shown that the two-point velocity-gradient moments and the two-point scalar-gradient moments can be expressed as a similarity solution. In fact, this is a necessary condition to ensure that the molecular diffusion terms and the convective terms in equations which govern the two-point correlation tensor evolve in an 'equilibrium' or 'similarity' manner. In this case, the two-point vorticity correlation tensor and the two-point rate-of-strain correlation tensor can also be expressed in similarity form. Consequently, the single-point vorticity correlation and the rate of dissipation of the kinetic energy per unit mass have similarity solutions when the two-point velocity correlation tensor has a similarity solution. Similarly, the similarity solution for the two-point scalar-gradient correlation can be used to demonstrate that a similarity solution exists for the rate

of dissipation of the scalar variance in this flow.

It is also straightforward to demonstrate that the second-order structure function for the velocity and the scalar fields can be written as similarity solutions. The solutions for both of the two-point velocity gradient correlations and the second-order structure function for the velocity field are consistent that purposed by Kolmogorov (1941) for the small-scale motions. Hence, when a similarity solution exists for the two-point velocity correlation tensor, the statistical measures of the small-scale motions will collapse when they are scaled by the Kolmogorov length and velocity scale, (in fact the statistics of all of the motion collapse with this scaling) even in finite-Reynolds-number flows. Of course, the profiles are a function of the Reynolds number. The present analysis does not indicate whether or not the profiles are universal for very high Reynolds numbers as proposed by Kolmogorov, but it does not exclude the possibility.

It can also be shown that the one-dimensional spectra of the two-point velocity and scalar correlations in the homogeneous directions can be expressed as similarity solutions. Further, the length scales that can be determined from these one-dimensional spectra or the two-point correlation tensor, such as the integral and the Taylor microscales, grow in proportion to the similarity length scale.

The similarity solutions for the two-point velocity correlation tensor and the two-point scalar correlation in the wake flow are derived assuming the flow originated from a virtual source. Hence, for a temporally developing wake generated from an actual set of initial conditions, these similarity solutions must be viewed as a possible

asymptotic state of the turbulence. Further, the governing equations for the similarity profiles of the two-point correlation contain constants which may depend on the source conditions of the wake. Consequently, the asymptotic state of the wakes generated from actual sources may depend on the source used to generate the wake; *i.e.*, the asymptotic state of the turbulence in different wake flows may not be universal.

The similarity hypothesis for the two-point velocity correlation tensor and the two-point scalar correlation were examined using Direct Numerical Simulations of temporally evolving wakes computed by Moser and Rogers (1994): an unforced wake and a wake with two-dimensional forcing. It is not possible to simulate a wake that is infinite in extent in the x_1 - and x_3 -directions, so the flow was modeled by a wake in a box that is periodic in the x_1 - and x_3 -directions. It is argued that motions significantly smaller than the dimensions of the box evolve like those in a wake evolving in an infinite environment.

The one-dimensional spectra of the two-point velocity correlation tensor in the x_1 and x_3 -directions are utilized to compare the predictions of the two-point similarity
hypothesis and the data from the simulations. Overall, the agreement between the
data and the predictions of the theory in both wakes is good for all but the largest
scales in the computation, particularly for the central region of the wake. Further
from the centerline there is more scatter owing to the highly intermittent nature of
the flow in this region (which caused poor statistical convergence). A comparison
of the Taylor microscales calculated from the one-dimensional spectra demonstrated
that these lengths scales grow approximately in proportion with the similarity length
scales for the points between the half-deficit points in the wake, as predicted by the

similarity hypothesis. The second order structure functions in the x_2 -directions were also used to test the similarity hypothesis. The functions collapse when they are scaled in the manner predicted by the similarity hypothesis for small and moderate separation distances.

The one-dimensional spectra of the two-point scalar spectra in the x_1 - and x_3 directions were also compared to the data from the simulation of the wake with a
two-stream mean scalar field. Again, the spectra except for the low-wave-number
region collapsed when they were scaled in the manner predicted by the similarity
hypothesis for positions between the half-deficit points of the wake. Outside of this
region the realizations from the simulations could not provide an accurate statistical
measure of the flow because the wake is too intermittent. The Taylor microscales
computed from these spectra are also approximately proportional to the similarity
length scale, as required by the similarity analysis.

Much of the variability in the statistical measures of the large-scale motions is attributable to a lack of sufficient independent samples for the motions of this scale, since the statistical measures are computed by spatially averaging over one full-field realization of the flow. An ensemble average over several simulations, would presumably yield better agreement with the predictions from the theory. Of course, there would never be exact agreement because the periodic boundary conditions in the wake simulations are incompatible with the boundary conditions used in the development of the two-point similarity hypothesis for an infinite environment. Overall, the good agreement between the theory and the data adds credence to both the two-point similarity hypothesis and the idea that the motions in the simulations resemble the

motions in wake evolving in an infinite environment.

In the similarity solution for the two-point velocity correlation tensor in the spatially developing axisymmetric jet it is necessary to define the similarity coordinate in the streamwise direction by normalizing the distances in this direction by the local length scale of the flow. (This is analogous to the methodology use in the analysis of the two-point, two time correlation in the temporally evolving wake). This similarity solution is valid for all separation distances. In fact, the two-point correlation tensor will collapse when it is normalized by any length and velocity scales that are proportional to the similarity scales, including those proposed by Kolmogorov, though, the functional form of the similarity profiles do depend on the ratios of the similarity variables chosen and the characteristic length and velocity scales of the turbulence (which are dependent on the Reynolds number of the flow). The growth rate of the axisymmetric jet also appeared as a parameter in the equations for the similarity profiles, indicating that they may be depend on the source conditions of the jet, to the extent that such conditions control this parameter.

The functional form of the pressure-velocity correlation was determine by solving a Poisson-type equation for the pressure field (c.f. Townsend 1956). The pressure field required to produce the motion in the thin vortical region of the jet yielded a pressure-velocity correlation that is consistent with the solution required in the analysis of the two-point velocity correlation tensor. But, it was also evident that the equations of motion would not admit similarity solutions unless the pressure field required to satisfy the boundary conditions on the flow yielded a pressure-velocity correlations that is also consistent with the hypothesized similarity solution. In theory,

such a set of boundary conditions should exist, in which case the governing equations for the two-point correlation tensor admit similarity solutions.

It was also straightforward to demonstrate that the velocity-gradient moments in the axisymmetric jet can be written in a similarity form, when the two-point velocity correlation tensor has a similarity solution. In this case, the rate of dissipation of the kinetic energy per unit mass, the two-point vorticity correlation, and the single point vorticity moments can be written in the similarity form.

Unlike the previous two flows, many free-shear flows, such as the plane jet, are not constant-Reynolds-number flows. In the plane jet, the Reynolds number of the flow increases as the flow evolves downstream. In this flow, the equations governing the two-point velocity correlation tensor do not admit similarity solutions. Instead, the equations that govern the correlation tensor for large separation distances (which emphasize the large-scale motions) and the equations that govern the second-order structure functions (which emphasize the small-scale motions) were examined separately. Each of these equation sets can be reduced to an equation set that admits similarity solutions, by neglecting the higher-order terms in the infinite-Reynolds-number limit. These solutions can, of course, be considered to be a first-order approximation of the two-point correlation tensor in a finite-Reynolds-number flow. The similarity solution derived for the second-order structure function (in the infinite-Reynolds-number limit) are consistent with the similarity solution proposed by Kolmogorov (1941). Again the analysis did not indicate that the similarity solutions for the scale-motions are unique, but it did not exclude this possibility.

The analyses outlined in this thesis demonstrate that similarity solutions do exist for the two-point velocity correlation tensor in several free-shear flows. Hence, the equations governing the statistical moments in these flows are consistent with the hypothesis that the turbulent structure (and the related probability density function) is similar at least to the level of the two-point velocity correlation tensor. It seems reasonable to expect that similarity solutions exist for the higher order moments, particularly for the constant Reynolds number flows, although this is obviously a point that must be investigated further in the future. Of course, the similarity solutions outlined here must be considered as an asymptotic solution of a flow from a real source, so the same would be true of the similar turbulent structure, if it exists. The governing equations also indicate that this asymptotic state may not be independent of the source conditions of the flow. The boundary conditions of the flow also play a crucial role in determining whether, in fact, the flow reaches an asymptotic state, and if is does, what that state is. It is reasonable to expect that the boundary conditions will influence the evolution of the large-scale structures more than the smaller structures in the flow. Thus, it is far more likely that evidence of the two-point similarity solution can be found for the moderate- to small-scale motions, as is, in fact, observed in the data from the temporally developing wake simulations.

Bibliography

Batchelor, G. K. (1947). Kolmogoroff's theory of locally isotropic turbulence. *Proc. Camb. Phil. Soc.* **43**, 533.

Batchelor, G. K. (1948). Energy decay and self-preserving correlation functions in isotropic turbulence. Q. Appl. Math 6, 192.

Batchelor, G. K. (1953). Homogeneous Turbulence. Cambrigde University Press.

Batchelor, G. K. (1967). An Introduction to Fluid Dynamics. Cambridge University Press, New York.

Berkooz, G., Holmes, P., and Lumley, J. L. (1993). The proper orthgononal decomposition in the analysis of turbulent shear flows. *Ann. Rev. of Fluid Mech.* **25**, 538–575.

Bernard, C. G. Speziale P. (1992). The energy decay in self-preserving isotropic turbulence revisited. *J. of Fluid Mech.* **241**, 645–47.

Bonnet, J. P., Delville, J., and Garem, H. (1986). Space and space-time longitudinal velocity correlations in the turbulent far wake of a flat plate in incompressible flow. Expts. in Fluids 4, 189–196.

Burmeister, L. C. (1983). Convective Heat Transfer. John Wiley & Sons, New York.

Cantwell, B. J. and Coles, D. (1983). An experimental study of entrainment and transport in the turbulent near wake of a circular cylinder. *J. of Fluid Mech.* **136**, 321–374.

Champagne, F. H. (1978). The fine-scale structure of the turbulent velocity field. J. of Fluid Mech. 86, 67–108.

Cohen, J. and Wygnanski, I. (1987). The evolution of instabilities in the axisymmetric jet. part 1. the linear growth of disturbances near the nozzle. *J. of Fluid Mech.* **176**, 191–219.

Ewing, D. and George, W. K. (1994). Application of a similarity hypothesis to the proper orthogonal decomposition for spatially evolving flows. In *Proc. of the Int. Symp. on Turbulent Heat and Mass Transfer*, Lisbon, Portugal.

George, W. K. and Gibson, M. M. (1992). The self preservation of homogeneous shear flow turbulence. *Expts. in Fluids* **13**, 229.

George, W. K., Castillo, L., and Knecht, P. (1995). The zero pressure gradient turbulent boundary layer. *Phys. Fluids*. submitted for publication.

George, W. K. (1978). Processing of random signals. In *Proc. of the Dynamic Flow Conference*.

George, W. K. (1989). The self-preservation of turbulent flows and its relation to initial conditions and coherent structures. In George, W. K. and Arndt, R. E., editors, *Advances in Turbulence*, pages 39–73. Hemisphere, New York.

George, W. K. (1990). Governing equations, experiments and the experimentalist. Expt. Fluid and Therm. Sci. 3, 557–566.

George, W. K. (1992). Decay of homogeneous isotropic turbulence. *Phys. of Fluids* A 4, 1492–1508.

George, W. K. (1994). Some new ideas for similarity of turbulent shear flows. In *Proc. of the Int. Symp. on Turbulent Heat and Mass Transfer*, Lisbon Portugal.

Glauser, M., Zheng, X., and George, W. K. (1995). An analysis of the turbulent axisymmetric jet mixing layer utilizing the proper orthogonal decomposition. *J. of Fluid Mech*. to be published.

Grant, H. L. (1958). The large eddies of turbulent motion. J. of Fluid Mech. 3, 149–190.

Grinstein, F. F. (1994). Open boundary conditions in the simulation of subsonic turbulent shear flows. J. of Comp. Phys. 115, 343-55.

Hayakawa, M. and Hussain, F. (1989). Three-dimensionality of the organized structures in a plane turbulent wake. J. of Fluid Mech. 206, 375–404.

Hinze, J. O. (1975). Turbulence. McGraw-Hill, New York.

Hussein, H. J., Capp, S. P., and George, W. K. (1994). Velocity measurements in a high-reynolds-number, momentum-conserving, axisymmetric, turbulent jet. *J. of Fluid Mech.* **258**, 31–75.

Kolmogorov, A. N. (1941). Local structure of turbulence in an incompressble fluid at a very high reynolds number. *Dokl. Akad. Nauk SSSR* **30**, 299–303.

Kolmogorov, A. N. (1963). A refinement of previous hypothesis concerning the local structure of turbulence in a viscous incompressible fluid at high reynolds number. J. of Fluid Mech. 1, 82–85.

Lighthill, M. J. (1956). An Introduction to Fourier Analysis and Generalized Functions. Cambridge University Press, London.

Lumley, J. L. (1970). Stochastic Tools. Academic Press.

Monin, A. S. and Yaglom, A. M. (1975). Statistical Fluid Mechanics Vol. II. MIT Press.

Moser, R. D. and Rogers, M. M. (1994). Direct simulation of a self-similar plane wake. Technical Report TM 108815, NASA Tech. Memo.

Mumford, J. C. (1983). The structure of the large eddies in fully developed turbulent shear flows. part 2. the plane wake. J. of Fluid Mech. 137, 447–456.

Panchapakesan, N. R. and Lumley, J. L. (1993). Turbulence measurements in axisymmetric jets of air and helium. part 1. air jet. J. Fluid Mech. 246, 197–223.

Payne, F. R. and Lumley, J. L. (1967). Large eddy structure of the turbulent wake behind a circular cylinder. *Phys. of Fluids Supp.* **10**, S194–S196.

Prasas, A. and Williamson, C. H. K. (1993). A new mechanism for oblique wave resonance in the 'natural' far wake. *J. of Fluid Mech.* **256**, 269–313.

Spalart, P. R., Moser, R. D., and Rogers, M. M. (1991). Spectral methods for the navier-stokes equations with one infinite and two periodic directions. *J. of Comp. Phys.* **96**, 297.

Spalart, P. R. (1988). Direct simulation of a turbulent boundary layer up to r_{θ} =1410. J. of Fluid Mech. 187, 67.

Sreenivasan, K. R. (1983). The azimuthal correlations of velocity and temperature fluctuations. *J. of Fluid Mech.* **136**, 321–374.

Tennekes, H. and Lumley, J. L. (1972). A First Course in Turbulence. MIT Press.

Townsend, A. A. (1956). The Structure of Turbulent Shear Flow. Cambridge University Press, London.

Townsend, A. A. (1979). Flow patterns of large eddies in a wake and in a boundary layer. J. Fluid Mech. 95, 515–537.

Towsend, A. A. (1970). Entrainment and the structure of turbulent flow. *J. of Fluid Mech.* 41, 13–46.

von Karmen, T. and Howarth, L. (1938). On the statistical theory of isotropic turbulence. *Proc. Roy. Soc. London (A)* **164**, 476.

Weygandt, J. H. and Mehta, R. D. (1993). Three-dimensional structure of straight and curved plane wakes. Technical Report JIAA TR-110, Stanford University.

Wygnanski, I., Champagne, F., and Marasli, B. (1986). On the large-scale structures in two-dimensional small-deficit, turbulent wakes. *J. of Fluid Mech.* **168**, 31.

Zaman, K. B. M. Q. and Hussain, A. K. M. F. (1980). Vortex pairing in the circular jet under controlled excitation. part 1. general jet response. *J. of Fluid Mech*.

Zhou, Y. and Antonia, R. A. (1993). A study of turbulent vorticies in the near wake of a cylinder. J. of Fluid Mech. 253, 375–404.

Appendix A

Review of Single-Point Similarity Hypothesis for the Axisymmetric Jet

The similarity analysis of the single-point equations for the far field of the axisymmetric jet was reported previously by (George, 1989), but recent studies of other shear flows (George, 1994) have illustrated the need to vary the earlier approach outlined by George (1989) (see also appendix of Hussein et al., 1994). The derivation in this section is in keeping with this later work. The similarity analysis is carried out using only the leading-order terms in the Reynolds-averaged equations, so the solutions outlined in this section are first-order accurate.

Using the standard thin-shear-layer and high-Reynolds-number assumptions (v. Tennekes and Lumley, 1972), the first-order differential and integral equations for the

mean momentum are given by (Hussein et al. 1994)

$$U_1 \frac{\partial U_1}{\partial x_1} + U_2 \frac{\partial U_1}{\partial x_2} = -\frac{1}{x_2} \frac{\partial x_2 \overline{u_1 u_2}}{\partial x_2}$$
(A.1)

and

$$\int_0^\infty U_1^2 x_2 dx_2 = M_o, (A.2)$$

where U_i and u_i are the mean and fluctuating velocity, respectively, in the x_i -direction. The geometry of the axisymmetric jet and orientation of the coordinate system are illustrated in figure 3.1. The overbar in the equation A.1 indicates an ensemble average and M_0 in equation A.2 is the rate of momentum addition at the source.

It is hypothesized that a similarity solution exists for these equations where the mean streamwise velocity, U_1 , can be written as

$$U_1(x_1, x_2) = U_s(x_1) f(\eta)$$
(A.3)

and the turbulent Reynolds stress $\overline{u_1u_2}$ is given by

$$\overline{u_1 u_2} = R_s(x_1) g(\eta), \tag{A.4}$$

where

$$\eta = \frac{x_2}{\delta} \tag{A.5}$$

and $\delta(x_1)$ and $U_s(x_1)$ are the similarity length and velocity scales for the far field of the axisymmetric jet. In this analysis it is assumed that the far field of the axisymmetric jet is statistically homogeneous in the azimuthal direction, so the single-point moments are independent of the azimuthal coordinate. Note, in order to avoid overconstraining the analysis of the problem, the scale for the Reynolds stress is arbitrary at this point and has not been chosen equal to U_s^2 . The mean cross-stream velocity, U_2 , can be determined by integrating the averaged incompressible continuity equation for this flow given by

$$\frac{\partial U_1}{\partial x_1} + \frac{1}{x_2} \frac{\partial x_2 U_2}{\partial x_2} = 0 \tag{A.6}$$

Substituting the hypothesized similarity solution for U_1 (eq. A.3) into this equation A.6 and integrating the equation from the centerline (where the cross-tream velocity U_2 is zero) yields

$$U(x_1, x_2) = -\left(\left[\delta \frac{dU_s}{dx_1}\right] + 2\left[U_s \frac{d\delta}{dx_1}\right]\right) \frac{1}{\eta} \int_0^{\eta} \tilde{\eta} f(\tilde{\eta}) d\tilde{\eta} + \left[U_s \frac{d\delta}{dx_1}\right] \eta f(\eta). \tag{A.7}$$

Substituting equations A.3, A.4 and A.7 into the differential and integral mean momentum equations (eqn. A.1 and A.2) yields

$$\left[U_s \frac{dU_s}{dx_1}\right] f^2 - \left(\left[U_s \frac{dU_s}{dx_1}\right] + 2\left[\frac{U_s^2}{\delta} \frac{d\delta}{dx_1}\right]\right) \frac{df}{d\eta} \frac{1}{\eta} \int_0^{\eta} \tilde{\eta} f(\tilde{\eta}) d\tilde{\eta} = -\left[\frac{R_s}{\delta}\right] \frac{1}{\eta} \frac{d\eta g}{d\eta} \tag{A.8}$$

and

$$\left[U_s^2 \delta^2\right] \int_0^\infty f^2 \tilde{\eta} d\tilde{\eta} = M_0 \tag{A.9}$$

The x_1 -dependent portion of each term in equation A.8 and A.9 is contained in square brackets.

Mathematically, these equations admit similarity solutions if the x_1 dependence of all of the terms in each equation are proportional, so equations A.8 and A.9 can be transformed into equations that are only a function of the similarity variable η . Physically, this implies that the flow evolves such that all of the terms in each equation maintain a relative balance as the flow evolves downstream.

Thus, equations A.8 and A.9 admit similarity solutions if

$$\left[U_s \frac{dU_s}{dx_1}\right] \propto \left[\frac{U_s^2}{\delta} \frac{d\delta}{dx_1}\right] \propto \left[\frac{R_s}{\delta}\right] \tag{A.10}$$

and

$$\left[U_s^2 \delta^2\right] \propto M_0. \tag{A.11}$$

These constraints are satisfied if

$$R_s \propto U_s^2 \frac{d\delta}{dx_1},$$
 (A.12)

$$U_s \propto \frac{M_0^{1/2}}{\delta},\tag{A.13}$$

and

$$\frac{1}{U_s} \frac{\partial U_s}{\partial x_1} \propto \frac{1}{\delta} \frac{d\delta}{dx_1}.$$
 (A.14)

It is straightforward to demonstrate that equation A.14 is satisfied when the constraint in equation A.13 is satisfied, so there are only two independent equations. Note, the growth rate of the jet is not determined by these constraints because the ratio R_s/U_s^2 is not yet known.

It is also evident that the equations only admit similarity solutions when i.e.,

$$Re_{\delta} = \frac{U_s \delta}{\nu} \propto M_o,$$
 (A.15)

which is an important consideration in the analysis of the equations for the two-point velocity correlation tensor.

In order to determine the growth rate of the jet, George (1989) examined the turbulent kinetic energy equation using scales for the rate of dissipation of the turbulent kinetic energy determined from physical arguments. Later analysis (George, 1994) indicated that it is more appropriate to examine the individual Reynolds stress component equations.

The first-order equation for the Reynolds stress $\overline{u_1u_1}$ is given by

$$U_k \frac{\partial \overline{u_1 u_1}}{\partial x_k} = 2 \frac{\overline{p} \frac{\partial u_1}{\partial x_1}}{\overline{p} \frac{\partial u_1}{\partial x_1}} - \frac{1}{x_2} \frac{\partial}{\partial x_2} x_2 \overline{u_2 u_1^2} - 2 \overline{u_1 u_2} \frac{\partial u_1}{\partial x_2} - \epsilon_{11}, \tag{A.16}$$

where ϵ_{11} is the rate of dissipation of $\overline{u_1u_1}$ per unit mass.

It is hypothesized that this equation admits a similarity solution where the moments are given by

$$2\frac{\overline{p}\frac{\partial u_1}{\partial x_1}}{P} = P^1(x_1)p_1(\eta), \tag{A.17}$$

$$\overline{u_2 u_1^2} = T^1(x_1) t_1(\eta), \tag{A.18}$$

and

$$\epsilon_{11} = D^1(x_1)d_1(\eta).$$
 (A.19)

It is straightforward to demonstrate that equation A.16 only admits a similarity solution of the hypothesized form when

$$K^1 \propto U_s^2,$$
 (A.20)

$$D^1 \propto P^1 \propto \frac{U_s^3}{\delta} \frac{d\delta}{dx_1},$$
 (A.21)

and

$$T^1 \propto U_s^3 \frac{d\delta}{dx_1}.$$
 (A.22)

Similar analyses can be carried out for first-order equations that govern the other Reynolds stresses $\overline{u_2u_2}$, $\overline{u_3u_3}$, and $\overline{u_1u_2}$, given by

$$U_k \frac{\partial \overline{u_2 u_2}}{\partial x_k} = 2 \frac{\overline{p} \frac{1}{\rho} \frac{\partial x_2 u_2}{\partial x_2}}{\partial x_2} - \frac{1}{x_2} \frac{\partial}{\partial x_2} \left\{ x_2 \overline{u_2 u_2^2} 2 x_2 \overline{p u_2} \right\} + 2 \frac{\overline{u_3^2 u_2}}{x_2} - \epsilon_{22}, \tag{A.23}$$

$$U_k \frac{\partial \overline{u_3 u_3}}{\partial x_k} = 2 \frac{\overline{p} \frac{\partial u_3}{\partial x_3}}{\rho \frac{\partial u_3}{\partial x_3}} - \frac{1}{x_2} \frac{\partial}{\partial x_2} (x_2 \overline{u_2 u_3^2}) - 2 \frac{\overline{u_3^2 u_2}}{x_2} - \epsilon_{33}, \tag{A.24}$$

and

$$U_k \frac{\partial \overline{u_1 u_2}}{\partial x_k} = \frac{\overline{p} \left(\frac{\partial u_1}{\partial x_2} + \frac{\partial u_2}{\partial x_1} \right)}{\overline{p} \left(\frac{\partial u_2}{\partial x_2} + \frac{\partial u_2}{\partial x_2} \right)} - \frac{1}{x_2} \frac{\partial}{\partial x_2} (x_2 \overline{u_1 u_2^2}) - \overline{u_2 u_2} \frac{\partial U_1}{\partial x_2} + \frac{\overline{u_3^2 u_1}}{x_2}. \tag{A.25}$$

Expressing each of the moments in these equations in a similarity form analogous to those in equations A.17 - A.19, it is straightforward to demonstrate that these equations only admit similarity solutions of the hypothesized form when

$$P^2 \propto D^2 \propto \frac{U_s K^2}{\delta} \frac{d\delta}{dx_1},$$
 (A.26)

$$T^{2_1} \propto T^{2_2} \propto U_s K^2 \frac{d\delta}{dx_1},$$
 (A.27)

$$P^3 \propto D^2 \propto \frac{U_s K^3}{\delta} \frac{d\delta}{dx_1},$$
 (A.28)

$$T^{3_1} \propto T^{3_2} \propto U_s K^3 \frac{d\delta}{dx_1},$$
 (A.29)

$$P^{12} \propto R_s U_s \frac{d\delta}{dx_1},\tag{A.30}$$

$$K^2 \propto R_s \frac{d\delta}{dx_1},$$
 (A.31)

and

$$T^{12_1} \propto T^{12_2} \propto U_s R_s \frac{d\delta}{dx_1}.\tag{A.32}$$

In addition, for incompressible flows the sum of the pressure-strain terms in equations A.16, A.23, and A.24 must be zero; *i.e.*,

$$\frac{\overline{p}\frac{\partial u_1}{\partial x_1}}{\rho} + \frac{\overline{p}\frac{1}{\rho x_2}\frac{\partial x_2 u_2}{\partial x_2}}{\partial x_2} + \frac{\overline{p}\frac{\partial u_3}{\partial x_3}}{\rho} = 0 \tag{A.33}$$

Substituting the hypothesized form of the similarity solutions into this equation yields

$$[P^1] p_1 + [P^2] p_2 + [P^3] p_3 = 0.$$
 (A.34)

Therefore, the hypothesized similarity solutions for the Reynolds-stress equations are only consistent with the equations of motion if the scales for the pressure-strain terms are proportional; *i.e.*,

$$[P^1] \propto [P^2] \propto [P^3],$$
 (A.35)

which can only be satisfied when

$$K^1 \propto K^2 \propto K^3 \propto U_s^2$$
. (A.36)

Comparing the constraints outlined in equations A.12, A.31, and A.36 yields

$$K^2 \propto U_s^2 \propto R_s \frac{d\delta}{dx_1} \propto U_s^2 \left(\frac{d\delta}{dx_1}\right)^2$$
 (A.37)

Thus, a similarity solution for the Reynolds-stress equations is only possible when

$$\frac{d\delta}{dx_1} \propto const,\tag{A.38}$$

which is analogous to the result obtained by George (1994) in an analysis of the plane jet.

There are two different choices for the scale in equation A.37 and it is not obvious from this analysis which of these choices is more appropriate when scaling data from jets with different growth rates. One consequence of having these two choices, is that the final set of equations that govern the similarity solutions have terms multiplied

by constants that depend on the growth rate of the jet.¹ Therefore, the functional form of the similarity solutions (e.g. $k_2(\eta)$) may implicitly depend on the growth rate of the jet, or more properly on the initial conditions of the jet (George 1989).

These constraints in the equations also define the scale for the dissipation rate terms in the Reynolds-stress equations. It is straightforward to demonstrate that the scales for all of the dissipation terms in these equations are proportional to a single scale given by

$$D^i \propto \frac{U_s^3}{\delta}.\tag{A.39}$$

The constant of proportionality may differ for the individual components and it may be a function of the growth rate or Reynolds number of the jet.

¹Here it is assumed that the length scale is chosen such that the mean velocity profiles collapse.

Appendix B

Transport Equation for the

Structure Function

Following the methodology Batchelor (1947) outlined for isotropic turbulence, it is straightforward to derive an equation governing the evolution of the mean-square velocity difference (or the second-order structure function) for non-homogeneous turbulence.

For a Cartesian coordinate system, the governing equations for the two-point velocity correlation tensor are given by (Hinze, 1975)

$$U_{k} \frac{\partial \overline{u_{\alpha} u_{\beta}'}}{\partial x_{k}} + U_{k}' \frac{\partial \overline{u_{\alpha} u_{\beta}'}}{\partial x_{k}'} = -\frac{1}{\rho} \frac{\partial \overline{p u_{\beta}'}}{\partial x_{\alpha}} - \frac{1}{\rho} \frac{\partial \overline{p' u_{\alpha}}}{\partial x_{\beta}'}$$
$$-\frac{\partial \overline{u_{k} u_{\alpha} u_{\beta}'}}{\partial x_{k}} - \frac{\partial \overline{u_{k}' u_{\alpha} u_{\beta}'}}{\partial x_{k}'} - \overline{u_{\beta}' u_{k}} \frac{\partial U_{\alpha}}{\partial x_{k}} - \overline{u_{\alpha} u_{k}'} \frac{\partial U_{\beta}'}{\partial x_{k}'}$$
$$+\nu \left\{ \frac{\partial^{2}}{\partial x_{k} \partial x_{k}} + \frac{\partial^{2}}{\partial x_{k}' \partial x_{k}'} \right\} \overline{u_{\alpha} u_{\beta}'}, \tag{B.1}$$

where the primed variables are evaluated at of one of the arbitrary points in space

and the unprimed variables are evaluated at the other.

The equation that governs the evolution of the correlation $\overline{u'_{\beta}u'_{\beta}}$ (no summation for greek indicies) in Cartesian coordinates is given by

$$U_{k}^{\prime} \frac{\partial \overline{u_{\beta}^{\prime} u_{\beta}^{\prime}}}{\partial x_{k}^{\prime}} = -\frac{2}{\rho} \frac{\partial \overline{p^{\prime} u_{\beta}^{\prime}}}{\partial x_{\beta}^{\prime}} + 2 \frac{\overline{p} \frac{\partial u_{\beta}^{\prime}}{\partial x_{\beta}^{\prime}} - \frac{\partial \overline{u_{k}^{\prime} u_{\beta}^{\prime} u_{\beta}^{\prime}}}{\partial x_{k}^{\prime}} - 2 \overline{u_{\beta}^{\prime} u_{k}^{\prime}} \frac{\partial U_{\beta}^{\prime}}{\partial x_{k}^{\prime}} + \nu \frac{\partial^{2} \overline{u_{\beta}^{\prime} u_{\beta}^{\prime}}}{\partial x_{k}^{\prime} \partial x_{k}^{\prime}} - 2 \nu \frac{\overline{\partial u_{\beta}^{\prime}} \frac{\partial u_{\beta}^{\prime}}}{\partial x_{k}^{\prime}} \frac{\partial u_{\beta}^{\prime}}{\partial x_{k}^{\prime}}$$
(B.2)

where the index notation is used for the subscript k in this equation. Similarly, the equation that governs the evolution of the correlation $\overline{u_{\alpha}u_{\alpha}}$ is given by

$$U_{k}\frac{\partial \overline{u_{\alpha}u_{\alpha}}}{\partial x_{k}} = -\frac{2}{\rho}\frac{\partial \overline{\rho}u_{\alpha}}{\partial x_{\alpha}} + 2\overline{\frac{\rho}{\rho}\frac{\partial u_{\alpha}}{\partial x_{\alpha}}} - \frac{\partial \overline{u_{k}u_{\alpha}u_{\alpha}}}{\partial x_{k}} - 2\overline{u_{\alpha}u_{k}}\frac{\partial U_{\alpha}}{\partial x_{k}} + \nu\frac{\partial^{2}\overline{u_{\alpha}u_{\alpha}}}{\partial x_{k}\partial x_{k}} - 2\nu\overline{\frac{\partial u_{\alpha}}{\partial x_{k}}\frac{\partial u_{\alpha}}{\partial x_{k}}}.$$
(B.3)

The equation for the mean square velocity difference can be determined by adding equation B.2 to equation B.3 and subtracting twice equation B.1 to yield

$$U_{k}' \frac{\partial \overline{u_{\beta}u_{\beta}'}}{\partial x_{k}'} + U_{k} \frac{\partial \overline{u_{\alpha}u_{\alpha}}}{\partial x_{k}} - 2\left(U_{k} \frac{\partial \overline{u_{\alpha}u_{\beta}'}}{\partial x_{k}} + U_{k}' \frac{\partial \overline{u_{\alpha}u_{\beta}'}}{\partial x_{k}'}\right) =$$

$$+2\frac{\overline{\rho}}{\rho} \frac{\partial u_{\beta}'}{\partial x_{\beta}'} + 2\frac{\overline{\rho}}{\rho} \frac{\partial u_{\alpha}}{\partial x_{\alpha}} - \frac{2}{\rho} \frac{\partial \overline{\rho'u_{\beta}'}}{\partial x_{\beta}'} - \frac{2}{\rho} \frac{\partial \overline{\rho u_{\alpha}}}{\partial x_{\alpha}} - 2\left(\frac{1}{\rho} \frac{\partial \overline{\rho u_{\beta}'}}{\partial x_{\alpha}} + \frac{1}{\rho} \frac{\partial \overline{\rho'u_{\alpha}}}{\partial x_{\beta}'}\right)$$

$$-\frac{\partial \overline{u_{k}u_{\alpha}u_{\alpha}'}}{\partial x_{k}} - \frac{\partial \overline{u_{k}'u_{\beta}u_{\beta}'}}{\partial x_{k}'} - 2\left(\frac{\partial \overline{u_{k}u_{\alpha}u_{\beta}'}}{\partial x_{k}} + \frac{\partial \overline{u_{k}'u_{\alpha}u_{\beta}'}}{\partial x_{k}'}\right)$$

$$-2\overline{u_{\beta}'u_{k}'} \frac{\partial U_{\beta}'}{\partial x_{k}'} - 2\overline{u_{\alpha}u_{k}} \frac{\partial U_{\alpha}}{\partial x_{k}} - 2\left(\overline{u_{\beta}'u_{k}} \frac{\partial U_{\alpha}}{\partial x_{k}} + \overline{u_{\alpha}u_{k}'} \frac{\partial U_{\beta}'}{\partial x_{k}'}\right)$$

$$+\nu \frac{\partial^{2}\overline{u_{\beta}'u_{\beta}'}}{\partial x_{k}'\partial x_{k}'} + \nu \frac{\partial^{2}\overline{u_{\alpha}u_{\alpha}}}{\partial x_{k}\partial x_{k}} - 2\left(+\nu \left\{\frac{\partial^{2}}{\partial x_{k}\partial x_{k}} + \frac{\partial^{2}}{\partial x_{k}'\partial x_{k}'}\right\} \overline{u_{\alpha}u_{\beta}'}\right) - v_{\alpha\alpha} - v_{\beta\beta}, \quad (B.4)$$

where

$$v_{\beta\beta} = 2\nu \frac{\overline{\partial u_{\beta}'}}{\partial x_{k}'} \frac{\partial u_{\beta}'}{\partial x_{k}'}.$$
 (B.5)

This equation can be simplified by noting that

$$\frac{\partial \overline{u_{\beta}' u_{\beta}'}}{\partial x_k} = 0 \tag{B.6}$$

and

$$\frac{\partial \overline{u_{\alpha}u_{\alpha}}}{\partial x_{k}'} = 0 \tag{B.7}$$

since the dependent values evaluated at x'_k are not a function of x_k and vice versa. For example, by adding

$$U_{k} \frac{\partial \overline{u_{\beta}' u_{\beta}'}}{\partial x_{k}} + U_{k}' \frac{\partial \overline{u_{\alpha} u_{\alpha}}}{\partial x_{k}'} = 0$$
(B.8)

to the convective terms in equation B.4 (the first line) they can be rewritten as

$$U_{k} \frac{\partial}{\partial x_{k}} \left[\overline{u_{\alpha} u_{\alpha}} - 2 \overline{u_{\alpha} u_{\beta}'} + \overline{u_{\beta}' u_{\beta}'} \right] + U_{k}' \frac{\partial}{\partial x_{k}'} \left[\overline{u_{\alpha} u_{\alpha}} - 2 \overline{u_{\alpha} u_{\beta}'} + \overline{u_{\beta}' u_{\beta}'} \right]$$

$$= U_{k} \frac{\partial}{\partial x_{k}} \overline{\left(u_{\alpha} - u_{\beta}' \right)^{2}} + U_{k}' \frac{\partial}{\partial x_{k}'} \overline{\left(u_{\alpha} - u_{\beta}' \right)^{2}}. \tag{B.9}$$

Similarly adding

$$\frac{\partial}{\partial x_k} \overline{u_k u_\beta' u_\beta'} + \frac{\partial}{\partial x_k'} \overline{u_k' u_\alpha u_\alpha},\tag{B.10}$$

which is zero for incompressible flow, to the turbulent transport terms (the third line in eq. B.4) yields

$$-\frac{\partial}{\partial x_k} \overline{u_k \left(u_\alpha - u_\beta'\right)^2} - \frac{\partial}{\partial x_k'} \overline{u_k' \left(u_\alpha - u_\beta'\right)^2}.$$
 (B.11)

The viscous diffusion terms (the two-point term in the last line of eqn. B.4) can be written in a similar form by adding

$$\nu \frac{\partial^2 \overline{u'_{\beta} u'_{\beta}}}{\partial x_k \partial x_k} + \nu \frac{\partial^2 \overline{u_{\alpha} u_{\alpha}}}{\partial x'_k \partial x'_k} = 0$$
(B.12)

to these terms to yield

$$\nu \left\{ \frac{\partial^2}{\partial x_k \partial x_k} + \frac{\partial^2}{\partial x_k' \partial x_k'} \right\} \overline{\left(u_\alpha - u_\beta'\right)^2}.$$
 (B.13)

Finally, the pressure terms and the production terms can be manipulated to yield

$$U_{k} \frac{\partial}{\partial x_{k}} \overline{\left(u_{\alpha} - u_{\beta}'\right)^{2}} + U_{k}' \frac{\partial}{\partial x_{k}'} \overline{\left(u_{\alpha} - u_{\beta}'\right)^{2}} = +2 \frac{\overline{p} \frac{\partial u_{\beta}}{\partial x_{\beta}'}}{\rho \frac{\partial u_{\beta}}{\partial x_{\beta}'}} + 2 \frac{\overline{p} \frac{\partial u_{\alpha}}{\partial x_{\alpha}}}{\rho \frac{\partial u_{\alpha}}{\partial x_{\alpha}}}$$

$$-\frac{2}{\rho} \frac{\partial}{\partial x_{\alpha}} \overline{p} \left(u_{\alpha} - u_{\beta}'\right) - \frac{2}{\rho} \frac{\partial}{\partial x_{\beta}'} \overline{p}' \left(u_{\beta}' - u_{\alpha}\right) - \frac{\partial}{\partial x_{k}} \overline{u_{k}} \left(u_{\alpha} - u_{\beta}'\right)^{2} - \frac{\partial}{\partial x_{k}'} \overline{u_{k}'} \left(u_{\alpha} - u_{\beta}'\right)^{2}$$

$$-2 \overline{\left(u_{\alpha}' - u_{\alpha}\right) u_{k}'} \frac{\partial U_{\beta}'}{\partial x_{k}'} - 2 \overline{\left(u_{\beta} - u_{\beta}'\right) u_{k}} \frac{\partial U_{\alpha}}{\partial x_{k}} - 2 \overline{\left(u_{\beta}' - u_{\alpha}'\right) u_{k}'} \frac{\partial U_{\beta}'}{\partial x_{k}'} - 2 \overline{\left(u_{\alpha} - u_{\beta}\right) u_{k}} \frac{\partial U_{\alpha}}{\partial x_{k}}$$

$$+ \nu \left\{ \frac{\partial^{2}}{\partial x_{k} \partial x_{k}} + \frac{\partial^{2}}{\partial x_{k}'} \frac{\partial}{\partial x_{k}'} \left(u_{\alpha} - u_{\beta}'\right)^{2} - v_{\alpha\alpha} - v_{\beta\beta}. \right\}$$
(B.14)